The Thesis Committee for Thomas Alexander Ivanoff
Certifies that this is the approved version of the following thesis:

Retrogression-Reaging and Hot Forming of AA7075

APPROVED BY
SUPERVISING COMMITTEE:

Supervisor:

Eric M. Taleff

David L. Bourell

Retrogression-Reaging and Hot Forming of AA7075

by

Thomas Alexander Ivanoff, B.S.M.E.

Thesis

Presented to the Faculty of the Graduate School of

The University of Texas at Austin

in Partial Fulfillment

of the Requirements

for the Degree of

Master of Science in Engineering

The University of Texas at Austin

May 2014

Dedication

I would like to dedicate this to my parents and my family. They have always given me their love and support.

Acknowledgements

I would like to thank my advisor, Dr. Eric Taleff, for his help and guidance during the course of this project. His support and knowledge were invaluable to me and the success of this project.

I would like to thank Andrew Weldon for his assistance during equipment fabrication and testing, and for his pure friendship. I would also like to thank the other members of my research group who provided help and technical expertise, and gave me their support during my studies.

Abstract

Retrogression-Reaging and Hot Forming of AA7075

Thomas Alexander Ivanoff, M.S.E.

The University of Texas at Austin, 2014

Supervisor: Eric M. Taleff

The retrogression-reaging (RRA) and hot forming behavior of AA7075 were studied. AA7075 is a high-strength alloy used in applications where weight is of particular importance, such as in automobiles. Like many of the high-strength aluminum alloys, AA7075 requires elevated temperature forming to achieve ductility comparable to steels at room temperature. Since AA7075 is a precipitation hardening alloy, heat treatments during forming and production need to be closely controlled to limit any loss of strength due to changes in the microstructure. Two new forming concepts are introduced to explore the feasibility of forming AA7075 in manners compatible with current automotive manufacturing processes. They are RRA forming and solution forming. These concepts seek to improve upon the room-temperature formability of AA7075-T6 and incorporate the paint-bake cycle (PBC) into the heat treatment process. The PBC is a mandatory heat treatment used to cure the paint applied to automobiles during production. Currently, the PBC is conducted at 180 °C for 30 minutes.

RRA behavior was studied with molten salt bath treatments between 200 and 350 °C. The PBC was used in lieu of the standard 24 hour reaging treatment conducted at 121 °C. It was determined that retrogression treating below 250 °C was acceptable for RRA forming, with retrogressing at 200 °C producing the hardest material after reaging by the PBC. The formability of AA7075-T6 during RRA forming was evaluated by tensile testing at 200 and 225 °C. Ductility of AA7075-T6 at RRA forming temperatures was double compared to those produced at room temperature. RRA forming was demonstrated to achieve this improved ductility and a final material hardness after the PBC of only slightly less than the peak-aged condition. In addition, solution forming behavior was studied at 480 °C. Solution forming can increase ductility compared to RRA forming, but it requires aging at 121 °C prior to the PBC to produce peak-aged hardness.

Table of Contents

List of Tables

List of Figures

Chapter 1: Introduction

1.1. Purpose of Study

Improving fuel efficiency throughout the transportation industry is one of the most challenging and important problems currently facing auto manufacturers. The need to improve fuel efficiency arises from both stricter government regulations and rising fuel costs. Under current CAFE standards, combined fuel efficiency for an auto manufacturer's line must achieve 35.5 mpg by 2016 and 54.5 mpg by 2025 [1]. The difficulty in achieving this is not in the technology to improve fuel efficiency, but rather how to do so without dramatically raising the cost of products or services. This can be accomplished, at least in part, through the utilization of light-weight structural materials. High-strength aluminum alloys have been used extensively in the aerospace industry for years, and auto manufacturers have recently shown interest in developing aluminum forming processes suitable for automobile components. Applications of particular interest include both external body panels and interior structural members for the body-in-white. Conventionally, high-strength steel sheet has been used for these applications. However, aluminum alloys can offer large weight reductions compared to steels while maintaining similar strengths. Aluminum alloys are 2/3 lighter than steel and can offer strength to density ratios over 3 times greater than high-strength steels [2-4].

In automotive applications, exterior body panels experience considerable bending loads during service. Luo developed a method to compare the bending strength of light-weight metal alloys to steel using ASM performance indices, where m is mass, ρ is density, E is elastic modulus, and Y is tensile yield strength [5]. The cost associated with replacing steel with aluminum was not considered.

$$\frac{m_1}{m_2} = \frac{\rho_1}{\rho_2}\sqrt[3]{\frac{E_2}{E_1}} \qquad (1.1)$$

$$\frac{m_1}{m_2} = \frac{\rho_1}{\rho_2}\sqrt{\frac{Y_2}{Y_1}} \qquad (1.2)$$

These equations determine the mass savings that can be obtained by using high-strength aluminum, subscript 1, over steel, subscript 2, for automotive applications. Equation 1.1 applies for structures of equivalent bending stiffness, while Equation 1.2 applies for structures of equivalent bending strength. A ratio of less than one implies mass savings over steel. Bending stiffness and bending strength are important to auto manufactures because they determine the denting resistance of exterior body panels. Table 1.1 presents the material constants and mass ratios of high-strength and medium-strength aluminum alloys compared to two steels.

Table 1.1: Material properties of aluminum alloys and steel used for the mass ratio calculations.

Material	Density (g/cm^3)	Yield Strength (MPa)	Young's Modulus (GPa)	Bending Stiffness Mass Ratio	Bending Strength Mass Ratio
AA7075-T6 [2]	2.81	503	71.7	0.515	0.227
AA6061-T6 [2]	2.7	276	68.9	0.502	0.295
HSLA Steel A715 [5]	7.83	410	200	1.02	0.701
Standard Low Carbon Steel [3]	7.8	200	210	1	1

The high-strength aluminum alloy, AA7075-T6, can produce mass savings of 48 and 77 percent for structures of equivalent bending stiffness and bending strength, respectively. For exterior body panels, high-strength aluminum alloys can reduce component mass by half without a sacrifice in dent resistance. High-strength aluminum alloy structural components can possess bending strengths and tensile yield strengths equivalent to high-strength steels. This allows auto manufacturers to maintain the crashworthiness of vehicles, but with a greatly reduced mass.

Several previous studies on the forming of medium-strength 5000-series aluminum alloys demonstrated increased ductility at elevated temperatures from the grain-boundary-sliding and solute-drag creep deformation mechanisms [7]. These alloys,

however, lack the ability to be age hardened to greater strength after forming. Thus, high-strength 7000-series aluminum alloys are of interest for strengths superior to 5000-series aluminum alloys. In particular, the alloy AA7075, used for structural components in the aerospace industry, is of interest. The yield strength of AA7075 is comparable to high-strength steels, it can be age hardened considerably, and it is commercially produced. In addition, the behavior of AA7075 is indicative of most 7000-series aluminum alloys. For these reasons, this study focuses on developing new forming processes for the auto industry using AA7075 sheet.

Retrogression and reaging (RRA) treatments were first developed in 1974 by Cina [8]. RRA is a multi-step heat treatment consisting of two distinct steps: retrogression and reaging. The retrogression is a short-duration, high-temperature heat treatment followed by a rapid cooling. During the retrogression, it is thought that the strengthening microstructural precipitates within the aluminum matrix partially dissolve, or retrogress, back into solution. This step reduces part strength. Reaging is a low-temperature heat treatment performed after the retrogression. It is performed at the optimal temperature for precipitation and regrowth of the strengthening precipitates. Reaging returns the part strength to its initial value by reforming partially dissolved precipitates or precipitating new strengthening precipitates.

Like all the aluminum alloys, AA7075 must be formed at elevated temperatures to achieve ductilities comparable to steels formed at room temperature [2-3, 9]. The high-strength aluminum alloys, including AA7075, derive their strength from precipitation

hardening heat treatments, i.e. aging. Consequently, thermal history throughout the forming and manufacturing processes must be rigorously controlled to achieve the desired final part strength. In the auto industry, after forming, parts are assembled and painted. Currently, in order to cure the paint, manufacturers require components to endure a paint-bake cycle (PBC). The typical PBC is a 30 minute baking procedure at 180 ºC [10]. RRA treatments may be useful for developing new forming procedures of AA7075. Forming AA7075 sheet during retrogression will increase ductility and decrease forming stresses during stamping. Following forming, the mandatory PBC can potentially be utilized as the reaging step to return the final part to the desired strength. Forming AA7075 within a RRA schedule may potentially improve ductility while maintaining the desired final part strength.

Medium-strength, age hardening aluminum alloys will also be briefly addressed in this study. In particular, AA6061 is another alloy useful in studying RRA forming. AA6061 is representative of many medium-strength 6000 series aluminum alloys, and its peak aging temperature coincides with current PBC temperatures. AA6061 is artificially aged to peak strength at 160 to 180 ºC. AA6061 exhibits tensile elongations of 28 percent at 205 ºC and 60 percent at 260 ºC [2]. RRA behavior of AA6061 provides a comparison to AA7075. High-strength aluminum alloys, such as AA7075, can offer much greater weight savings than medium-strength aluminum alloys. Thus, the primary focus of this study is to investigate whether a RRA heat treatment combined with traditional auto manufacturing processes results in advantageous aging and forming behavior of AA7075.

1.2. Literature Review

1.2.1. Aging and Microstructure

AA7075 is a precipitation-hardening aluminum alloy that contains several alloying elements. The principle alloying additions are Zn, Mg, and Cu. In addition, minor amounts (less than 0.3 Wt. percent) of Ti, Mn, Cr, and Zr are commonly added to the alloy to benefit solidification, grain refinement, and various other purposes [2, 4, 11]. AA7075 is considered one of the strongest aluminum alloys commercially available. It is widely accepted that this alloy derives its strength from fine η'-phase and η-phase (MgZn) precipitates. Park and Ardell produced a generally accepted description of the precipitation sequence for AA7075 from the homogenized condition [12]. When aging occurs between 75 to 130 ºC two precursory precipitates form prior to the formation of η precipitates. Spherical G.P. zones initiate precipitation and are then followed by formation of the η'-phase [12]. If aging is conducted between 100 to 180 ºC, η' and η do not necessarily require prior G.P. zone formation to precipitate [12]. According to Park and Ardell, when over-aged below 190 ºC, the resulting microstructure is predominantly composed of η type precipitates [12]. Both the η' and η precipitates were determined to be plate like and hexagonal in structure [12]. In addition to the η-phase, the T-phase can form when aging occurs above 190 ºC. There are three commonly used tempers, or aging treatments, of AA7075. They are designated as the T6, T7, and Retrogression and Reaging (RRA) tempers [2]. Each of these tempers relies principally on controlling precipitation of the η'-phase and η-phase to varying extents. The T-phase produces large

cubic precipitates and was shown to reduce strength [12]. It is not desired for most tempers. The T6, T7, and RRA tempers will now be discussed in detail.

The strongest aging condition of AA7075 is the T6 temper, denoted as AA7075-T6. Because of its strength, the T6 temper is also referred to as the "peak-aged" condition. The standard procedure for its production after solution treatment is a single aging for 24 to 48 hours at 121 ºC [2]. The resulting microstructure consists primarily of finely distributed η' precipitates, lesser quantities of η precipitates, and any surviving G.P. zones [12]. The size and distribution of the η' and η precipitates critically influence the final strength. The orientation, composition, and size of these precipitates within the aluminum matrix were extensively characterized through TEM microscopy [12-16]. These studies verified that aging to the T6 temper primarily produces a dense and consistent distribution of fine η' precipitates [12]. The η-phase was also confirmed to exist, but to a much lesser extent than the η'-phase. It is generally accepted though, that the number density, distribution, and precipitate size of either precipitate has a greater impact on strength than the particular precipitate present [12]. Aging at 121 ºC beyond 48 hours will begin to reduce the final strength because of continued growth of η precipitates and evolution of η' precipitates into larger η precipitates. According to Park and Ardell, the η-phase prefers precipitation along grain boundaries [12, 16]. This is particularly important to the development of the T7 temper.

The T7 temper, also known as the "over-aged" condition, has a lower overall strength than the T6 temper. Over-aged sheet material is traditionally obtained by aging

for 6 to 8 hours at 107 ºC and then aging for 24 to 30 hours at 163 ºC [2]. Compared to the T6 temper, the T7 microstructure contains far fewer η' and η precipitates, with more η precipitates forming than η' precipitates. The η precipitates are generally larger in the T7 condition than they are in the T6 temper [12]. Park and Ardell showed that after aging at 100 ºC for 8 hours and 165 ºC for 24 hours, the resulting microstructure consists of large η precipitates along the grain boundaries and fewer smaller η precipitates lightly dispersed throughout the aluminum matrix [12]. The lack of η' precipitates and low quantity of total precipitates within the aluminum matrix is primarily responsible for the reduced strength of the T7 temper compared to the T6 temper [12]. Furthermore, studies suggest that over aging at temperatures above 190 ºC also permit the precipitation of the T-phase [12, 16]. The T-phase precipitates are generally much larger than η precipitates and are commonly believed to reduce strength even further.

Retrogression and reaging (RRA) treatments of AA7075 were first patented in 1974 by Baruch M. Cina [8]. A RRA treatment is a multi-step aging process. Typically the initial aging for RRA is similar if not identical to a peak aging (T6) treatment [8, 13-20]. After the initial peak aging, a retrogression heat treatment is performed. The retrogression is a short-duration, high-temperature heat treatment. Following the retrogression, a reaging completes the RRA treatment. The reaging is usually performed at the same temperature as the peak aging treatment. Cina first characterized the retrogression times and temperatures useful for RRA treatments of AA7075 [8]. According to Cina, retrogression can be successfully performed from 160 to 260 ºC. The

recommended retrogression times for 160 and 260 ºC are 30 minutes and 7 seconds, respectively [8].

Danh, Rajan, and Wallace suggested that during recommended retrogression treatments the η' precipitates already present from peak aging undergo a partial dissolution [13-20]. Park and Ardell concluded that nearly 1/3 of the η' precipitates formed during peak aging either fully dissolve or partially dissolve during typical retrogression treatments [16]. In addition, it is believed that the larger η' precipitates present from peak aging that do not dissolve evolve into η precipitates. The existing η precipitates undergo slight coarsening [13-16, 20]. Park and Ardell demonstrated that the dissolution and evolution of the η' precipitates occurs during the earliest stages of retrogression [16]. Kanno and Araki came to the same conclusions as Park and Ardell [17]. They used TEM microscopy to show a combination of partial dissolution of η' precipitates formed during peak-aging and slight growth of the η precipitates formed during peak aging after retrogression treatments of AA7075 [17]. Longer retrogression times, beyond the recommended retrogression times, predominantly cause growth of η precipitates, with precipitates present along grain boundaries coarsening the most [13-20]. The final microstructure following retrogression, regardless of retrogression time, contains far fewer precipitates than before. Though similar to a T7 tempered microstructure, the retrogressed structure is not equivalent. An over-aged sheet cannot be recovered to T6 strength without solution treating, whereas a properly retrogressed sheet can. This is generally thought to be because η' precipitates formed during peak aging only

partially dissolve during recommended retrogression treatments [13-20]. Reaging is conducted after the retrogression treatment is completed. The typical reaging procedure is conducted at 121 ºC for 24 to 48 hours [2, 8, 13-20]. Park and Ardell demonstrated that some η' precipitates form, essentially replacing those dissolved during retrogression and partially dissolved η' precipitates regrow during reaging [16].

The density and distribution of precipitates in the RRA microstructure are similar to those of the T6 microstructure. In both, η' precipitates are evenly and densely distributed throughout the grains. The RRA microstructure, however, contains large η precipitates along the grain boundaries. It is thought these are mainly precipitated and/or grown during retrogression and then undergo slight coarsening during reaging [16]. The final microstructure resulting from a RRA treatment is a combination of large η precipitates along the grain boundaries and a fine dispersion of smaller η' precipitates throughout the aluminum matrix [13-20]. RRA treatments, however, are very sensitive to alloy composition and the aging performed before RRA treatment. Because of this, RRA treatments depend strongly upon the material processing history. This is evident from the slight variation across the literature in the optimal retrogression parameters determined for maintaining peak strength after reaging.

1.2.2. Mechanical Behavior

In the peak aged, or T6 temper, AA7075-T6 exhibits a hardness of 175 to 190 HV and tensile yield strength of 503 MPa (73 ksi) [2]. Park and Ardell suggested that the greatest gains in strength were a result of fine η' or η precipitates distributed throughout the aluminum matrix [12]. It is believed that the strength gains are more dependent on the number of precipitates present and precipitate size than on precipitate type [12]. In practice though, the η' precipitate forms more than the η precipitate during T6 aging. Later investigations have consistently supported this claim [2, 11, 14-15]. While AA7075-T6 is considerably stronger than many other aluminum alloys, it is also highly susceptible to stress corrosion cracking (SCC). It is generally accepted that small η precipitates distributed along the grain boundaries are the primary cause of poor SCC behavior [12-15].

In response, the T7 temper was developed as a way to reduce SCC susceptibility. Park found a crack velocity of 4×10^{-4} mm/hr for AA7075-T7 compared to 2×10^{-2} mm/hr for AA7075-T6 during SCC experiments [13].The reduction in crack growth rate is accomplished primarily by the growth of η precipitates along grain boundaries [13-16, 20, 21-25]. This reduces the number of η precipitates along grain boundaries. Wallace, Rajan, and Beddoes suggested that the large grain boundary precipitates provide crack retardation through crack-tip blunting mechanisms [14]. While over aging treatments improve SCC resistance, they also reduce overall strength compared to peak aging [2, 12, 16, 21-25]. This is commonly attributed to the low quantity of η' precipitates present in

the over-aged microstructure. AA7075-T7 exhibits tensile yield strength of 435 MPa (63.1 ksi) and a hardness of 155 HV [2]. Over aging results in a 16 percent reduction in yield strength and a 13 percent reduction in hardness compared to peak-aged AA7075.

In 1974 Cina proposed RRA treatments for AA7075-T6 as a way of reducing SCC susceptibility while still maintaining peak-aged strength [8]. Rajan et al. studied the SCC behavior of AA7075-RRA and confirmed that SCC susceptibility was reduced by RRA treatments while the strength remained comparable to the peak-aged condition [14]. Several studies since then have reaffirmed the conclusions by Rajan et al. [13, 15-17, 21-24]. The final strength of AA7075-RRA is highly dependent upon the temperature and duration of the retrogression step. The change in hardness during retrogression of AA7075-T6 is shown in Figure 1.1. The typical hardness profiles for both low and high temperature retrogressions are shown as T_1 and T_2, respectively. Numerous studies have established that retrogressing beyond the recovery limits denoted in Figure 1.1 will prevent the strength lost during retrogression from being fully recovered during reaging [13-14]. Typical hardnesses are shown as a function of retrogression time in Figure 1.2.

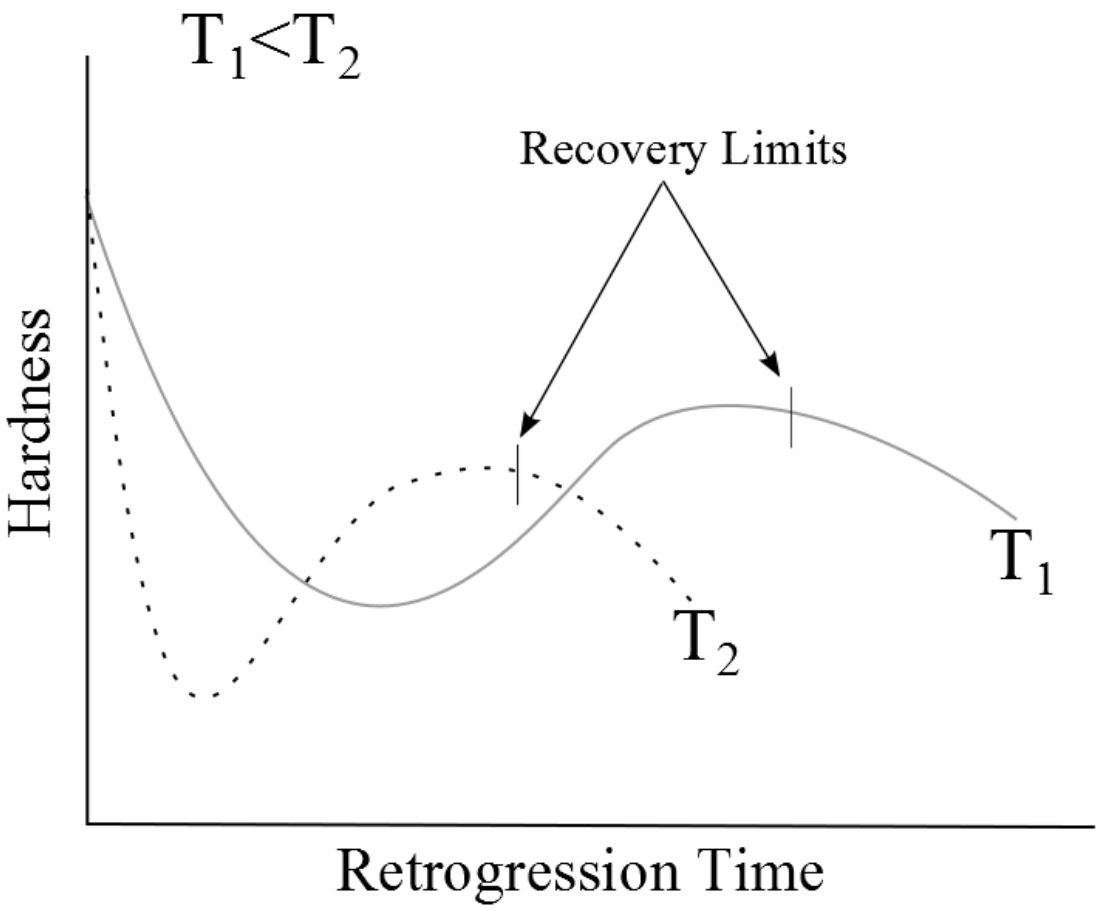

Figure 1.1: Typical hardness profiles of low (T_1) and high (T_2) temperature retrogressions as a function of retrogression time.

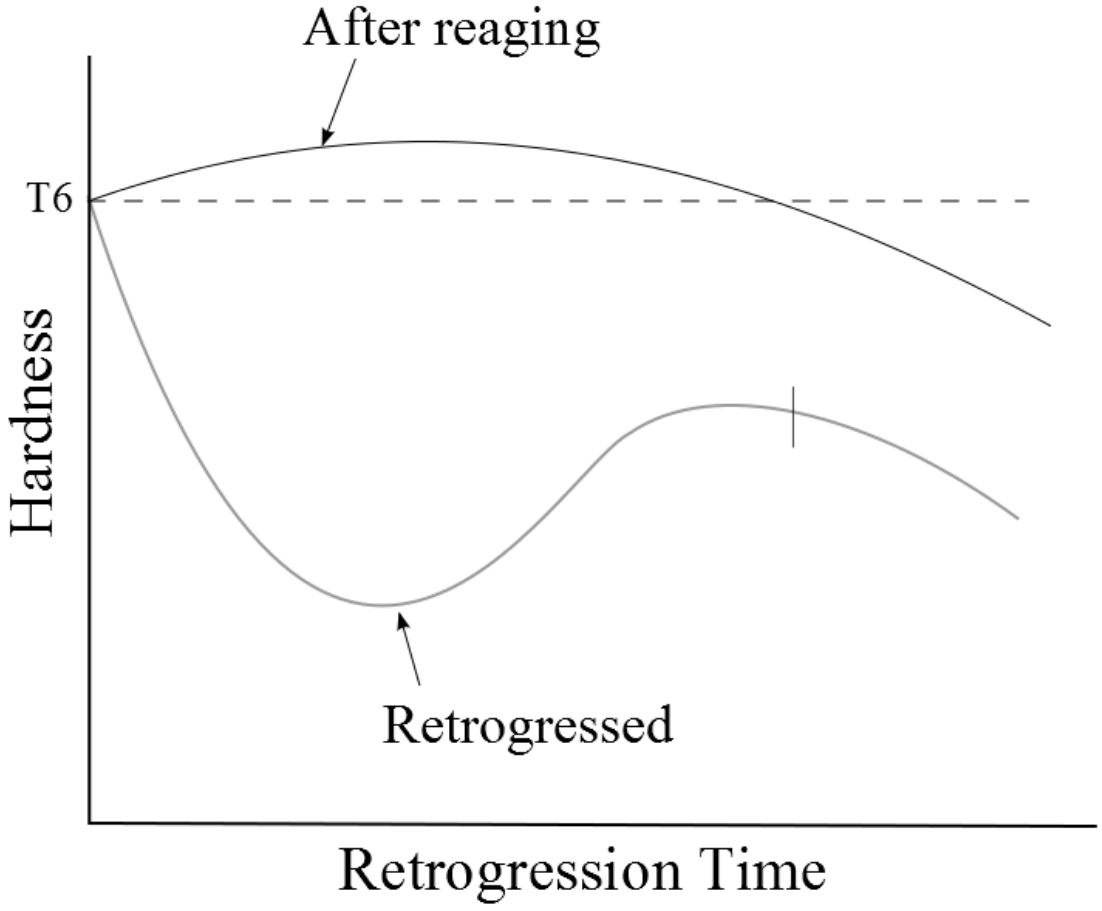

Figure 1.2: Typical hardness profiles of a retrogressed material (lower curve) and of a retrogressed material reaged at 121 ºC for 24 to 48 hours (upper curve) as functions of retrogression time.

Shorter retrogression times and lower retrogression temperatures typically result in a greater recovered strength and less SCC resistance compared to longer retrogression times and higher retrogression temperatures [13-24]. During longer and higher

temperature retrogression treatments, η' precipitates will dissolve to a greater extent than at lower temperatures and shorter times. In addition, the coarsening rate of η precipitates increases with time and temperature. The dissolution of η' precipitates adversely affects final strength, while growth of η precipitates along grain boundaries improves SCC resistance [13-24]. For AA7075, low-temperature retrogression treatments typically range from 160 to 180 ºC and last for 20 to 30 minutes. High-temperature retrogression treatments typically range from 230 to 240 ºC and last for 10 to 20 seconds [13-20]. The upper threshold for retrogression temperature is generally limited to 260 ºC. The short retrogression times necessary at these temperatures become impractical to obtain and control.

In addition to artificial aging procedures, such as the tempers discussed above, natural aging has been shown to substantially affect certain aluminum alloys [10, 25]. Taleff et al. established this for several Al-Zn-Mg alloys similar to AA7075. Following exposure to a typical paint-bake cycle (PBC), several alloys regained 30 percent of their strength after 60 weeks of natural aging [10]. In contrast, several studies reported that a heat treatment similar to the PBC acts as a retrogression treatment for AA7075-T6. They did not report on subsequent natural aging of these specimens [13, 20]. Consequently, the natural aging behavior of AA7075 following the PBC was considered during the course of this study.

AA7075-T6 exhibits low ductility at room temperature, causing difficulties for forming processes such as stamping. At room temperature AA7075-T6 exhibits tensile

elongation of 11 percent [2]. This is less than a third of the elongation of most steels used for stamping at room temperature [2-3]. It has been shown, however, that ductility of AA7075-T6 can be increased twofold by forming at elevated temperatures [26-28]. Sotirov et al. performed tensile tests at 200 and 230 ºC that produced tensile elongations of 25 and 32 percent, respectively [26]. Furthermore, Hui et al. showed an increase in ductility at 220 ºC but achieved tensile elongations of only 18 percent during tensile testing [27]. Tensile tests performed at temperatures near 300 ºC produced even greater elongations. The ASM Aluminum Specialty Handbook reports tensile elongations of 65 percent at 265 ºC and 70 percent at 315 ºC [2]. McQueen reports that tensile elongation does not increase above 300 ºC [10]. Nevertheless, it appears that forming at elevated temperatures may allow for AA7075-T6 to be successfully used in stamping operations.

Medium-strength aluminum alloys are currently used by the auto industry with cold forming processes. AA6016 and AA6111 have been previously used for exterior body panels [29-30]. AA6061 was reviewed in this study because it exhibits potentially useful behavior and is more readily available for future testing. AA6061-T6 achieves a tensile yield strength of 276 MPa (40 ksi) and a hardness of 107 HV. This is the peak-aged condition for AA6061. Compared with AA7075-T6, this is a reduction of 54 percent in tensile yield strength and 58 percent in hardness. The recommended aging temperature for AA6061 is from 160 to 180 ºC. This currently coincides with the typical PBC temperatures used today [2, 10]. Because of this overlap, AA6061 may see appreciable

strength gains following the PBC. Indeed, Saga et al. reported a marked increase in hardness after a typical PBC for various pre-aging conditions of AA6061 [31].

1.3. New Forming Concepts

Auto manufacturers encounter several difficulties when attempting to use conventional stamping techniques for forming high-strength aluminum alloys. Room temperature forming applications are limited by low ductility, and hot forming applications are restricted by the desired final part strength. Possibilities exist to create new forming concepts to overcome these difficulties. In particular, developing new forming concepts by combining hot forming and RRA heat treatments with current PBC demands is of interest. The new forming concepts suggested by this study are RRA forming and solution forming.

1.3.1 RRA Forming

RRA forming is a new multi-step heat treatment and forming concept designed to improve formability and maintain the peak-aged strength of high-strength aluminum alloys during auto manufacturing. The new concept integrates hot forming and the mandatory PBC into a RRA heat treatment. To begin, the sheet material is aged to the T6 condition and then preheated for a controlled time before stamping. The heated sheet is

then stamped in either warm or cold dies. The hot stamping operation acts as a retrogression treatment. The material is quickly cooled to room-temperature in the dies either during or at the end of the forming procedure. After the forming/retrogression operation, the sheet must be reaged back to peak strength. The PBC is used as the reaging treatment in lieu of the optimal reaging treatment. AA7075 is a practical alloy to investigate for this study. AA7075 provides the strength and light-weighting desired by auto manufacturers, and RRA treatments of AA7075 have been studied in the past. Furthermore, RRA treatments can improve SCC resistance while maintaining the peak-aged strength of AA7075. Two RRA forming concepts were proposed for this study. A processing map for each RRA forming concept is shown in Figure 1.3.

AA7075-T6 can be successfully retrogressed at 200 to 250 ºC for times from 2 minutes to 1 minute, respectively. The retrogression procedure includes the heat-up, forming, and cool-down operations. Two distinct reaging treatments for AA7075 were investigated during this study. The first, shown in Figure 1.3 (a), implements the PBC as the only reaging treatment. It was hypothesized that a proper retrogression could be paired with the PBC to mimic the effects of a traditional RRA treatment. The second option, shown in Figure 1.3 (b), is a two-step reaging treatment. After forming, an intermediate aging is performed at the optimal reaging temperature of 121 ºC for 3 to 24 hours. Then reaging is completed by the PBC. This option was investigated to determine how the PBC affected partially reaged AA7075. RRA forming can potentially address the

current barriers to forming AA7075 by improving ductility during stamping and maximizing final part strength.

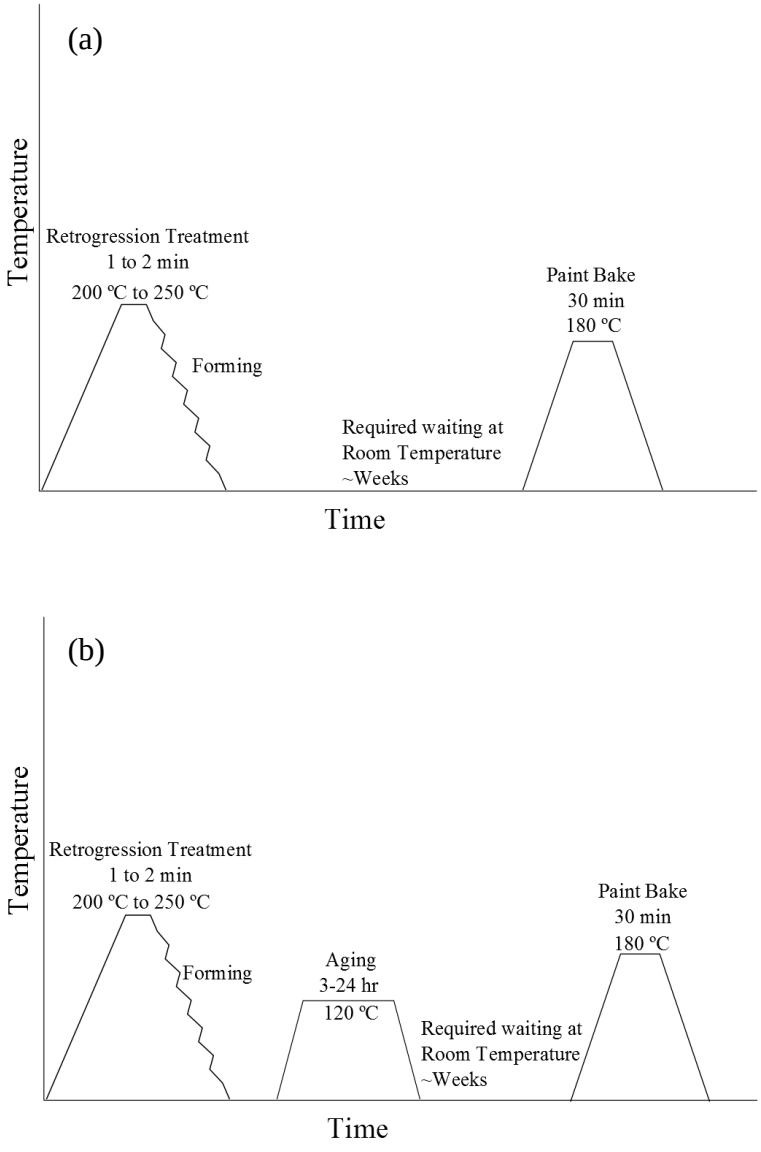

Figure 1.3: RRA forming concept for AA7075-T6 with (a) single-stage reaging and (b) dual-stage reaging.

AA6061 is another alloy that may benefit from RRA forming. Retrogression treatments for AA6061 are similar to those for AA7075, but the preferred aging temperature of AA6061 is from 160 to 180 ºC. Because this coincides with standard PBC temperatures, AA6061 is expected to respond favorably to the PBC. Saga et al. demonstrated that the PBC improves the hardness of AA6061 aged at 100 ºC for 300 seconds from 45 to 90 HV [31]. Combined with improvements in ductility at elevated temperatures, AA6061 could potentially be used with RRA forming operations.

1.3.2. Solution Forming

Solution forming is a new forming concept designed to greatly improve ductility and incorporate the PBC into a peak-aging heat treatment. The process map for solution forming is shown in Figure 1.4.

To begin, AA7075-O is heated to 480 ºC, the solution treatment temperature, and forming is performed. Cold dies are used for the stamping operation to provide rapid cooling. After forming is completed, the solution treated microstructure should still be intact. Next, a two-step aging treatment is performed. Initial aging is performed at 120 ºC for 3 to 24 hours, such that the material is slightly under-aged upon completion. The PBC is then used to complete the aging treatment. Aging with only the PBC would not likely be sufficient to reach peak-aged strength. It is suggested that aging at 120 ºC prior to the PBC can provide the appropriate pre-aging required to optimize the final part strength

[2]. Solution forming improves ductility compared to RRA forming, but requires higher temperatures and more aging treatments than the latter.

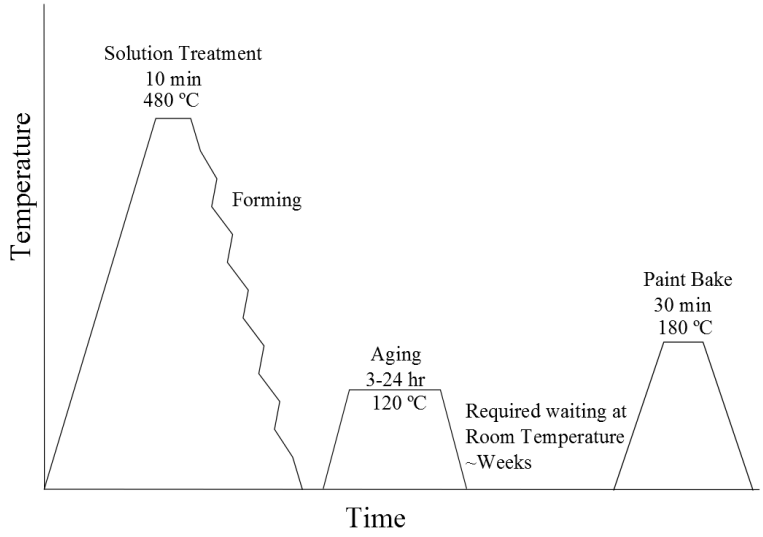

Figure 1.4: Solution forming concept for AA7075.

1.3.3. Comparison and Evaluation

There are several key differences between solution forming and RRA forming. They are in formability, operating cost and difficulty, and aging requirements. The ductility of AA7075 is greater at solution forming temperatures than at RRA forming temperatures [2]. This greater ductility allows more complex forming operations to be conducted with solution forming. Solutionizing requires heating to temperatures in excess

of 480 ºC. RRA forming operations only require heating to 250 ºC, or slightly less. This is both cheaper and easier to achieve than solution forming temperatures. Another distinction is that solution forming is not constrained by the short retrogression times of RRA forming. This creates a larger processing window for solution forming that is easier to manage. However, RRA forming requires less aging after forming than solution forming to reach peak-aged strength. This is because in the retrogressed condition, AA7075, contains a greater quantity of formed or partially dissolved η' and η precipitates than the solution-treated condition. AA7075-O should be void of nearly all strengthening precipitates and requires a rigorous aging treatment to reach peak-aged strength. In summary, RRA forming offers less ductility and shorter processing windows, but is conducted at lower temperatures and requires less aging than solution forming.

In order to further develop RRA forming and solution forming, the aging and forming behaviors of AA7075 were thoroughly evaluated. Hardness testing was used to assess the effects of various RRA heat treatments of AA7075-T6. These tests were then used to determine the heat treatment temperature and durations potentially useful for RRA forming. Tensile tests were performed at RRA forming and solution forming temperatures to evaluate the improvements in ductility obtainable from these new forming concepts.

Chapter 2: Experimental Procedures

2.1. Overview

The aging and forming behaviors of two AA7075-T6 sheet materials, generously provided by General Motors, are investigated. Both sheets were cold rolled to a final thickness of 2 mm and were received in the T6 condition [2]. One sheet was produced by ALCOA and the other by Austria Metall AG (AMAG). The nominal chemical composition of AA7075 is given in Table 2.1. The specific alloy compositions of the two AA7075-T6 materials tested were not provided. The two alloy sheets investigated in this study were subjected to the same heat treatments and tensile testing procedures. Samples for aging treatments were machined from the as-received material and subjected to multiple retrogression and reaging (RRA) treatments. Aging treatments were conducted, and hardness, an indirect measure of strength, was measured after the various RRA treatments. These data were used to determine the acceptable temperatures and times for RRA forming. Separate tensile coupons were machined from the as-received material for tensile testing. Tensile testing was conducted at temperatures of 18 ºC (room-temperature), 200 and 225 ºC with rapid direct electrical resistance heating, and 300 and 480 ºC with a resistance heating furnace. A constant cross-head velocity was used for all these tensile tests to provide an initial strain rate of 0.05 s^{-1}. All tensile coupon geometries were designed and machined per ASTM E8 standards, and elevated

temperature testing was conducted per ASTM E21 standards [32-33]. The tensile coupon geometries used in this study are described in detail in section 2.3. Tensile testing was conducted to evaluate the ductility obtainable from forming AA7075 at the elevated temperatures proposed for the solution forming and RRA forming concepts.

Table 2.1: Nominal AA7075 chemical composition in weight percent (wt. percent) [34].

Alloy	Zn	Mg	Cu	Cr	Si	Fe	Mn	Ti	Al
7075	5.1 - 6.1	2.1 - 2.9	1.2 - 2.0	0.18 - 0.28	< 0.4	< 0.5	< 0.3	< 0.2	bal.

2.2. Aging Procedures

A flow chart describing the five aging procedures investigated is presented in Figure 2.1. Path 1 kept material in the as-received condition and was used as a control. Path 2 produced retrogression treated material in order to characterize the hardness as a function of retrogression time for specific retrogression temperatures. It was of particular interest to locate the local minimum hardness produced by retrogression treating at short times. Reaging at 120 ºC from that local minimum hardness results in the greatest recovery in strength [16, 19-23]. Path 3 produced material reaged at 120 ºC for various times following retrogression treating. This treatment was completed to determine the effect of various 120 ºC reaging times on hardness. Path 4 produced paint-baked material

following retrogression treating. It was completed in order to determine if the paint-bake cycle (PBC) could replace a traditional reaging treatment at 120 ºC. Path 5 produced paint-baked material following retrogression treating and intermediate aging at 120 ºC for various times. This was studied to determine if pre-aging at 120 ºC before the PBC increased part strength compared to paint baking alone.

The specific temperatures and times investigated for the retrogression, reaging, and PBC steps are presented in Table 2.2. A total of 96 different heat treatment conditions were examined for each material. Specimens for RRA heat treatments, shown in Figure 2.2, were 3 cm long by 1 cm wide by 2 mm thick strips machined from the as-received material. Retrogression treatments used a molten salt bath. The molten salt bath and small specimen size ensured that the retrogression temperature was reached in no more than a few seconds. A resistance tube furnace was used for both the 180 ºC PBC and the optional 120 ºC intermediate aging treatments. Specimens were immediately water quenched to room temperature following the completion of each heat treatment. During heat treatments, temperature was monitored with two type-K thermocouples. Micro-Vickers hardness tests were conducted after the completion of each heat treatment. Specimens were naturally aged for 3 to 7 days between heat treatments. Specimens from each processing path were examined throughout testing, as shown in Figure 2.1. Several aging treatments were repeated during this study. Tests that were repeated one additional time are marked with a superscript † in Table 2.1. The data were consistent between the repeated tests. In addition, 3 to 5 hardness measurements were usually made for each

specimen. At least 3 hardness measurements were always made for the first examination following the completion of a heat treatment. For subsequent monitoring of natural aging, 3 or more measurements were taken only if the first measurement was not consistent with previous measurements. The uncertainty associated with hardness measurements was calculated to be ± 5 HV. This was calculated from the average of the standard deviations of tests where 3 or more hardness measurements were taken. The error was consistent between both sheet materials and between the different aging treatments. The largest standard deviation calculated from an individual examination was 13.8 HV, but this was caused by an individual outlier in the hardness measurements.

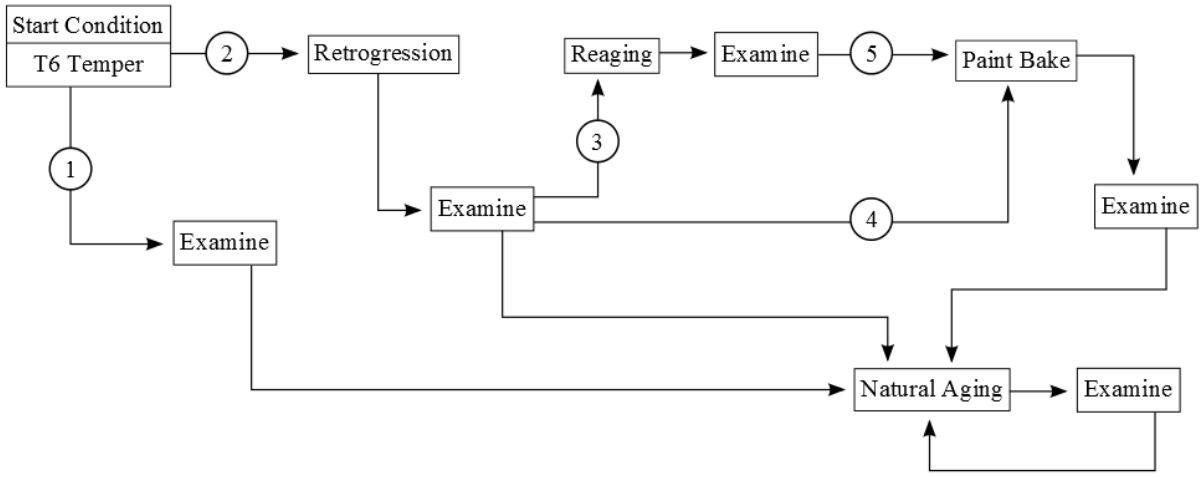

Figure 2.1: Flow chart of the aging treatments investigated. Path 1 provides material in the as-received condition. Path 2 provides material after retrogression treating; Path 3 provides material after retrogression treating and 120 ºC reaging; Path 4 provides material after retrogression treating and paint baking; Path 5 provides material after retrogression treating, 120 ºC reaging, and paint baking.

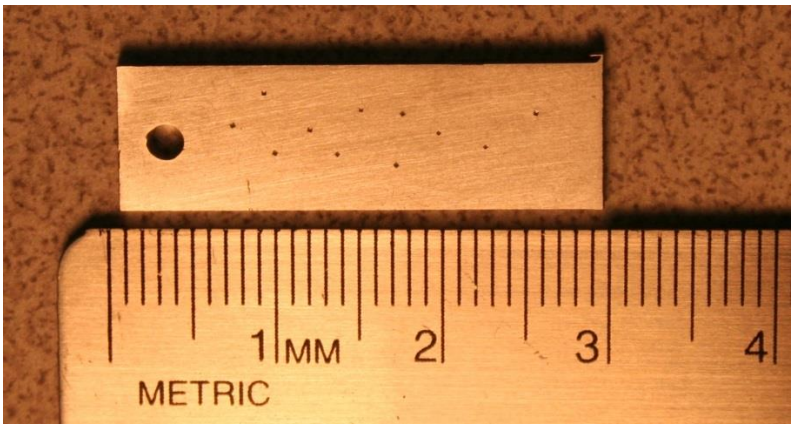

Figure 2.2: An example of the aging specimens used for studying heat treatments.

Table 2.2: Heat treatment temperatures and times used for this study. Each section corresponds to heat treatments for a path shown in Figure 2.1. Tests that were repeated one additional time are marked with a superscript †.

1	Control – Material in the as receive condition	
2	Retrogression Temp (°C)	Retrogression time (s)
	200†	10†
		30†
		90†
		150†
	225	10
		30
		90
		150
	250†	10†

Table 2.2 continued

	30†
	90†
	150†
300	10
	30
	90
	150
350	10
	30
	90
	150

3	Retrogression Temp (°C)	Retrogression time (s)	Reage Temp (°C)	Reage time (hrs)
	200	10	120	3
				6
				12
				24
		30	120	3
				6
				12
				24
		90	120	3
				6
				12
				24
		150	120	3
				6
				12
				24
	225	10	120	3
				6
				12
				24
		30	120	3
				6

Table 2.2 continued

			12
			24
	90	120	3
			6
			12
			24
	150	120	3
			6
			12
			24
250	10	120	3
			6
			12
			24
	30	120	3
			6
			12
			24
	90	120	3
			6
			12
			24
	150	120	3
			6
			12
			24
300	10	120	24
	30	120	24
	90	120	24
	150	120	24
350	10	120	24
	30	120	24
	90	120	24
	150	120	24

Table 2.2 continued

4 Retrogression Temp (°C)	Retrogression time (s)	Reage Temp (°C)	Reage time (hrs)	Paint Bake Temp (°C)	Paint Bake time (min)
200†	10†	none†	none†	180†	30†
	30†	none†	none†	180†	30†
	90†	none†	none†	180†	30†
	150†	none†	none†	180†	30†
225	10	none	none	180	30
	30	none	none	180	30
	90	none	none	180	30
	150	none	none	180	30
250†	10†	none†	none†	180†	30†
	30†	none†	none†	180†	30†
	90†	none†	none†	180†	30†
	150†	none†	none†	180†	30†
300	10	none	none	180	30
	30	none	none	180	30
	90	none	none	180	30
	150	none	none	180	30
350	10	none	none	180	30
	30	none	none	180	30
	90	none	none	180	30
	150	none	none	180	30

5 Retrogression Temp (°C)	Retrogression time (s)	Reage Temp (°C)	Reage time (hrs)	Paint Bake Temp (°C)	Paint Bake time (min)
200	10	120	3	180	30
			6	180	30
			12	180	30
			24	180	30
	30	120	3	180	30
			6	180	30
			12	180	30
			24	180	30
	90	120	3	180	30

Table 2.2 continued

			6	180	30
			12	180	30
			24	180	30
	150	120	3	180	30
			6	180	30
			12	180	30
			24	180	30
225	10	120	3	180	30
			6	180	30
			12	180	30
			24	180	30
	30	120	3	180	30
			6	180	30
			12	180	30
			24	180	30
	90	120	3	180	30
			6	180	30
			12	180	30
			24	180	30
	150	120	3	180	30
			6	180	30
			12	180	30
			24	180	30
250	10	120	3	180	30
			6	180	30
			12	180	30
			24	180	30
	30	120	3	180	30
			6	180	30
			12	180	30
			24	180	30
	90	120	3	180	30
			6	180	30
			12	180	30
			24	180	30
	150	120	3	180	30
			6	180	30

Table 2.2 continued

			12	180	30
			24	180	30
300	10	120	24	180	30
	30	120	24	180	30
	90	120	24	180	30
	150	120	24	180	30
350	10	120	24	180	30
	30	120	24	180	30
	90	120	24	180	30
	150	120	24	180	30

Path 1, shown in Figure 2.1 and Table 2.1, retained material in the as-received condition for future testing. The other paths described were used to produce material in various conditions of interest for potential forming technologies. Path 1 was used to quantify the changes in hardness produced by the various aging treatments investigated.

Path 2 produced material in the retrogressed state for further testing. Available literature suggests that retrogression treating at from 200 to 250 ºC for 10 to 150 seconds allows the peak-aged hardness to be recovered with an optimal reaging treatment. Consequently, samples were retrogressed at temperatures of 200, 225, and 250 ºC for 10, 30, 90, and 150 seconds. These span the potentially useful retrogression conditions for AA7075. Retrogression treating at 300 and 350 ºC was performed to quantify the effects of retrogression treatments at temperatures above the limit to recover hardness during reaging. Retrogression time was measured from the moment the specimen was submerged in the molten salt bath. Specimens were immediately water quenched to room temperature upon completion of the retrogression. These specimens were used to

determine the times and temperatures potentially useful for retrogression treatments of AA7075.

Path 3 produced material in the retrogressed and reaged condition for further testing. Specimens were reaged at 120 ºC for 3, 6, 12, and 24 hours after retrogression treating. Specimens were immediately water quenched to room temperature upon completion of the reaging. This was performed to determine how reaging time affects the hardness recovered after retrogression treatments. Reaging was also used to determine if peak-aged hardness was recoverable for each of the retrogression treatments investigated.

Paths 4 and 5 produced material with a simulated paint-baked condition at the end of the prior aging treatments. All retrogression treated specimens and specimens retrogressed and intermediately aged at 120 ºC were subjected to a simulated paint-bake cycle (PBC). Specimens were subjected to the PBC because it is a mandatory procedure in the automobile manufacturing process. Heat treating at 180 ºC for 30 minutes was used to simulate the typical PBC currently used by the automobile industry. The timing of the PBC was started the moment the specimens were loaded into the tube furnace. Specimens were immediately water quenched to room temperature upon completion of the PBC. These specimens were used to determine hardness after the PBC for various pre-aging conditions and whether or not the PBC could be used instead of an optimal reaging treatment. Part hardness after the PBC would need to be near the peak-aged hardness to consider RRA forming practical.

Natural aging was monitored for select specimens from the as-received and retrogressed conditions and for all specimens subjected to the PBC. Natural aging was conducted in a temperature-controlled environment maintained between 18 to 21 ºC. At least 3 hardness values were measured immediately following the completion of each heat treatment. A logarithmically increasing time span was adapted between subsequent hardness tests, as in the previous work by Taleff et al. [10]. Natural aging was monitored to measure any change in hardness over extended periods of time. This is important for ensuring parts behave as expected during service. Loss in hardness over time would be detrimental, whereas hardness gains may reduce artificial aging requirements.

2.3. Tensile Testing Procedures

Hardness data gathered from the aging treatments were used to determine the appropriate temperatures for evaluating RRA forming and solution forming behaviors. In order for a retrogression temperature to be considered suitable for RRA forming, peak-aged hardness must be recoverable by reaging after a minimum retrogression time of 30 seconds. RRA forming was explored at 200 and 225 ºC, and solution forming was explored at 300 and 480 ºC. The tensile testing procedures and test fixtures used are illustrated in Figure 2.3. Cold forming was simulated by tensile testing at room temperature. Solution forming was simulated by tensile testing in a three-zone resistance

tube furnace. RRA forming was simulated by tensile testing with rapid direct electrical resistance heating. The procedures for each of these tests are discussed in the following.

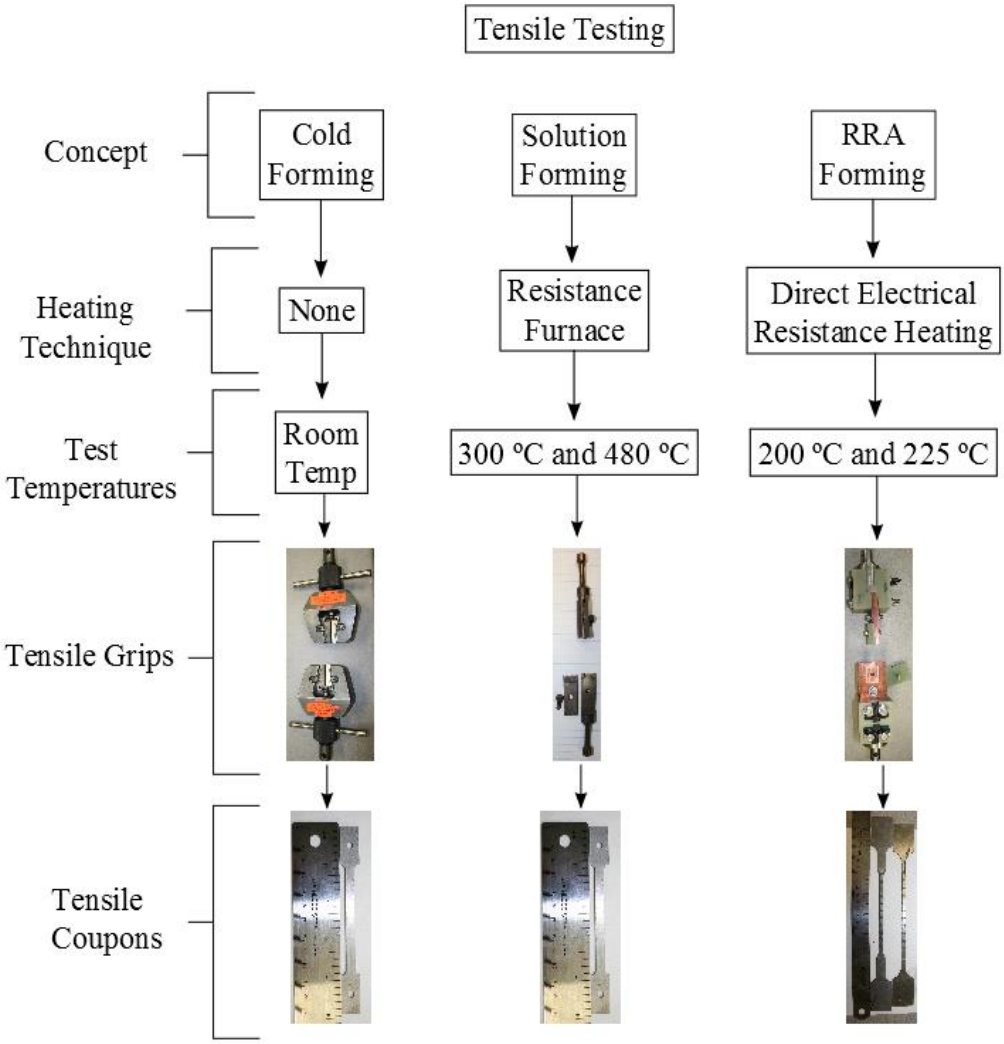

Figure 2.3: This figure displays the test temperatures and testing equipment used to evaluate cold forming (left), solution forming (middle), and RRA forming (right).

2.3.1. Room-Temperature Tensile Testing

Room-temperature tensile tests used specimens with a dog-bone geometry having a 70-mm gauge length and a 6-mm gauge width. A technical drawing of this tensile coupon geometry is presented in Figure 2.7. The rolling direction was oriented along the tensile direction. Tensile elongations were imposed by a computer controlled electro-mechanical test frame capable of maintaining a constant displacement rate. Tests were conducted on the as-received AA7075-T6 and on solution-treated AA7075. Solutionizing was conducted at 480 ºC for 48 hours in a tube furnace. Specimens were immediately water quenched to room temperature upon completion of the solution treatment. Peak-aged and solution-treated AA7075 were tensile tested at room-temperature to gauge the improvements in ductility gained by forming at retrogression and solution treatment temperatures. An extensometer was used to monitor elongation during testing. The extensometer could not be used in elevated-temperature tests. The test setup for room-temperature tensile testing is shown in Figure 2.4. Reduction-in-area was measured at the point of fracture with calipers accurate to ± 0.001 inches after testing.

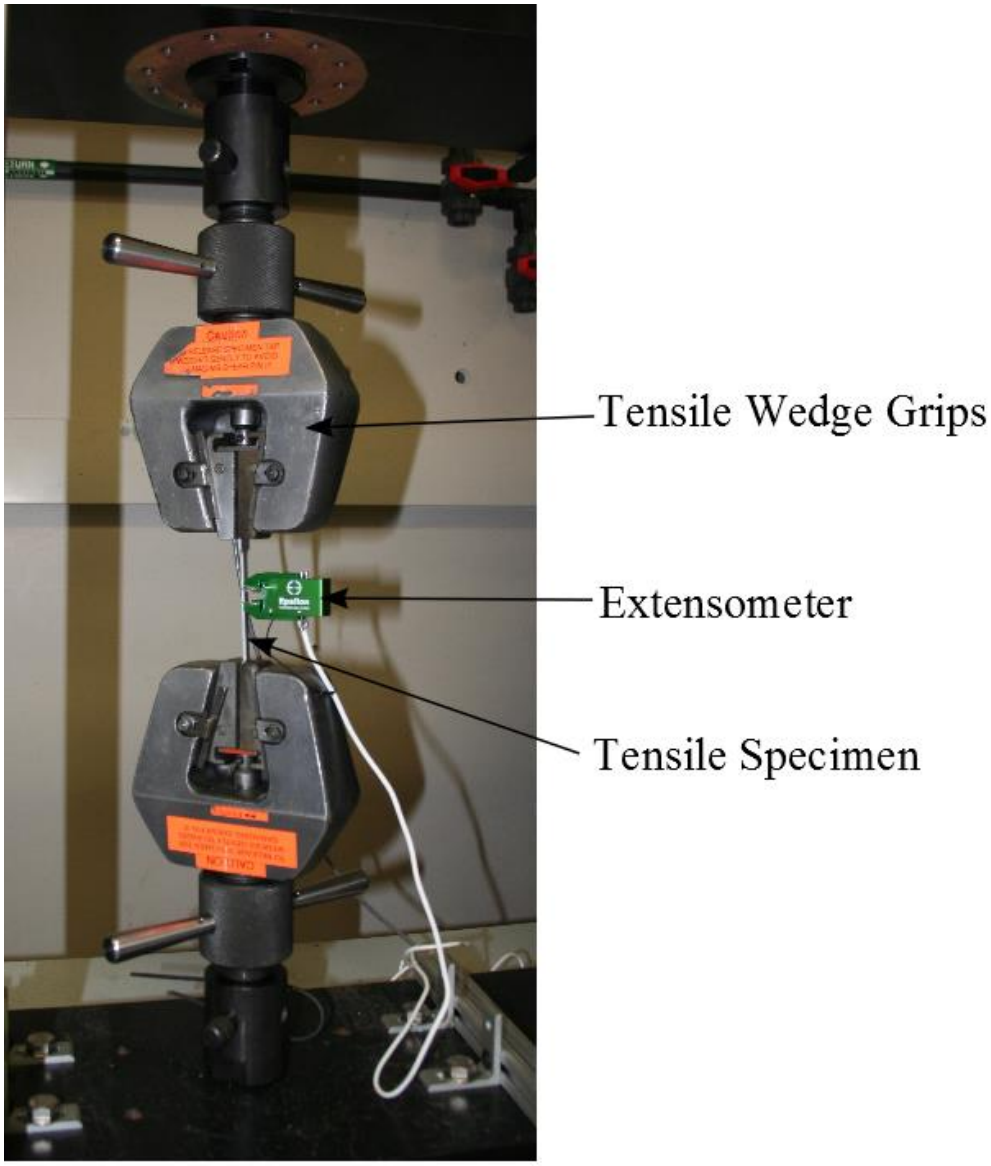

Figure 2.4: Room-temperature tensile test setup.

2.3.2. Solution Forming Temperature Tensile Testing

Solution forming tests were conducted at 300 and 480 ºC in a resistance tube furnace. These tests were conducted to measure ductility of AA7075 at solution forming temperatures. Testing was conducted at 480 ºC because that is the typical solution treatment temperature of AA7075. Very little tensile data exist for AA7075 at 480 ºC. Data are more readily available for tensile tests conducted at 300 ºC. Therefore, testing was also conducted at 300 ºC to produce data that could be compared to the data available from literature. Testing at 300 ºC also provided a closer comparison to RRA forming temperatures. Solution forming tensile testing was performed with the same tensile coupon geometry used for room-temperature tensile tests. The rolling direction was oriented along the tensile direction. Each specimen was brought to the desired testing temperature within 15 to 20 minutes by a three-zone resistance tube furnace. The three-zone furnace was used because rapid heating was not required. The furnace was controlled by a three-zone furnace controller that provided individual control of each heating zone during testing. The experimental setup for solution forming tensile testing is shown in Figure 2.5. Temperature was monitored during each test using two type-K thermocouples in contact with the specimen. Each specimen was immediately water quenched to room-temperature after test completion. Tensile elongations were imposed by a computer controlled servo-hydraulic test frame capable of maintaining a constant displacement rate. Tensile elongation was calculated from the crosshead displacement. The machine compliance was accounted for by adjusting the force and displacement data

after testing. This was accomplished by forcing the elastic loading portion of the data to match the known value of Young's modulus at the respective testing temperature. The unrelaxed temperature dependent Young's modulus for aluminum used for these corrections is described by Equation 1. This equation is from a fit to the data of Köster, where Young's modulus (E) is in MPa and temperature (T) is in Kelvin [35].

$$E(MPa) = 77{,}630 - 12.98T - 0.03084T^2 \qquad (2.1)$$

Reduction in area was measured at the point of fracture with calipers accurate to ± 0.001 inches for each specimen tested.

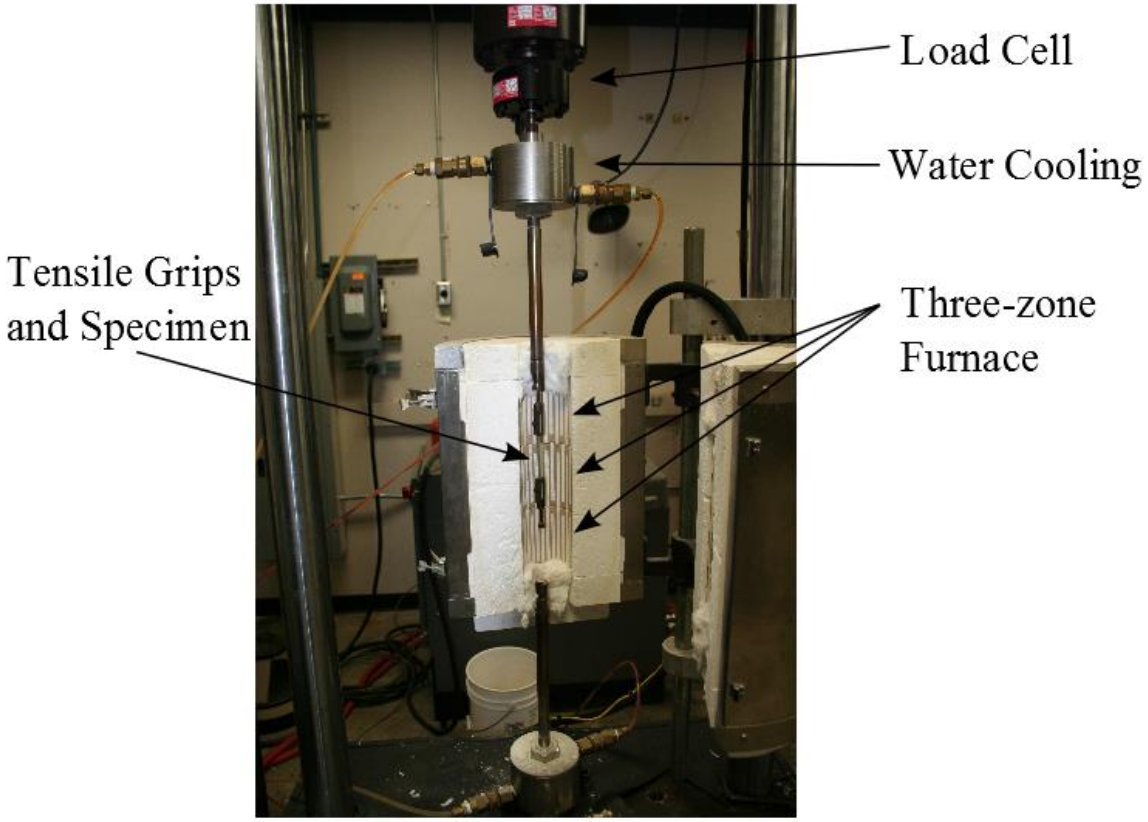

Figure 2.5: Solution forming tensile testing setup.

2.3.3. RRA Forming Temperature Tensile Testing

Tensile tests were performed at 200 and 225 ºC to evaluate RRA forming behavior. Typical retrogression treatments for AA7075 at temperatures above 200 ºC last for roughly 1 minute or less [8, 13-24]. Because of this, direct electrical resistance heating was used to heat the tensile coupons rapidly enough to appropriately simulate retrogression treatments during deformation. The electrical heating system was

comprised of three parts: the power system, the control system, and the tensile testing fixtures. A schematic and a picture of the electrical heating system are shown in Figure 2.6.

The power system consisted of a Miller XMT 350 MPA welding power unit, which provided up to 350 amps at 1 to 2 volts. This unit was chosen because it was available and provided well regulated amperage at low voltage. The power system was remotely controlled by computer to automate the heating procedure. Automation was implemented in order to provide precise control of the temperature and heating rate during testing. The control system consisted of an Omega 0S0550 Series infrared pyrometer (IR), Dell computer, National Instruments data acquisition and output modules, and LabVIEW routine. This system controlled, monitored, and recorded the specimen temperature during each test. The IR pyrometer measured the infrared emission from the specimen, and temperature was inferred from that measurement. Each tensile coupon was painted flat black to provide a constant, known emissivity. Emissivity was taken to be 0.95. A PID algorithm was implemented in LabVIEW to control specimen temperature during testing. The amperage supplied by the welder was continually adjusted through a computerized interface based on a heating profile input by the user and the temperature determined from the IR pyrometer. The IR pyrometer was used in lieu of contact temperature measurement techniques because of the high currents required for direct electrical resistance heating. Various National Instruments DAQ boards were used to connect all of the components of the system to a single command computer. This

system did not monitor deformation, i.e. force and displacement. A separate computer controlled and recorded the deformation data obtained from tensile testing. Tensile elongations were imposed by a computer controlled electro-mechanical test frame capable of maintaining a constant displacement rate. The tensile testing fixtures consisted of the tensile grips and tensile coupons. The design of each of these is discussed in the following.

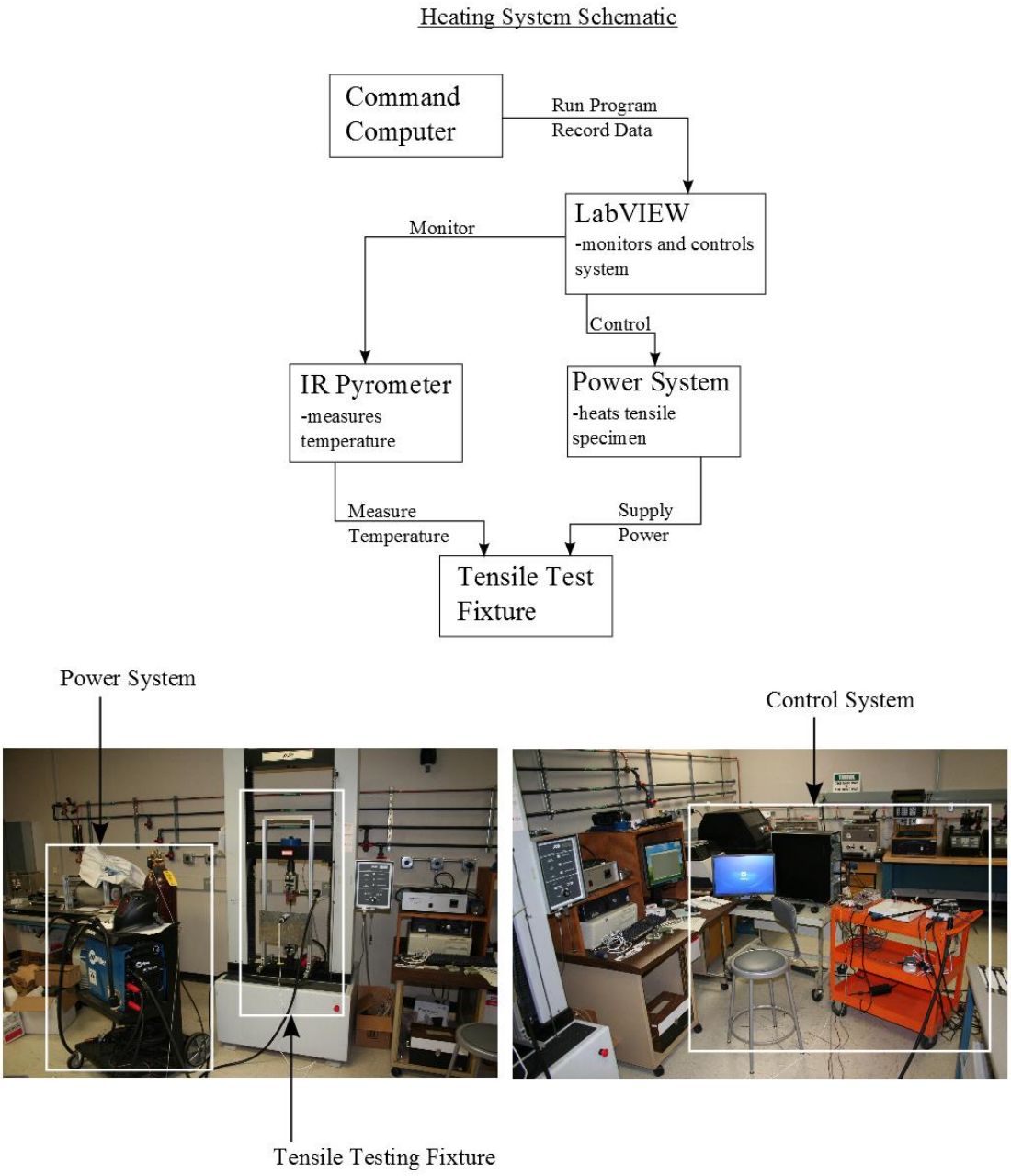

Figure 2.6: Schematic representation of the direct electrical resistance heating system (top) and photographs of the direct electrical resistance heating system (bottom).

Tensile coupons were designed specifically for rapid heating immediately prior to tensile testing. A one-dimensional finite difference transient temperature model was developed to aid in the design of an appropriate tensile coupon. The model was adapted from the work of Karunasena on electrical resistance heating of flat bar geometries [36-37]. The heating rate and temperature profile of the tensile coupon are determined by the width and length of the gauge region. Temperature was assumed to be constant across the width and thickness of the coupon but vary along the length of the gauge region. Boundary conditions needed to be specified before the model could be run. This included specifying the ambient air temperature and the temperature of each end of the gauge region. The ambient air was held constant at 20 ºC. The initial temperature at each end of the gauge region was also taken to be 20 ºC, but was linearly increased to 100 ºC during the simulation. This was done because Karunasena observed a temperature increase at the ends of the bar [36]. The convective and radiative heat transfer coefficients used were first determined by a fit to the data of Karunasena. They were later refined by fitting to data obtained with the tensile coupons used in this study. A detailed description of the heat transfer model is provided in Appendix A.

Using the model, two tensile coupon geometries were designed. The rolling direction was oriented perpendicular to the tensile direction. The technical drawings for these are provided in Figure 2.7. A long double-dog-bone geometry with an 11-cm gauge length and 5-mm gauge width was first designed. This specimen produced a heating rate of 15 ºC per second in the middle of the gauge region using the rapid heating system. The

resulting temperature profile provided a ± 5 ºC temperature variation across a 1-inch length at the center of the gauge region. The double-dog-bone geometry was chosen to concentrate the current and localize heating to the inner-most gauge region. Because the double dog-bone is an unusual geometry, a single-dog-bone geometry was also designed. The single-dog-bone geometry has a 15.3-cm gauge length and 5-mm gauge width. This geometry produces a slightly larger constant-temperature region in the gauge region and a quicker heating rate than the double-dog-bone geometry. The heating characteristics of both geometries are shown in Figure 2.8. The single-dog-bone-coupon was tested to verify the data from the double-dog-bone geometry. Test results were consistent between both of these geometries and with data from the available literature. The tensile coupons were given large grip faces to improve conduction between the tensile coupon and the specimen holder. Both geometries used in this study are significantly longer than traditional tensile coupons. This was required to provide a reasonably long constant-temperature zone in the inner-most gauge region and to limit the conductive heat loss from the gauge region to the tensile grips.

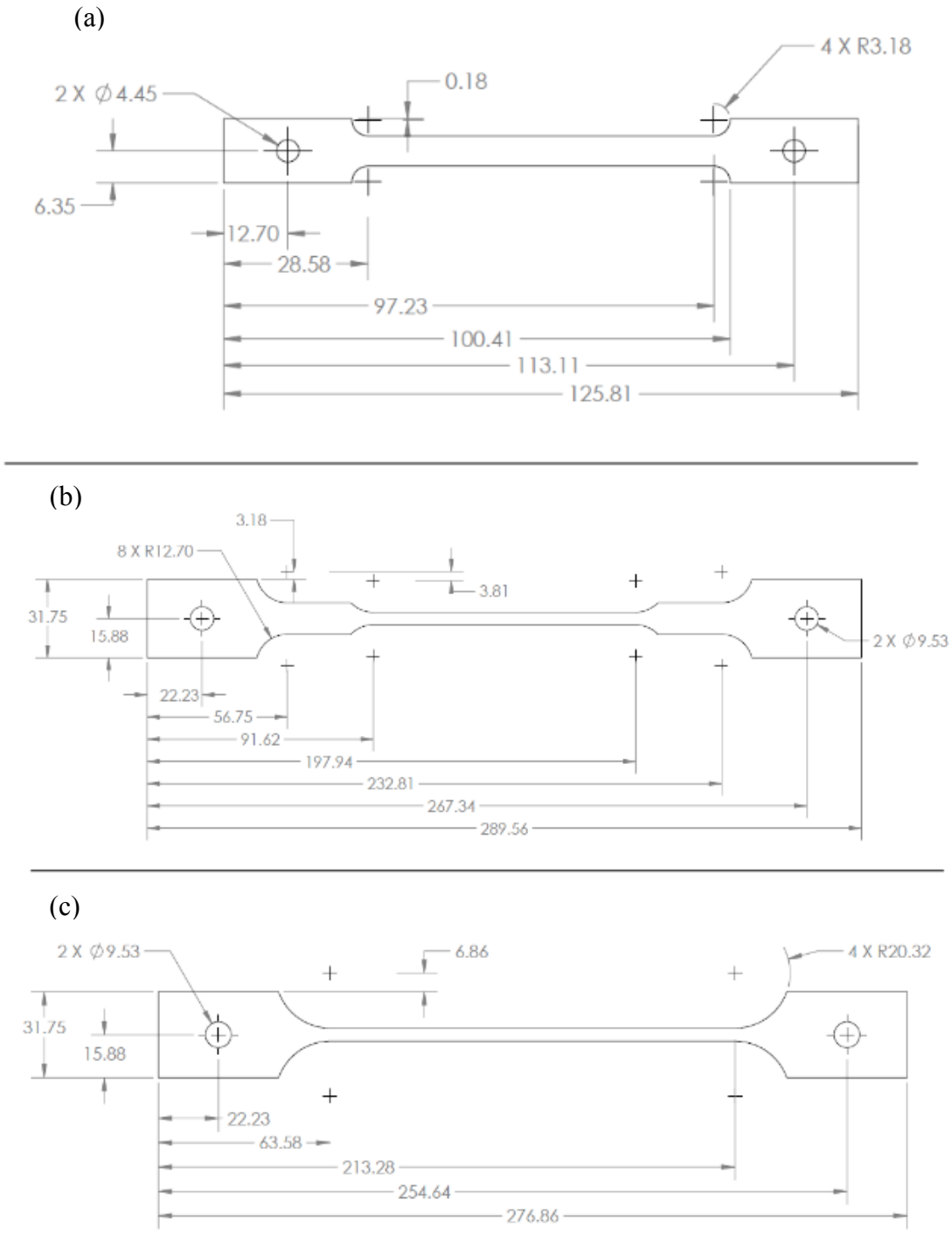

Figure 2.7: Technical drawings of (a) the room-temperature tensile coupon, (b) the rapid heating double-dog-bone tensile coupon, and (c) the single-dog-bone tensile coupon. All dimensions are in millimeters.

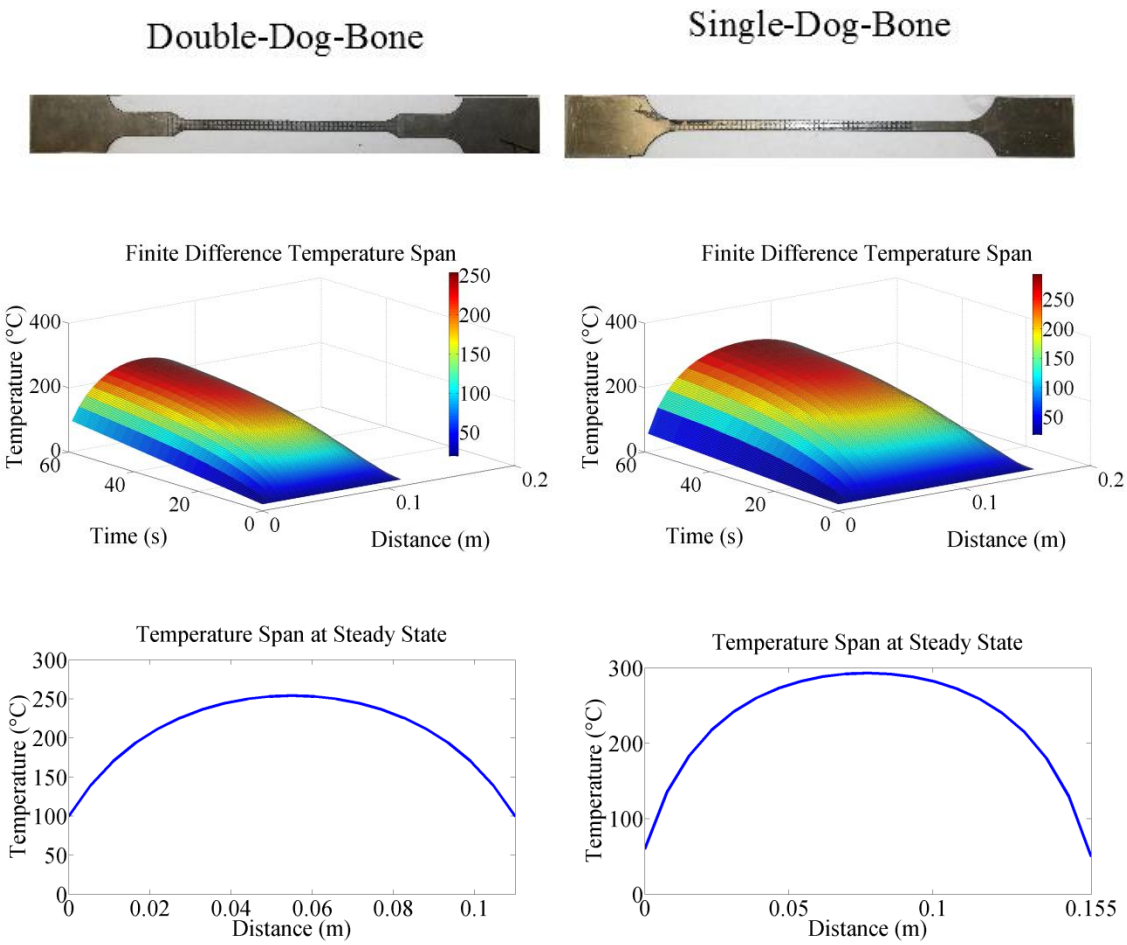

Figure 2.8: Heating rates and profiles for the double-dog-bone (left) and single-dog-bone (right) tensile coupons predicted by the heat transfer model. The heating rates and temperature profiles were calculated with a constant current of 250 amps.

The rapid-heating system was tested with a static table-top testing rig, shown in Figure 2.9, prior to testing in the tensile testing frame. This was to test the control and power systems and to compare the actual heating profiles and heating rates produced by the tensile geometries with those predicted by the numerical model simulations. Both

geometries behaved similarly to the model predictions, and only minor adjustments were made to the heat transfer coefficients to more accurately match the experimental temperature profiles across the inner-most gauge length. The temperature determined by the IR pyrometer was verified at 100 and 500 ºC using two Omega temperature indicating lacquers.

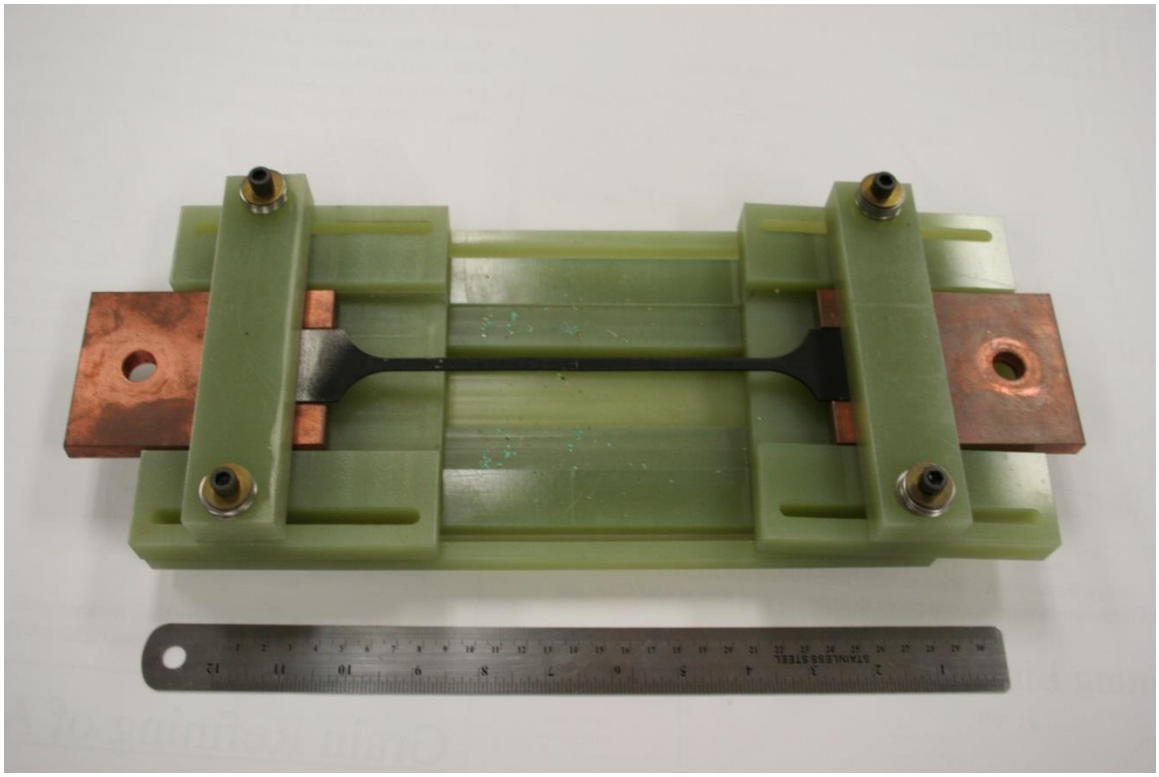

Figure 2.9: Static table-top testing rig.

New tensile grips were also designed for rapid heating tensile testing. The grips, shown in Figure 2.10, were designed to electrically isolate 500 amps at 5 volts, bear over 2000 lbs, and provide proper axial alignment of the specimen within the testing frame. The specimen holders were machined from C110-H02 copper to provide ample electrical conduction to the tensile specimen. The wire leads from the power supply were bolted directly to the specimen holder. Care was taken to ensure that each wire and connection was robust enough to safely conduct 350 amps without excessive heating. Furthermore, the specimen holder was designed to provide a large enough thermal mass to avoid over-heating of the grip assembly. Tensile specimens were shoulder loaded and held in place by a G-10 cover placed over the front of the specimen. A bolt through the assembly was used to secure the specimen and the G-10 cover to the specimen holder. G-10 phenolic composite was chosen to provide electrical isolation from the test frame because it combines a high dielectric strength with high tensile yield strength. G-10 phenolic is a glass-fiber and epoxy composite material with a dielectric strength of 800 V/mm and tensile yield strength of 310 MPa (45 ksi) [38]. Spacers were machined from a single block of G-10 material with the fibers oriented along the tensile direction. The spacer electrically isolated the specimen holder from the load cell. An adapter was machined from a solid three-inch diameter 303 stainless steel rod to connect the spacer with the load cell. 303 stainless steel was chosen because it combines sufficient strength and good machinability. The adapter, G-10 spacer, and specimen holder were secured to each other by four half-inch diameter 18-8 stainless steel bolts. Stainless steel was used for all bolts, nuts, and washers because the testing frame is located in a non-atmospherically

controlled environment. Technical drawings of the grip components are available in Appendix A.

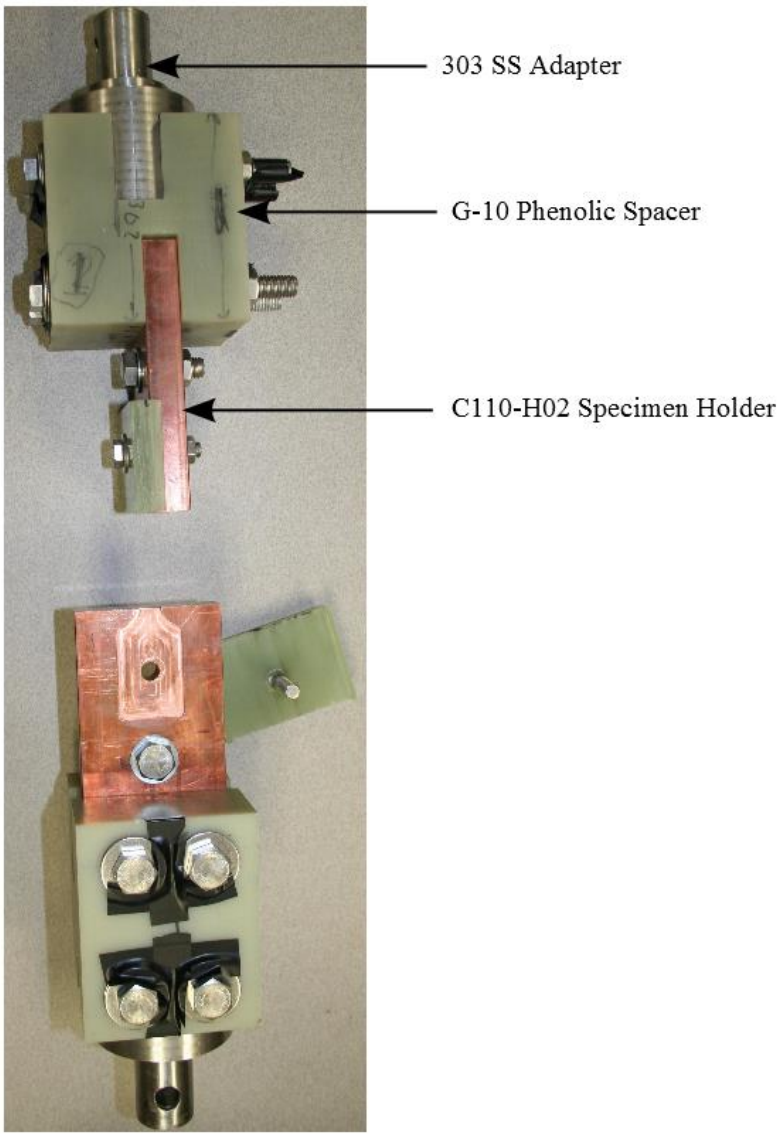

Figure 2.10: Tensile grips used for rapid heating tensile testing.

Rapid heating tensile testing was used to simulate forming operations at retrogression temperatures. Tensile specimens were brought to the appropriate testing temperature within 25 to 30 seconds by the rapid heating system. A predefined temperature profile was specified before the test began for automatic computer control of heating. Once the specimen reached the desired testing temperature, it was allowed to stabilize for 10 to 20 seconds before deformation was started. The power supply was shut off at the start of deformation testing so that the tensile coupon would not electrically arc at failure. Deformation testing typically lasted for 1.5 seconds, and the temperature remained nearly constant during deformation. No form of quenching or forced convection techniques were used to cool the tensile specimens. After failure, each tensile specimen was left to cool in the ambient room-temperature air. Cooling to room-temperature typically required 1 to 2 minutes.

Reduction in area was measured at the point of fracture after each test with calipers accurate to ± 0.001 inches, and cross-head displacement was measured in real time during each test. Elastic expansion of the grips and the temperature variations along the specimen gauge length made monitoring tensile elongation difficult. The temperature variations caused strain localization at the center of the inner-most gauge region, where temperature was the highest. As a result, it was not possible to determined local tensile elongation from the cross-head displacement alone. In order to measure local strains, circular gauge marks with a 0.1-inch diameter were electrochemically etched onto each specimen. A video camera captured images of the etched specimens during each test. A

frame-by-frame analysis was completed afterwards to measure the elongation of the gauge marks. These data provided local tensile elongations and local strain rates. The video analysis process is depicted in Figure 2.11.

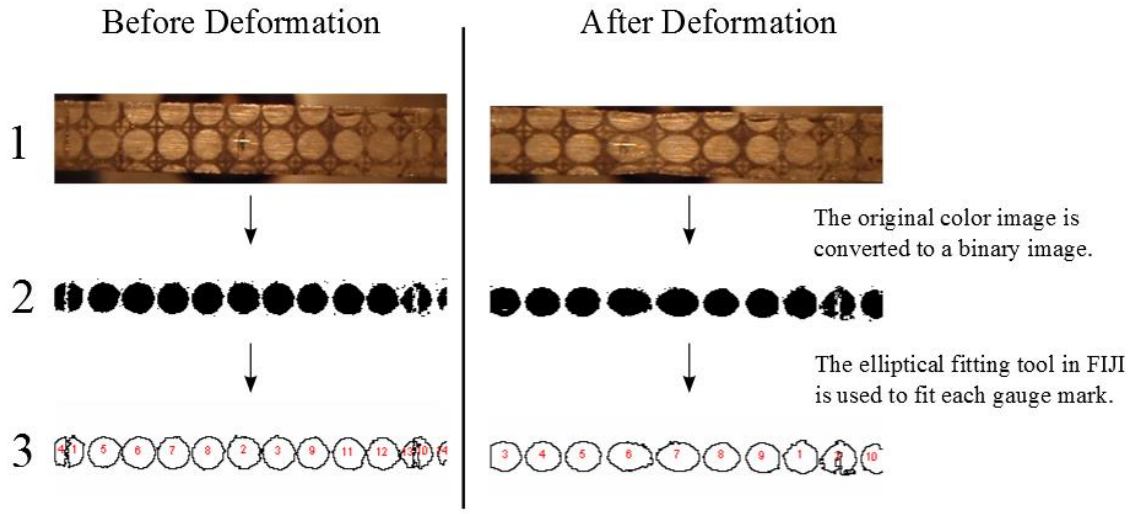

Figure 2.11: Example of the video analysis procedure used to measure local strain during rapid heating tensile testing.

In order to begin video analysis, the images associated with deformation had to be identified. It was assumed that the image captured immediately before the specimen fractured constituted the end of deformation testing. In reality, this is slightly inaccurate. Because the duration of deformation varied from test to test, different moments of testing were captured for each test. Consequently, the image assumed to be the end of

deformation testing was not captured at the same moment of final deformation for each test. The video camera recorded at a frame rate of 15 frames per second, resulting in a 0.07 second gap between images. Because this gap was small compared to the total deformation time, the discrepancy between tests was believed to be negligible. Force and displacement data were used to calculate the duration of deformation for each test. This value was then used to locate the image associated with the start of deformation testing. Every three images between the first and last images of deformation testing captured were analyzed. In total, 5 to 7 frames were analyzed for each test. The time elapsed between each frame analyzed was 0.2 seconds.

Analysis was completed by fitting ellipses to each gauge mark and measuring the major and minor axes of each ellipse. To accomplish this, the original image captured was converting to a binary image. This was so that each image could be interpreted by FIJI, an image analysis software program [39]. Each binary image was manually edited to ensure the shape of the gauge marks was completely preserved during the conversion. The original image was over-layed onto the binary image to aid in this procedure. Next, the elliptical fitting tool in FIJI was used to fit an ellipse to each gauge mark and measure the lengths of each major and minor axis. FIJI was used because it provided a systematic way of accurately and consistently fitting an ellipse to each gauge mark. Strain was calculated by measuring the elongation of each axis between images.

Note: Appendix A contains a more detailed description of the procedures used during this study. It also contains more information on the design and testing of the tensile grips and tensile coupons used for ERH testing.

Chapter 3: Experimental Results

3.1. Hardness Data

Hardness tests were used to evaluate AA7075-T6 after retrogression and reaging (RRA) heat treatments. The retrogression response was determined by the hardness as a function of retrogression time for multiple retrogression temperatures. It was of particular interest to locate the retrogression time associated with the local hardness minimum for each retrogression temperature. This information was then used to evaluate the retrogression times and retrogression temperatures potentially useful for RRA forming. Throughout this section, each figure will present plots for the two materials studied side-by-side. The plot shown on the left is for the material from ALCOA, and the plot shown on the right is for the material from AMAG.

3.1.1. Retrogression Treating Only

The hardness data for each retrogression temperature investigated are presented as a function of retrogression time in Figure 3.1.

ALCOA AMAG

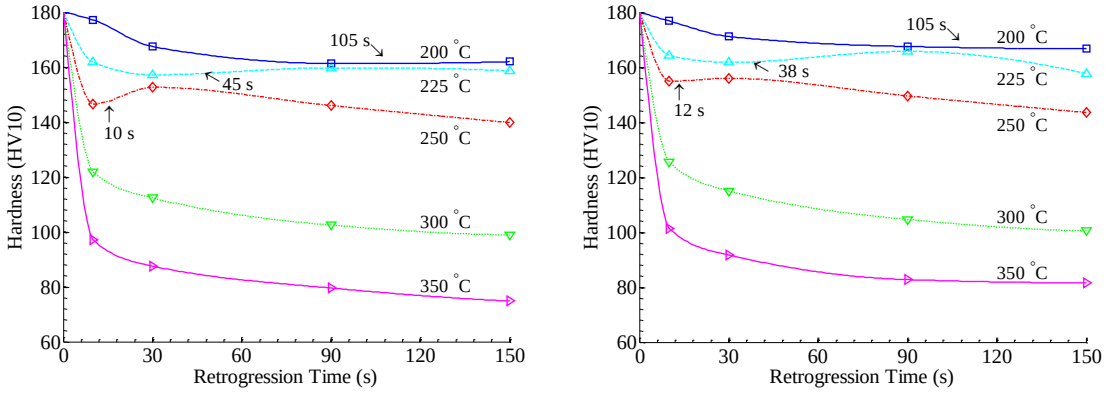

(a) ALCOA: retrogression treated.

(b) AMAG: retrogression treated.

Figure 3.1: Hardness is shown as a function of retrogression time for specimens retrogression treated at 200, 225, 250, 300, and 350 ºC. Data from ALCOA (a) specimens and AMAG (b) specimens are shown side-by-side.

As shown in Figure 3.1, both materials exhibit two types of retrogression behavior. The low-temperature behavior consists of retrogression treatments performed at 250 ºC and below, for which a local minimum in hardness occurs during retrogression. The high-temperature behavior consists of retrogression treatments performed at 300 and 350 ºC. The observed retrogression behavior is consistent with data from the available literature [8, 13-24].

Low-temperature retrogression treatments produced the typical hardness profile associated with retrogression treatments [8, 13-24]. Hardness is first reduced to a local minimum and then slightly recovers as retrogression time increases. After the slight

increase, hardness then gradually descends with increasing retrogression time. The location and depth of the initial reduction in hardness is highly dependent upon retrogression temperature. Retrogression treatments performed at 250 ºC produced a quicker and more severe reduction in hardness than retrogression treatments performed at 200 and 225 ºC. Retrogression treatments conducted at 200 ºC did not produce a significant increase in hardness after the local hardness minimum for the retrogression times investigated. It is expected that an increase in hardness would be observed if retrogression treatments at 200 ºC were performed for longer than 150 seconds. Overall, hardness decreased with increasing retrogression temperature.

Recovered hardness after reaging is greatest when specimens are retrogressed to the local hardness minimum prior to reaging. Reaging after retrogression treating beyond the local hardness minimum is detrimental to final part hardness [8, 16]. Therefore, it was of particular interest to determine the retrogression time associated with the local hardness minimum for each retrogression temperature. These times are noted in Figure 3.1 and listed in Table 3.1 for retrogression treatments performed at 250 ºC and below. The retrogression time necessary to reach the local hardness minimum decreased from 105 ± 20 to 10 ± 5 seconds as retrogression temperature increased from 200 to 250 ºC. The uncertainty in the retrogression time to reach the local minimum hardness was determined from a visual inspection of each hardness profile as a function of retrogression time.

Table 3.1: Local minimum hardness data and corresponding retrogression conditions for the (a) ALCOA and (b) AMAG materials.

(a)

ALCOA		
Retrogression Temperature (ºC)	Local Minimum Retrogression Time (s)	Local Minimum Hardness (HV)
200	90 ± 20	161
225	30 ±10	157
250	10 ± 5	147

(b)

AMAG		
Retrogression Temperature (ºC)	Local Minimum Retrogression Time (s)	Local Minimum Hardness (HV)
200	150 ± 20	167
225	30 ± 10	162
250	10 ± 5	155

High-temperature retrogression treatments at 300 and 350 ºC did not produce the typical hardness curve associated with retrogression behavior. Contrary to low temperature retrogression treatments, there was no evidence of achieving a local hardness minimum or subsequent recovery in hardness as retrogression time increased. Instead, a rapid decrease in hardness was initially observed and hardness continued to decrease with increasing retrogression time.

The hardness data obtained from each retrogression treatment were combined for both materials and used to create a "master" hardness profile as a function of

temperature-normalized retrogression time. Hardness after retrogression treating is related to partial dissolution of η' precipitates. This depends on the distance zinc diffuses away from η' precipitates during retrogression. It was hypothesized that hardness could be represented as a function of the diffusion distance of zinc in aluminum.

Equation 3.1 describes how the distance a diffusing species travels in a solid material depends on time and the diffusion coefficient of the diffusing species in the solid material. In this study, $\bar{x}$ (m) is the diffusion distance of zinc in the solid aluminum matrix, D (m^2/s) is the temperature dependent diffusion coefficient for zinc in aluminum, and t (s) is time.

$$\bar{x} \sim \sqrt{D \cdot t} \qquad (3.1)$$

The diffusion coefficient of a solute is described by Equation 3.2, where D_o (m^2/s) is the frequency factor, Q (J/mol) is the activation energy, R (J/mol-K) is the universal gas constant, and T (K) is the retrogression temperature.

$$D = D_o \cdot e^{-Q/RT} \qquad (3.2)$$

Equation 3.3 is obtained by combining Equation 3.1 with Equation 3.2 and can be used to relate the diffusion distance of zinc in aluminum to the retrogression temperature, T (K), and retrogression time, t (s). Because it was postulated that hardness, HV, depends on the diffusion distance of zinc in aluminum, hardness is assumed to be a function of retrogression temperature and retrogression time in the following manner,

$$HV = fn(\bar{x}) = fn\left(t \cdot e^{-Q/RT}\right) \qquad (3.3)$$

The activation energy for zinc diffusion in aluminum near η' precipitates was taken as 95 kJ/mol. This value is from Taleff et al. [10]. Smithell's and Hisayuki et al. list the activation energy of zinc diffusion in Al-Zn-Mg alloys near 120 kJ/mol [40-41]. This value was determined from high-temperature diffusion measurements. The activation energy listed by Taleff et al. was determined from differential scanning calorimetry of Al-Zn-Mg alloys undergoing peak-aging. It was not determined by diffusion measurements. The value from Taleff et al. was used because it was a direct measurement of the dissolution of η' precipitates.

Ignoring constant terms, Equation 3.3 presents hardness as a function of retrogression temperature (T) and retrogression time (t). The right side of Equation 3.3 represents retrogression time compensated for retrogression temperature and is referred to as temperature-normalized retrogression time, t^*. Hardness data are plotted against temperature-normalized retrogression time in Figure 3.2. A curve was drawn to the data in Figure 3.2 to highlight the shape of the hardness profile and enable hardness to be easily determined from retrogression temperature and retrogression time.

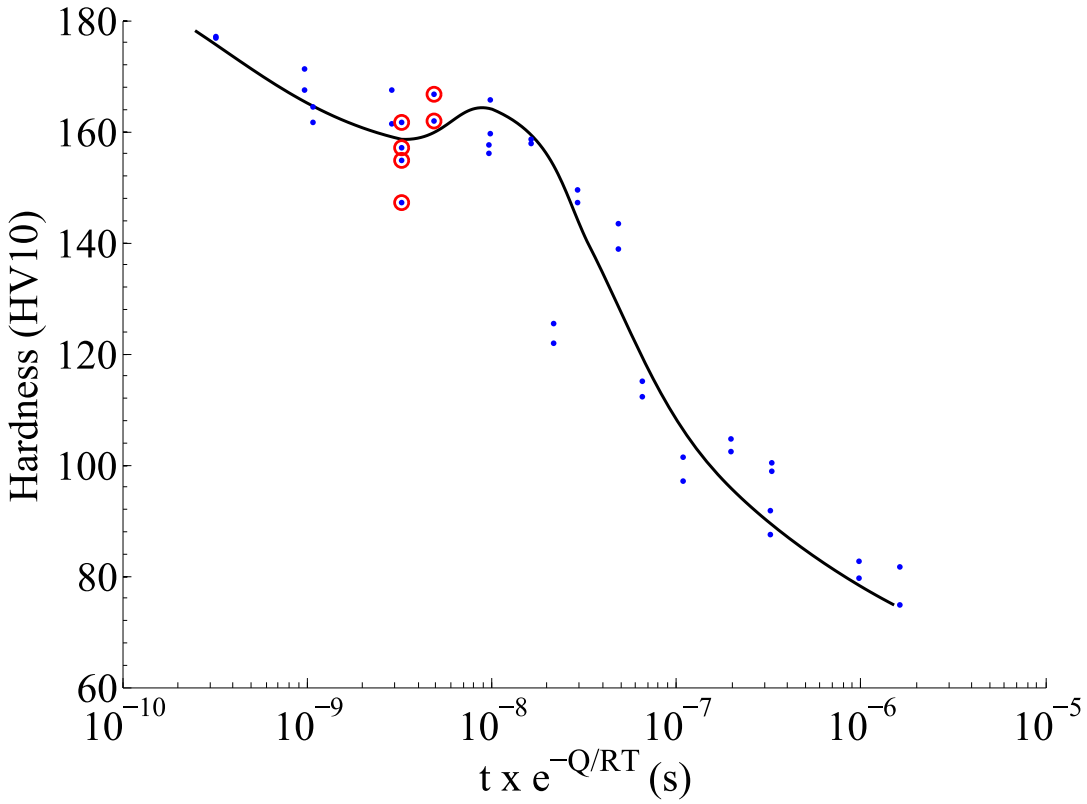

Figure 3.2: The hardness profile for retrogression of AA7075 is shown plotted against temperature-normalized retrogression time. The points enclosed in a circle denote local minimum hardness.

3.1.2. Retrogression Treating and Paint Baking

Typically, reaging is performed at 120 ºC for 24 hours after retrogressing to complete a RRA heat treatment. However, for the RRA forming concept introduced in section 1.3, the mandatory paint-bake cycle (PBC) is used as a reaging treatment instead. Thus, the retrogressed specimens were subjected to a simulated PBC, and their responses

were studied. The simulated PBC was conducted at 180 ºC for 30 minutes. The hardness data for specimens subjected to the PBC following retrogression treatments are shown as a function of retrogression time in Figure 3.3.

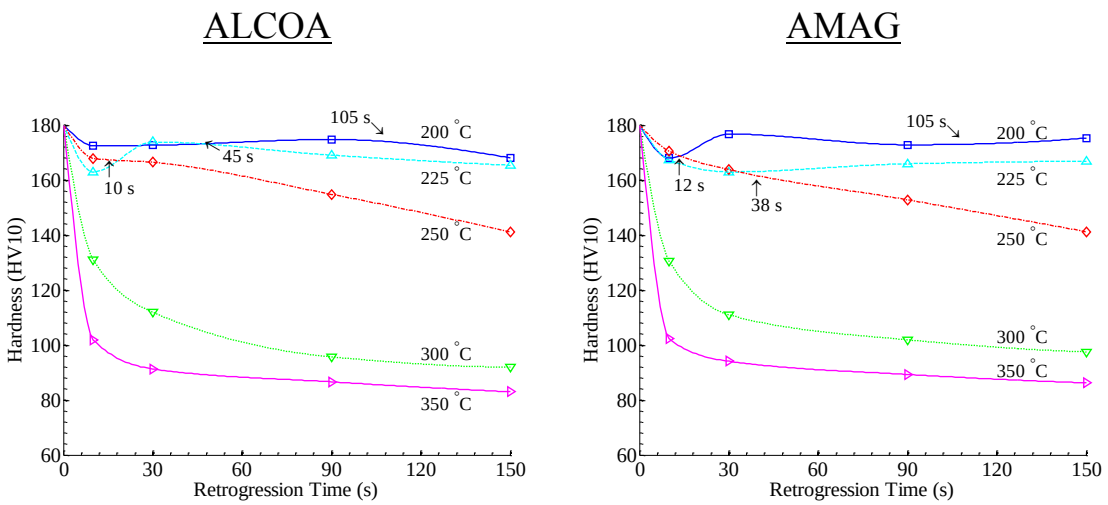

(a) ALCOA: retrogression treated and paint-baked.

(b) AMAG: retrogression treated and paint-baked.

Figure 3.3: Hardness is shown as a function of retrogression time for specimens subjected to the simulated PBC following retrogression treatments at 200, 225, 250, 300, and 350 ºC. Data from ALCOA (a) specimens and AMAG (b) specimens are shown side-by-side.

The PBC produced a measurable increase in hardness in many of the specimens retrogressed at 250 ºC and below. Specimens retrogressed at 200 ºC for over 10 seconds reached at least 83 percent of peak-aged hardness following the PBC. Hardness was reduced in the specimen retrogressed at 200 ºC for 10 seconds. It is suspected the PBC caused further retrogression in this specimen. This was most likely a result of the

specimen being under-retrogressed prior to paint baking. The PBC response for specimens retrogressed at 225 ºC depended upon the manufacturer. For these specimens, hardness increased following the PBC in the ALCOA specimens retrogressed for more than 10 seconds, while hardness did not increase or decrease following the PBC in the AMAG specimens for any retrogression time. Finally, the PBC increased hardness for specimens retrogressed at 250 ºC for 10 and 30 seconds, while specimens retrogressed for 90 and 150 seconds were not influenced by the PBC.

Overall, it was observed that the PBC generally improved hardness after low-temperature retrogression treatments. Hardness following the PBC generally decreased as retrogression temperatures and retrogression times increased.

For higher temperature retrogression treatments, the PBC had little effect on hardness for any of the retrogression times investigated. As expected, retrogression treating at temperatures above 300 ºC reduced hardness too severely to be recovered to peak-aged hardness by a reaging treatment. Because of this, these specimens were not considered for any of the multi-step heat treatments discussed later, but their natural aging behaviors were still monitored.

3.1.3. Retrogression Treating and Intermediate Aging at 120 ºC

Though the PBC was useful for reaging specimens retrogressed at low temperatures, none of the specimens fully recovered peak-aged hardness. Therefore, a

second RRA forming concept was introduced in section 1.3. It was suggested that an additional intermediate aging treatment performed after retrogression treating and before the PBC may improve the final hardness. Intermediate aging treatments were conducted at 120 ºC for 3, 6, 12, and 24 hours. It was of interest to determine if the final hardness, after the PBC, could be optimized by varying the intermediate aging time. Hardness is plotted against retrogression time for specimens retrogressed at 250 ºC and below and reaged at 120 ºC for various times in Figure 3.4.

ALCOA

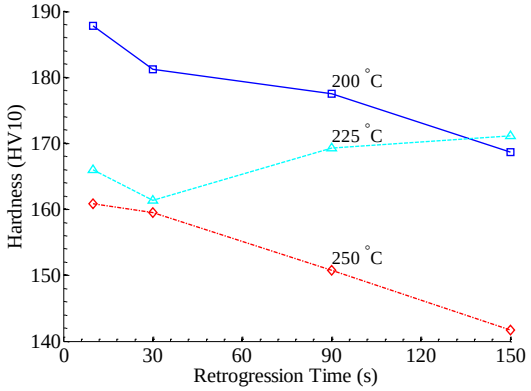

(a) ALCOA: retrogression treated and aged for 3 hours at 120 ºC.

AMAG

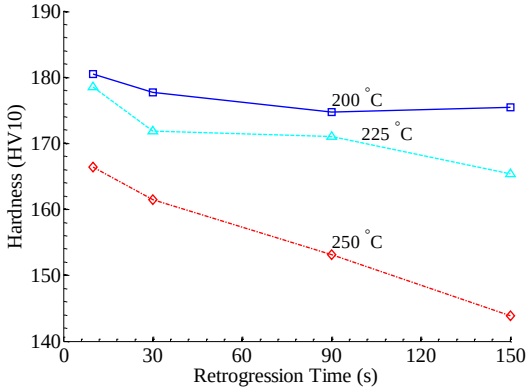

(b) AMAG: retrogression treated and aged for 3 hours at 120 ºC.

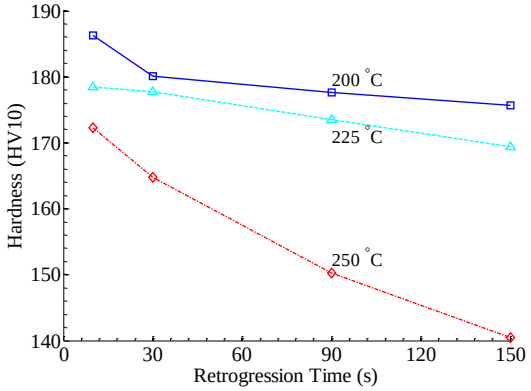

(c) ALCOA: retrogression treated and aged for 6 hours at 120 ºC.

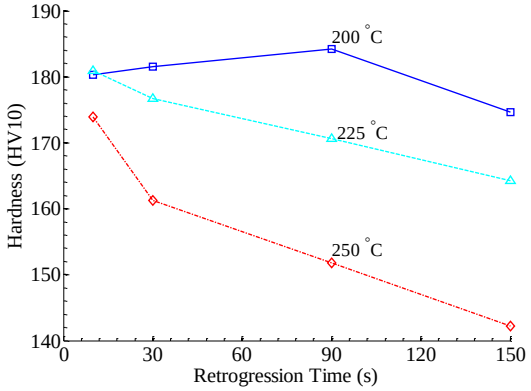

(d) AMAG: retrogression treated and aged for 6 hours at 120 ºC.

Figure 3.4: Hardness is shown as a function of retrogression time for specimens reaged at 120 ºC for various times following retrogression treatments at 200, 225, and 250 ºC. Aging times from top to bottom are (a,b) 3, (c,d) 6, (e,f) 12, and (g,h) 24 hours. Data from ALCOA (left) specimens and AMAG (right) specimens are shown side-by-side.

Figure 3.4 continued

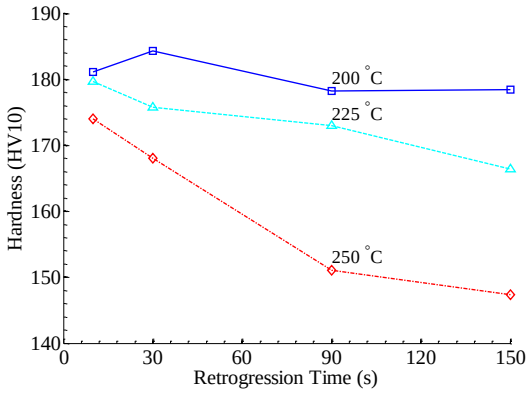

(e) ALCOA: retrogression treated and aged for 12 hours at 120 ºC.

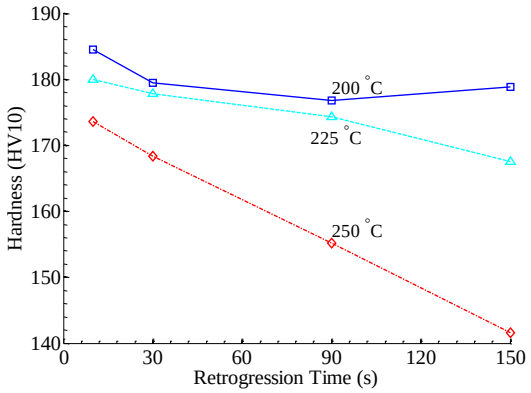

(f) AMAG: retrogression treated and aged for 12 hours at 120 ºC.

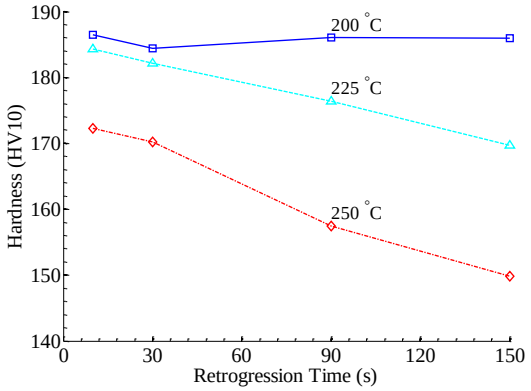

(g) ALCOA: retrogression treated and aged for 24 hours at 120 ºC.

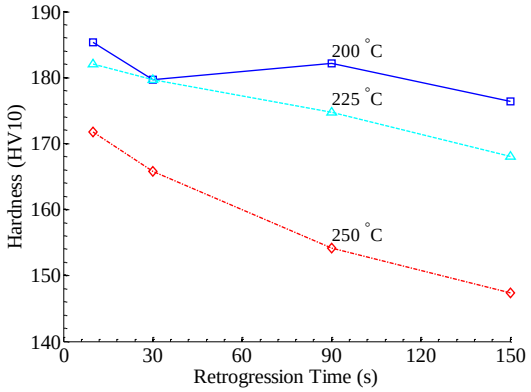

(h) AMAG: retrogression treated and aged for 24 hours at 120 ºC.

All specimens retrogressed at 200 ºC obtained nearly peak-aged hardness (HV = 180) following intermediate aging at 120 ºC for each intermediate aging time, with the exclusion of the ALCOA specimen retrogressed for 150 seconds and intermediate aged for 3 hours. For specimens retrogressed at 225 ºC, only those retrogressed for less than 90

seconds reached peak-aged hardness following intermediate aging. The intermediate aging treatment was less successful on specimens retrogressed at 250 ºC than for the lower retrogression temperatures. Peak-aged hardness was not recovered in any specimen retrogressed at 250 ºC following intermediate aging, regardless of retrogression time or intermediate aging time.

Overall, hardness decreased with increasing retrogression time and retrogression temperature for a constant intermediate aging time. Also, hardness increased with intermediate aging time for constant retrogression conditions. Intermediate aging for 24 hours typically produced the hardest material for each retrogression condition. The recovered hardness after intermediate aging of specimens retrogressed at 250 ºC fell significantly below the recovered hardness after intermediate aging of the material retrogressed at 200 ºC and 225 ºC.

3.1.4. Retrogression Treating, Intermediate Aging at 120 ºC, and Paint Baking

Specimens were subjected to the simulated PBC (180 ºC for 30 min.) following the completion of 120 ºC intermediate aging after retrogression treating. Hardness is plotted against retrogression time for these specimens in Figure 3.5.

ALCOA

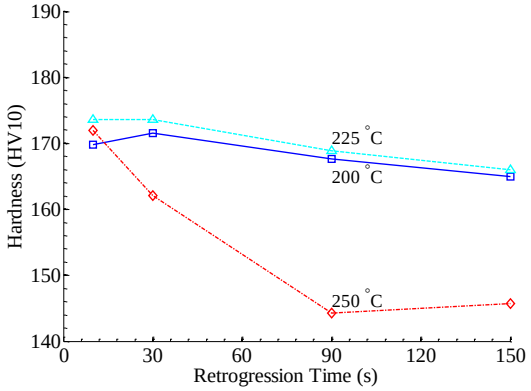

(a) ALCOA: retrogression treated, aged for 3 hours at 120 ºC, and paint baked.

AMAG

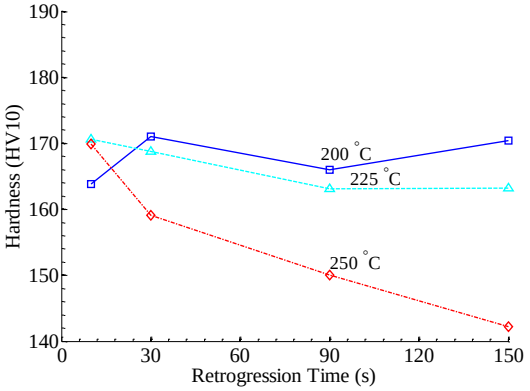

(b) AMAG: retrogression treated, aged for 3 hours at 120 ºC, and paint baked.

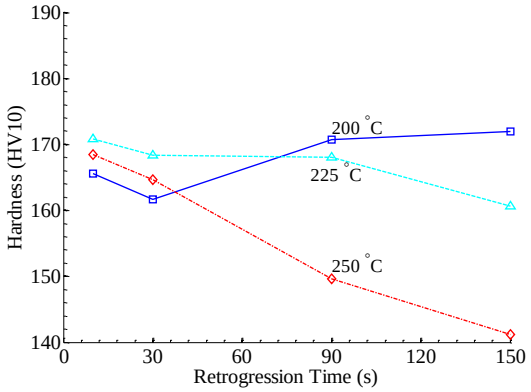

(c) ALCOA: retrogression treated, aged for 6 hours at 120 ºC, and paint baked.

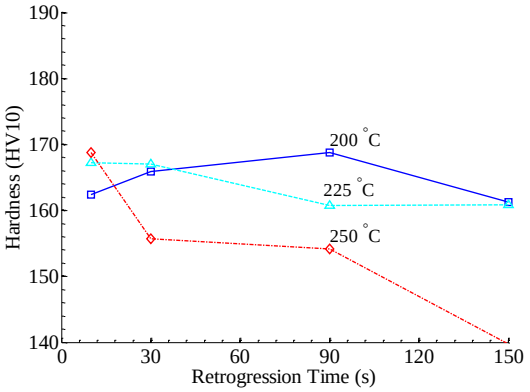

(d) AMAG: retrogression treated, aged for 6 hours at 120 ºC, and paint baked.

Figure 3.5: Hardness is shown as a function of retrogression time for specimens reaged at 120 ºC for various times and then paint baked following retrogression treatments at 200, 225, and 250 ºC. Aging time from top to bottom are (a,b) 3, (c,d) 6, (e,f) 12, and (g,h) 24 hours. Data from ALCOA (left) specimens and AMAG (right) specimens are shown side-by-side.

Figure 3.5 continued

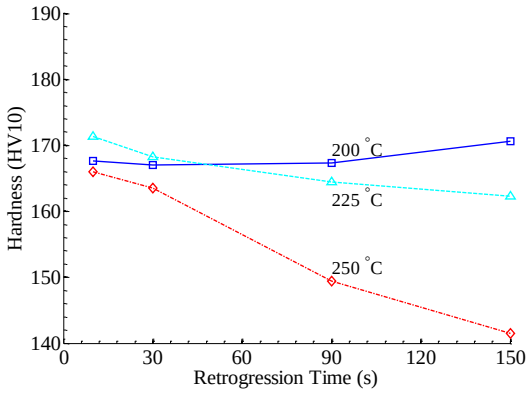

(e) ALCOA: retrogression treated, aged for 12 hours at 120 ºC, and paint baked.

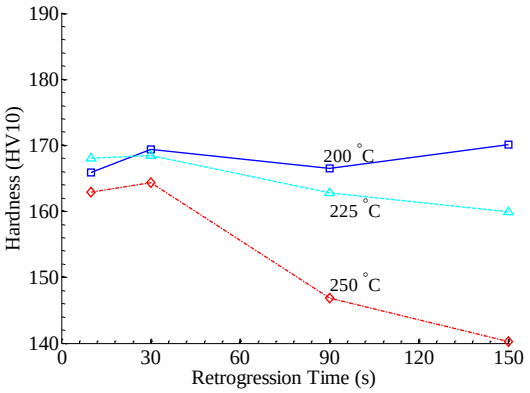

(f) AMAG: retrogression treated, aged for 12 hours at 120 ºC, and paint baked.

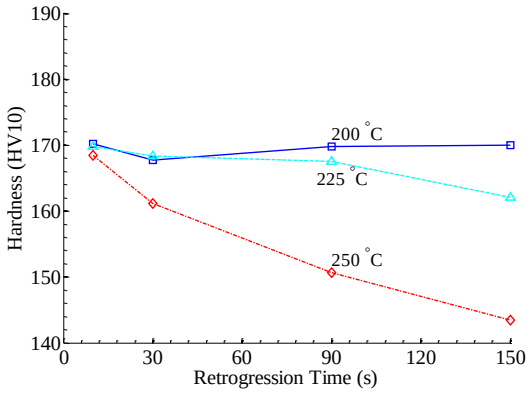

(g) ALCOA: retrogression treated, aged for 24 hours at 120 ºC, and paint baked.

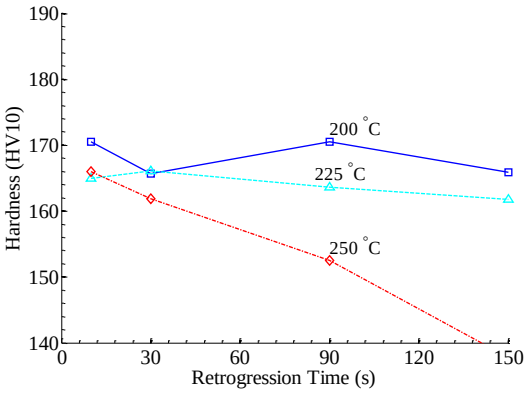

(h) AMAG: retrogression treated, aged for 24 hours at 120 ºC, and paint baked.

The PBC lowered hardness in many of the specimens retrogressed and intermediate aged at 120 ºC. Hardness was maintained around 170 HV for all of the specimens retrogressed at 200 and 225 ºC, regardless of intermediate aging time. This is comparable to retrogression treating, followed by the PBC alone, without any

intermediate aging. For the material retrogressed at 250 ºC, hardness decreased as retrogression time increased, regardless of the intermediate aging time.

In conclusion, the PBC eliminated any hardness gains obtained from intermediate aging at 120 ºC after retrogression treating. Intermediate aging at 120 ºC after retrogression treating and before the PBC did not significantly improve final hardness compared to reaging with the PBC alone.

3.1.5. Natural Aging Behavior

The long term stability of the microstructures produced by the various heat treatments investigated is of interest. The natural aging behavior of each heat treatment was monitored after completion of the PBC to investigate microstructural stability. Any increase in hardness during natural aging at room-temperature would improve part performance, while a reduction in hardness would detract from part performance during service. Natural aging of 7000-series alloys is a topic of previous investigation. Taleff et al. measured a significant improvement in hardness of several Al-Zn-Mg alloys after 60 weeks of natural aging [10]. In this study, each specimen was naturally aged for 30 weeks after a simulated PBC. Of all the heat treatments investigated, only specimens retrogressed at 350 ºC were affected by natural aging. The hardness data for specimens naturally aged after retrogression treating and paint baking are plotted against the

logarithm of natural aging time in Figure 3.6. The individual plots correspond to retrogression times of 10, 30, 90, and 150 seconds.

ALCOA

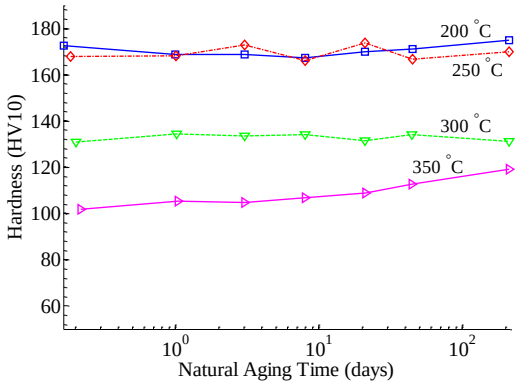

(a) ALCOA: retrogression treated for 10 seconds, paint baked, and naturally aged.

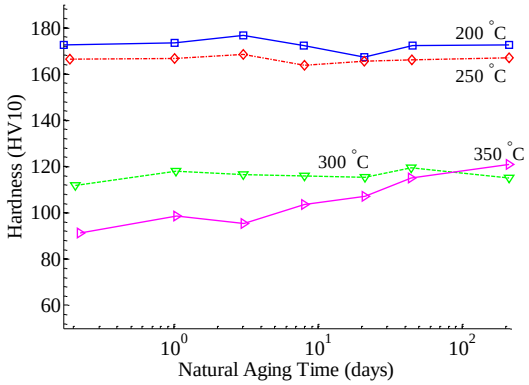

(c) ALCOA: retrogression treated for 30 seconds, paint baked, and naturally aged.

AMAG

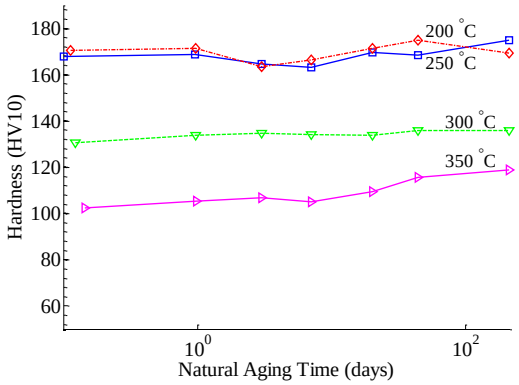

(b) AMAG: retrogression treated for 10 seconds, paint baked, and naturally aged.

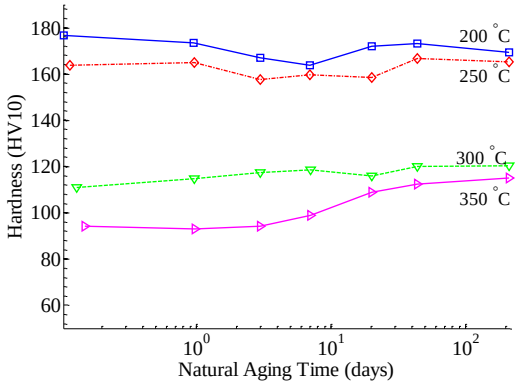

(d) AMAG: retrogression treated for 30 seconds, paint baked, and naturally aged.

Figure 3.6: Hardness is shown as a function of natural aging time for paint baked specimens following retrogression treatments at 200, 225, 250, 300, and 350 ºC. Retrogression times from top to bottom are (a,b) 10, (c,d) 30, (e,f) 90, and (g,h) 150 seconds. Data from ALCOA (left) specimens and AMAG (right) specimens are shown side-by-side.

Figure 3.6 continued

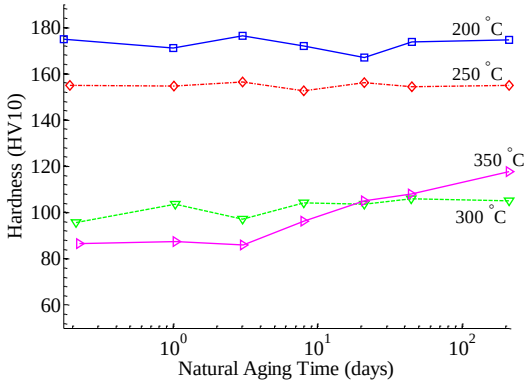

(e) ALCOA: retrogression treated for 90 seconds, paint baked, and naturally aged.

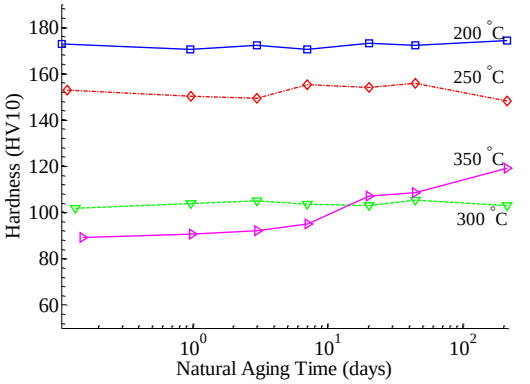

(f) AMAG: retrogression treated for 90 seconds, paint baked, and naturally aged.

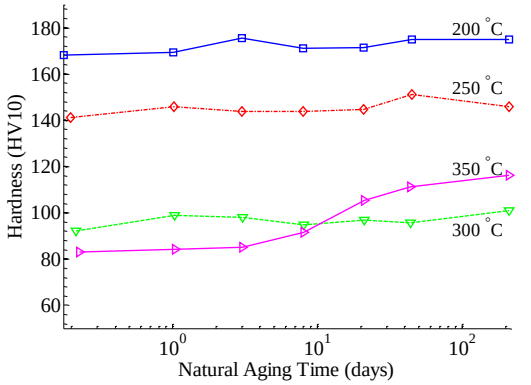

(g) ALCOA: retrogression treated for 150 seconds, paint baked, and naturally aged.

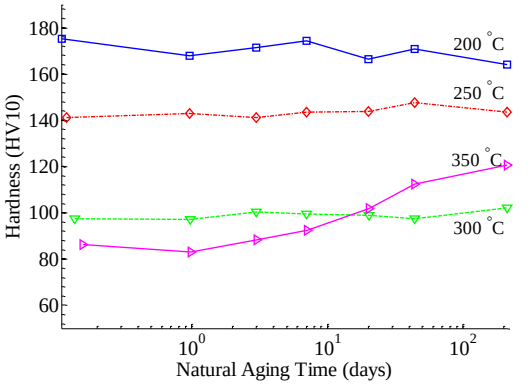

(h) AMAG: retrogression treated for 150 seconds, paint baked, and naturally aged.

Hardness substantially increased in all specimens retrogressed at 350 ºC after only 100 days of natural aging at room-temperature. The amount of hardness recovered increased with retrogression time and stabilized near 120 HV regardless of retrogression time. This result suggests that retrogressing at 350 ºC produced significant dissolution of precipitates, allowing new precipitates to form during natural aging from the solutes

previously put into solution. Though hardness was greatly improved by natural aging, it did not approach 180 HV, the peak-aged hardness of AA7075. None of the other retrogression temperatures were affected by natural aging. While natural aging did not improve part performance for lower temperature retrogression treatments, no softening was observed either. This is significant because it means near peak-aged hardness can be maintained after paint baking. Further natural aging is recommended to confirm these initial measurements for longer natural aging times.

3.2. Tensile Testing Data

Tensile testing was performed to measure the ductility of AA7075 at multiple temperatures. Tests were conducted at room-temperature to model cold forming, 200 and 225 ºC to model RRA forming, and 300 and 480 ºC to model solution forming.

3.2.1. Room-Temperature Tensile Tests

Room-temperature testing was performed on material in the T6 and solution-treated conditions. The rolling direction was oriented along the tensile direction. These tests provided baseline measures of ductility to compare with expected improvements in ductility at retrogression and solution-treating temperatures. True stress is plotted against true strain for tests conducted at room temperature in Figure 3.7. The solution treated

material was more ductile than the peak-aged material, as expected. Furthermore, the total elongations and yield strengths observed in these tests were consistent with data available from the literature [2]. A shear fracture was observed for each specimen upon failure.

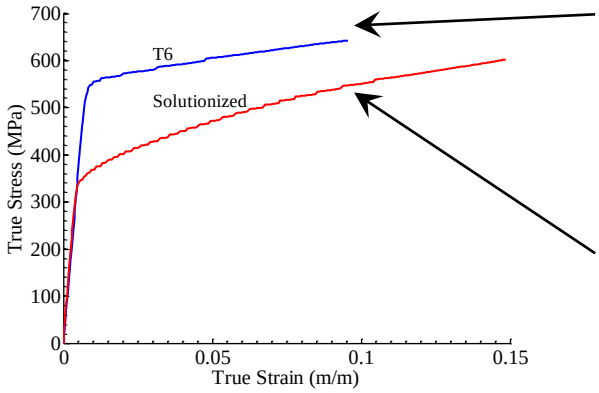

(a) ALCOA: Room-temperature true stress-strain data.

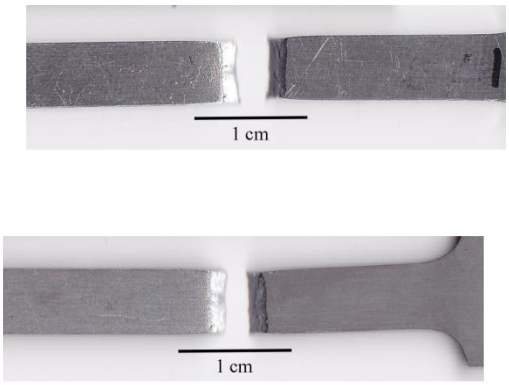

(b) ALCOA: Failed specimens.

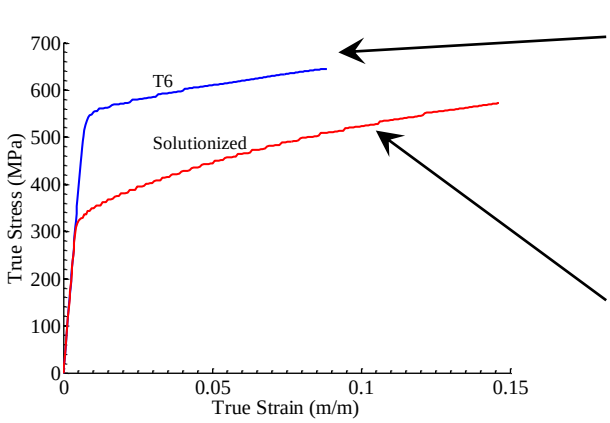

(c) AMAG: Room-temperature true stress-strain data.

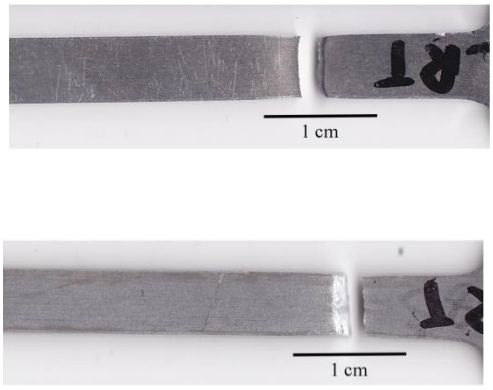

(d) AMAG: Failed specimens.

Figure 3.7: True stress is plotted against true strain for room-temperature tensile tests for (a) ALCOA and (c) AMAG material. Images of the failed tensile specimens (b,d) are shown for each tests.

3.2.2. Solution Forming Temperature Tensile Tests

Tensile tests were performed at solution treatment temperatures to measure ductility. Tests were performed at 300 and 480 ºC. The rolling direction was oriented along the tensile direction. Solution forming conditions were expected to greatly increase ductility, but these also require the most complicated aging treatments to reach peak-aged strength after forming. True stress is plotted against true strain for tensile tests conducted at 300 and 480 ºC in Figure 3.8. Specimens tested at 300 ºC failed earlier than expected. This was a result of rapid necking. Failure was ultimately caused by cavitation after necking. As a result of the necking, the true stress and true strain calculations do not hold for the final phase of each test. Necking limited total elongation of these specimens to 22 percent. Total elongation was much greater for tests at 480 ºC. Both materials elongated by over 70 percent and reached the elongation limit of the furnace and specimen size used for testing. A longer furnace might allow for even greater elongation at 480 ºC. Rapid necking was not observed in specimens tested at 480 ºC. Two specimens were tested at 480 ºC for each material. Each specimen failed by cavitation. Failures with and without necking were observed at 480 ºC in each material.

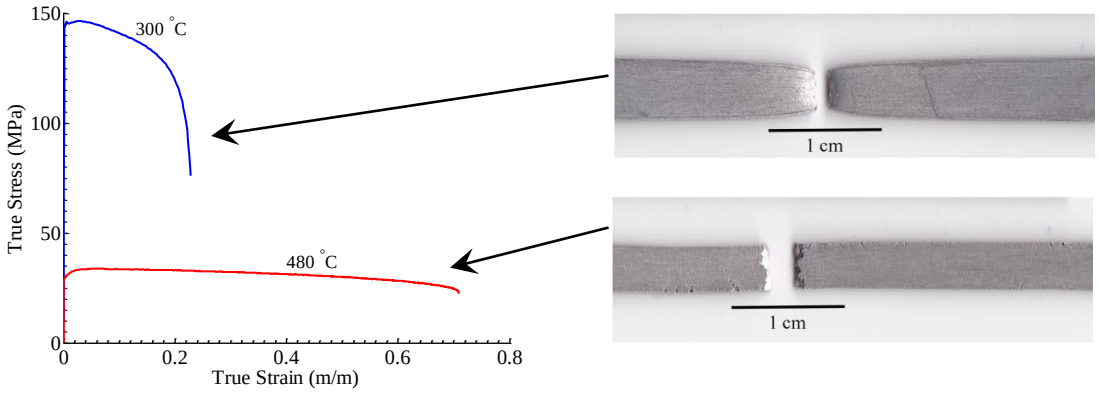

(a) ALCOA: Solution-temperature true stress-strain data.

(b) ALCOA: Failed specimens.

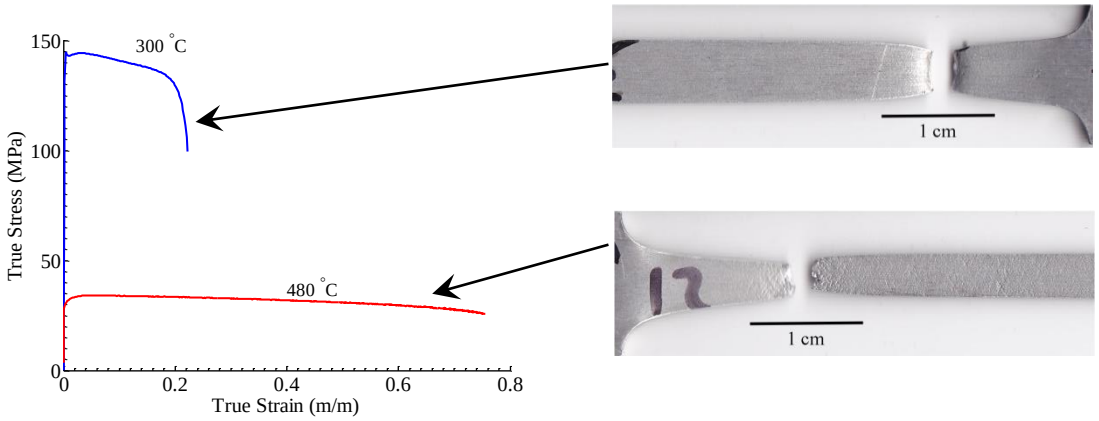

(c) AMAG: Solution-temperature true stress-strain data.

(d) AMAG: Failed specimens.

Figure 3.8: True stress is plotted against true strain for solution forming temperature tensile tests for (a) ALCOA and (c) AMAG material. Images of the failed tensile specimens (b,d) are shown for each tests.

3.2.3. RRA Forming Temperature Tensile Tests

RRA forming behavior was evaluated with tensile tests performed at 200 and 225 ºC with rapid electrical heating. These temperatures were chosen because they produced nearly peak-aged hardness after retrogression treating and reaging with the PBC. Specimens were tested in the T6 temper, and the rolling direction was oriented perpendicular to the tensile testing direction. Engineering stress is plotted against nominal (engineering) strain calculated from total cross-head displacement for these tests in Figure 3.9. True stress and true strain could not be calculated for rapid electrical heating tests because deformation was highly irregular along the gauge length. Engineering yield stresses at 200 and 225 ºC are consistent with data available from the literature [26-27]. Engineering yield stress was measured to be 320 MPa at 200 ºC and 290 MPa at 225 ºC. Because the testing temperature was only maintained for a small portion of the middlemost gauge region, strain was heavily localized to this region. As a result, total elongation measurements are not particularly meaningful. Local strain from the deformed region was subsequently determined from video analysis of each test and is reported in Table 3.2. Necking occurred before failure for each test conducted at RRA forming temperatures. Three to four tests were conducted at 200 and 225 ºC for each material. The tensile data and failure modes were consistent between the tests.

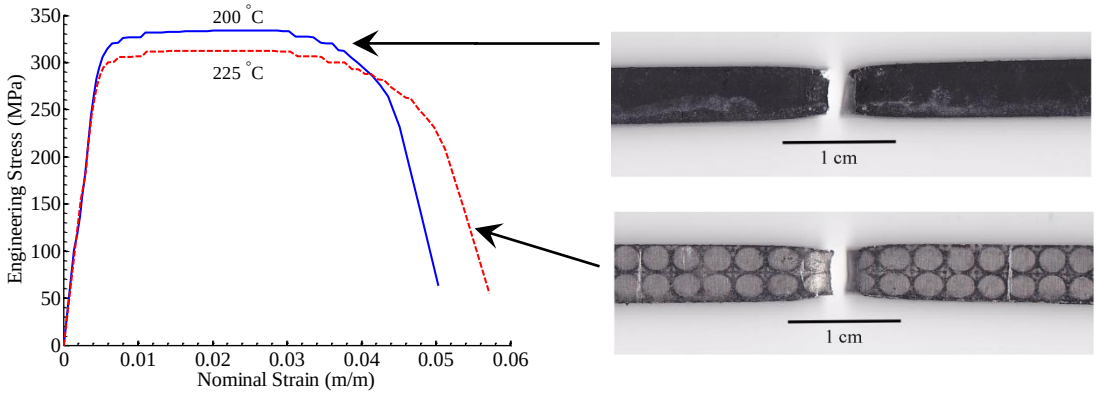

(a) ALCOA: Engineering stress is plotted against nominal strain for RRA-temperature tests.

(b) ALCOA: Failed specimens.

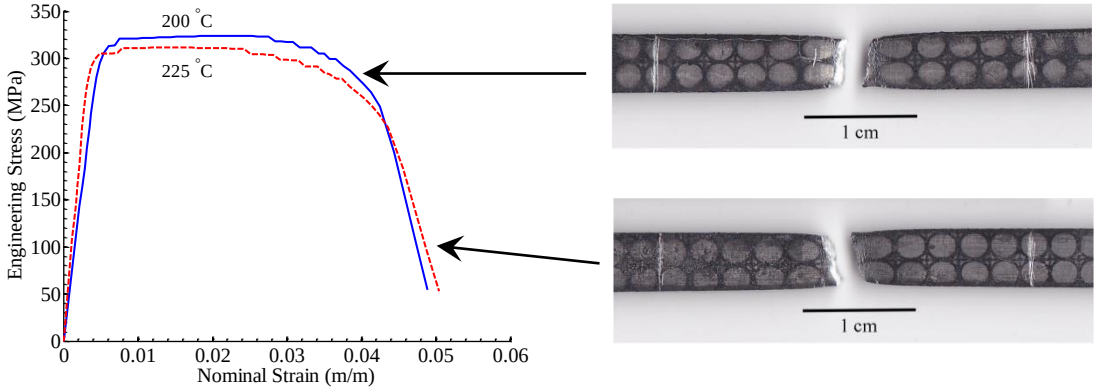

(c) AMAG: Engineering stress is plotted against nominal strain for RRA-temperature tests.

(d) AMAG: Failed specimens.

Figure 3.9: Engineering stress is plotted against nominal strain for rapid heating tensile tests for (a) ALCOA and (c) AMAG material. Images of the failed tensile specimens (b,d) are shown for each tests.

3.2.4. Ductility Measurements

Reduction in area was measured in addition to tensile elongation for each test. Percent elongation and percent reduction in area are presented in Table 3.2, along with the material condition before testing and the tensile failure mode. At room temperature slight necking was observed. The specimens tested at 300 ºC exhibited rapid necking. Necking at 300 ºC was more severe than at room-temperature. The ALCOA specimen tested at 480 ºC did not neck during testing. For this reason, reduction in area at 300 ºC was greater than at 480 ºC for the ALCOA material. In general, both percent reduction in area and percent elongation increased with temperature. Images of each specimen before and after testing are available in Appendix B.

Table 3.2: Material condition prior to testing, percent elongation, percent reduction in area, and failure mode are presented for the (a) ALCOA material and the (b) AMAG material for each tensile testing temperature investigated. Elongation measurements denoted with a * were determined from effective local elongations.

(a)

ALCOA					
Test Temperature ºC	Material Condition	% Elongation	% Reduction In Area	Failure Mode	Elongation Measurement
18	T6	10	20	Shear	Strain Gauge
18	Sol. treated	16	24	Shear	Strain Gauge
200	T6	52*	44	Neck, Shear	Local Video
225	T6	42*	48	Neck, Shear	Local Video
300	Sol. treated	23	73	Neck, Cavitation	Cross-head Dsip.
480	Sol. treated	71	64	Cavitation	Cross-head Dsip.

(b)

AMAG					
Test Temperature ºC	Material Condition	% Elongation	% Reduction In Area	Failure Mode	Elongation Measurement
18	T6	9.2	30	Shear	Strain Gauge
18	Sol. treated	16	31	Shear	Strain Gauge
200	T6	37*	42	Neck, Shear	Local Video
225	T6	47*	47	Neck, Shear	Local Video
300	Sol. treated	22	75	Neck, Cavitation	Cross-head Dsip.
480	Sol. treated	76	83	Neck, Cavitation	Cross-head Dsip.

Chapter 4: Discussion

4.1. Retrogression-Treated Material

Retrogression temperatures above 300 ºC are not suitable for RRA forming. Typical retrogression behavior was not observed for these conditions, and hardness was reduced too severely for practical RRA forming. However, retrogression between 200 and 250 ºC was suitable for RRA forming. Typical retrogression behavior was observed, suggesting hardness reductions during retrogression could be recovered through an appropriate reaging treatment.

Two 3-D contour plots of hardness after retrogression treating are shown as functions of retrogression time and retrogression temperature in Figures 4.1 and 4.2 for several retrogression conditions. Each hardness contour mesh was constructed by an interpolation of the data points obtained in this study, shown as black dots. Reduction in hardness during retrogression treatments depends more on retrogression temperature than retrogression time.

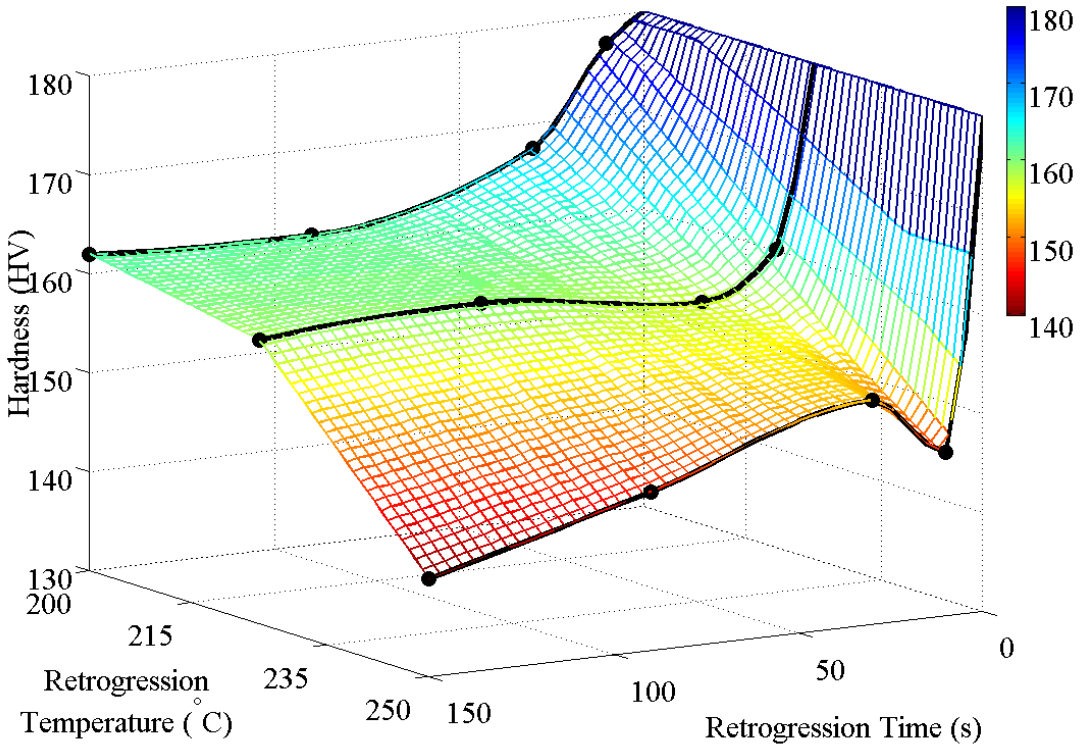

Figure 4.1: Contour plot of hardness for retrogressed ALCOA specimens as a function of retrogression time and retrogression temperature.

AMAG

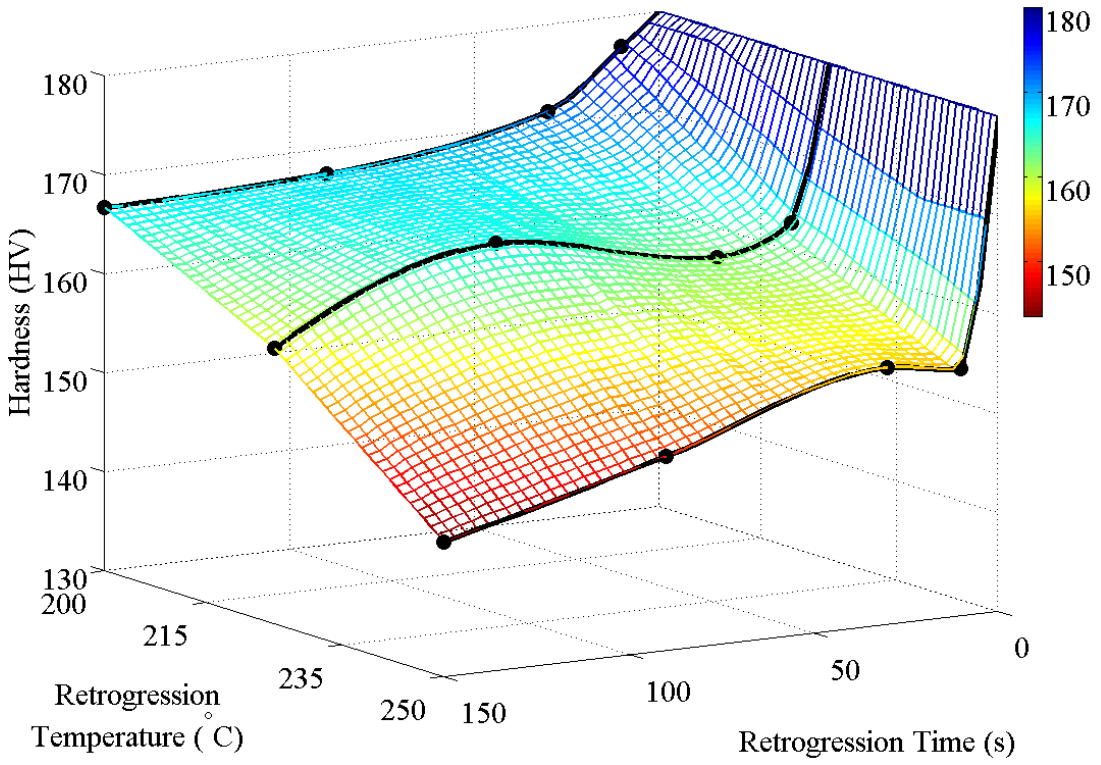

Figure 4.2: Contour plot of hardness for retrogressed AMAG specimens as a function of retrogression time and retrogression temperature.

Hardness loss depends on microstructural development during retrogression treating. The microstructural development for an individual retrogression temperature as retrogression time increases is described in the following discussion. According to Park and Ardell, during typical retrogression treatments, the initial reduction in hardness is primarily caused by the dissolution of η' precipitates. During these early retrogression

stages leading to the local minimum hardness, fine η' precipitates formed during peak-aging prior to retrogression either fully or partially dissolve, and larger η' precipitates transform to η-phase precipitates. This reduces the total quantity of precipitates in the microstructure, which causes the material to soften. Meanwhile, η precipitates already present from peak aging prior to retrogression treating tend to coarsen [13-20]. The subsequent increase in hardness that follows the local minimum hardness is attributed to the precipitation of new η-type precipitates [14-16]. This increases the total number of precipitates in the microstructure, which causes hardness to recover. Further retrogression treating, beyond the slight increase in hardness following the local hardness minimum, promotes coarsening of the η precipitates already present in the microstructure. As larger η precipitates grow and consume smaller precipitates, the total number of precipitates decreases and hardness is reduced [13-24].

Data available from the literature demonstrated that hardness after reaging is maximized when reaging is performed on material retrogressed to the local minimum hardness [8, 13-24]. According to literature, this is because at the local minimum hardness, many η' precipitates only partially dissolve to an extent that permits hardness to be recovered by an appropriate reaging treatment. This is effective because the larger η precipitates have not yet undergone coarsening, and new η precipitates have not yet formed.

Yield strength is important to the automobile industry. High hardness, which indicates high yield strength, allows automobile manufacturers to reduce component

weight and improve fuel efficiency. In addition, high hardness and yield strength can improve the crash worthiness and dent resistance of auto-body panels. To achieve the best hardness from reaging, it is necessary to determine the time associated with retrogressing to the local minimum hardness. These values are presented in Table 4.1 for specimens retrogressed at temperatures of 250 ºC and less.

Table 4.1: Local minimum hardness data and corresponding retrogression conditions for the (a) ALCOA and (b) AMAG materials.

(a)

ALCOA		
Retrogression Temperature (ºC)	Local Minimum Retrogression Time (s)	Local Minimum Hardness (HV)
200	90 ± 20	161
225	30 ±10	157
250	10 ± 5	147

(b)

AMAG		
Retrogression Temperature (ºC)	Local Minimum Retrogression Time (s)	Local Minimum Hardness (HV)
200	150 ± 20	167
225	30 ± 10	162
250	10 ± 5	155

The local minimum retrogression time is useful in defining the processing window for RRA forming. Retrogressing at low temperatures allows material to stay at the retrogression temperature longer and still recover most hardness by an appropriate reaging afterward. This increases the time available for RRA heating and forming operations. Low-temperature operations are also easier and cheaper to implement than high-temperature operations. As shown in Table 4.1, retrogression treating at 200 and 225 ºC permits heating and forming operations to last for 120 to 30 seconds, respectively. Whereas, retrogressing at 250 ºC is limited to a window of 10 seconds. Conducting heating and forming operations within 10 seconds is most likely not feasible, which limits the potential RRA forming temperatures to below 250 ºC.

Using these data, a processing window for RRA forming is recommended at temperatures from 200 to 225 ºC and times from 120 to 30 seconds. Retrogression temperatures below 200 ºC may also be potentially useful for RRA forming. They were not investigated in this study because higher temperatures are of most interest for potential high ductilities.

Hardness is plotted against temperature-normalized retrogression time in Figure 4.3. The hardness data produce a useful master retrogression curve using the temperature-normalized retrogression time, t^*, given in Equation 4.1, where t is retrogression time (s), Q is the activation energy of zinc diffusion in aluminum (kJ/mol), R is the universal gas constant (J/mol-K), and T is retrogression temperature (K). Q was taken as 95 kJ/mol as discussed in section 3.1.1. Data for hardness after retrogression treating that were

produced by Park and Kanno et al. also normalized well in Figure 4.3. The local minimum hardness was observed, on average, at a temperature-normalized time of t^*_{min} = 3.5 x 10^{-9} ± 8 x 10^{-10} seconds. Uncertainty in t^*_{min} was determined from the standard deviation of the data. It is a result of the uncertainty in determining the time associated with retrogressing to the local minimum hardness. Retrogression behavior appears to be a function of the distance zinc diffuses in aluminum during retrogression. This is likely why the local minimum hardness is well predicted by the retrogression temperature and retrogression time, using t^*_{min}.

$$t^* = \left(t \cdot e^{-Q/RT} \right) \qquad (4.1)$$

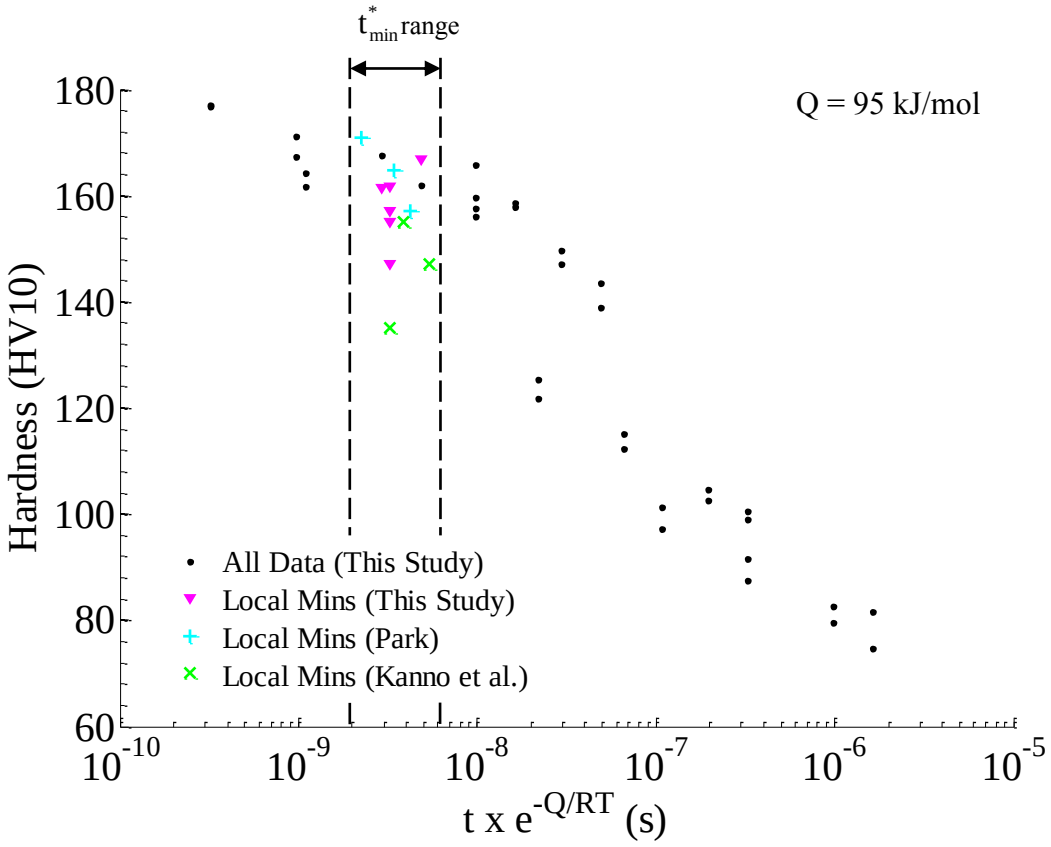

Figure 4.3: Hardness is plotted as a function of temperature-normalized retrogression time.

4.2. Retrogression-treated and Paint-baked Material

The paint-bake cycle (PBC) was used to reage retrogression treated specimens. Hardness is plotted against retrogression time in Figure 4.4 for specimens subjected to paint baking after retrogression treating and for specimens subjected to retrogression treating only. Hardness was generally higher after the PBC. Only the AMAG specimen retrogression treated at 225 ºC produced a negligible PBC response. Peak-aged hardness was never fully recovered by reaging with the PBC. Though, for certain retrogression

conditions shown in Figure 4.4, hardness was recovered to within 5 percent of the peak-aged condition (HV = 180). This is most likely a result of over-aging occurring during the PBC. The microstructure of peak-aged AA7075 consists of a fine even distribution of small η' precipitates throughout the aluminum matrix. Over-aging treatments reduce the number of η' precipitates compared to the peak-aged condition, which reduces hardness [2, 11-12]. Over-aging treatments designated by the T7 temper are accomplished by aging for 6 to 8 hours at 107 ºC and then aging for 24 to 30 hours at 163 ºC [2].

4.2.1. Microstructural Development during Paint Baking after Retrogressing to t^*_{min}

The reaging behavior of material retrogressed to the local minimum hardness is of particular interest. It is suspected that over-aging occurs during paint-baking in material previously retrogressed to the local minimum hardness. This is because current PBC temperatures (180 ºC) are greater than the recommended over-aging treatment temperature (163 ºC) and RRA reaging treatment temperature (121 ºC) [2].

Reaging at the recommended temperature of 121 ºC for 24 hours after retrogression treating to t^*_{min} produces numerous fine η' precipitates. New η' precipitates replace those dissolved during retrogression and η' precipitates that were partially dissolved during retrogression are regrown. Compared to the recommended reaging, it is suspected that reaging with the PBC precipitates fewer η' precipitates. This is most likely a result of three effects. During the PBC more η precipitates form, existing η´ precipitates

that survived retrogression evolve into larger η precipitates, and existing η precipitates tend to coarsen. As a result, the microstructure produced by retrogression followed by the PBC contains fewer fine η' precipitates compared to the peak-aged condition. Because of this, hardness is lower in the specimens paint-baked after retrogression treating than in the peak-aged condition. However, the hardness of these specimens is greater than the hardness of over-aged AA7075, which is typically 155 HV [2]. This suggests that over-aging during the PBC is not severe. Typical PBC times (30 mins.) are much shorter than over-aging times used for the T7 temper. Because of this, multiple specimens retrogressed to t^*_{min} produced nearly peak-aged hardness after the PBC. This suggests that some precipitation, regrowth, and stabilization of small η'-phases occurs during the PBC, but less than would during recommended reaging at 121 ºC. This assessment is based upon the data produced by Park and Ardell [12, 16].

Hardness was always improved by reaging with the PBC after retrogression to t^*_{min}. It is believed that hardness is recovered during the PBC because η' precipitates which were partially dissolved during the retrogression treatment are regrown. However, hardness is not recovered to the peak-aged condition because aging at 180 ºC also causes larger η precipitates to form and existing η precipitates to coarsen. This is an unavoidable consequence of aging at high temperatures. As a result, the microstructure after retrogressing to the local minimum hardness and reaging by the PBC contains fewer fine η' precipitates than when reaging is performed at 121 ºC.

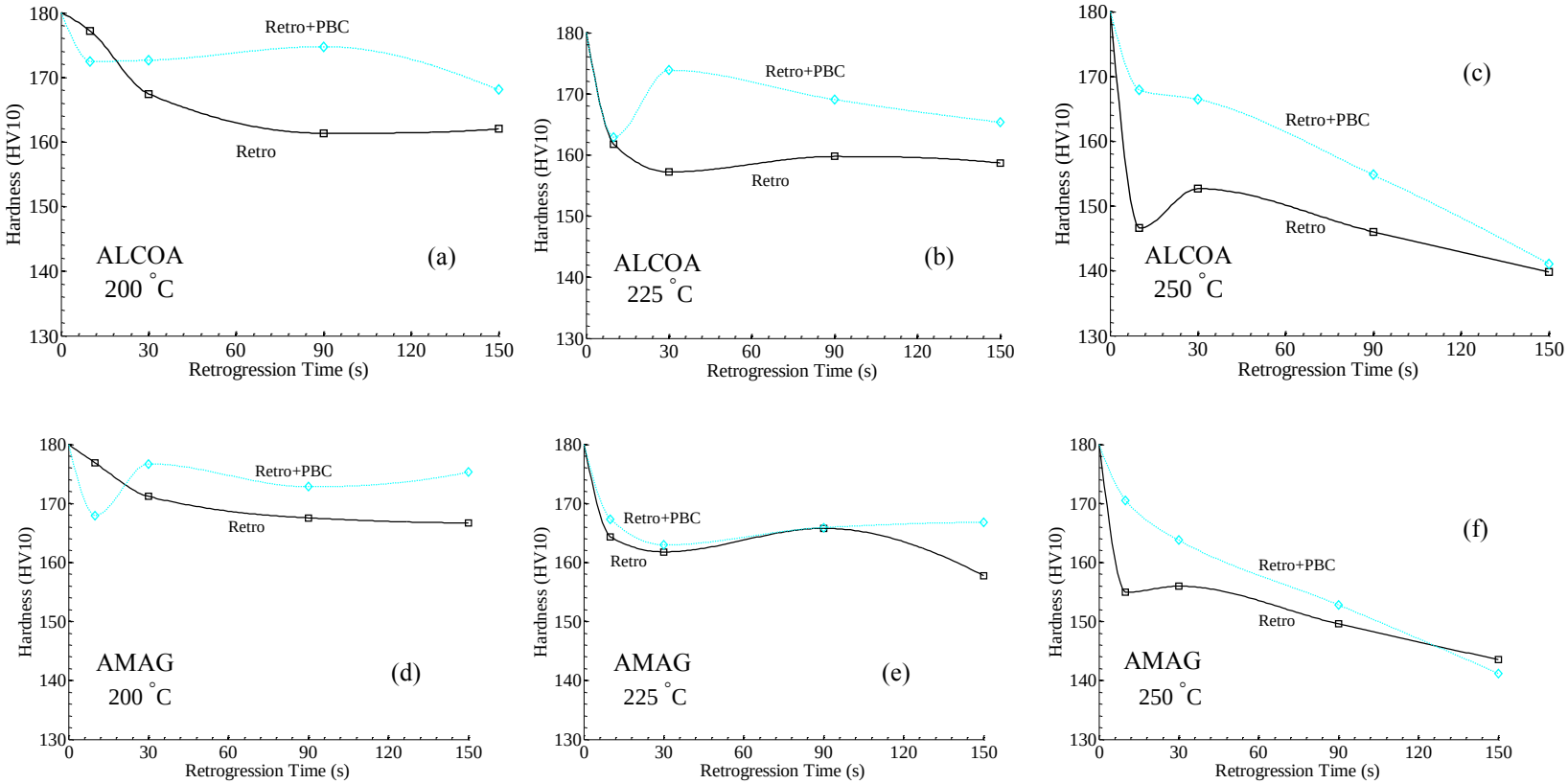

Figure 4.4: Hardness data are plotted against retrogression time for specimens paint baked after retrogression treating and specimens retrogression treated only. Retrogression temperatures of 200, 225, and 250 ºC are shown individually for (a,b,c) ALCOA and (d,e,f) AMAG materials.

As expected, specimens are hardest after reaging with the PBC when previously retrogressed to the local minimum hardness. The hardness of specimens paint-baked after retrogression treating to t^*_{min} at 250 ºC and below are presented in Table 4.2.

Table 4.2: Hardness data for specimens paint baked after retrogression treating to the local minimum hardness and corresponding retrogression conditions for the (a) ALCOA and (b) AMAG materials.

(a)

ALCOA				
Retrogression Temperature (ºC)	Retrogression Time (s)	Hardness after Retro Only (HV)	Hardness after PBC (HV)	Change in Hardness from PBC (HV)
200	90 ± 20	161	175	14
225	30 ±10	157	174	17
250	10 ± 5	147	168	21

(b)

AMAG				
Retrogression Temperature (ºC)	Retrogression Time (s)	Hardness after Retro Only (HV)	Hardness after PBC (HV)	Change in Hardness from PBC (HV)
200	150 ± 20	167	175	8
225	30 ±10	162	163	1
250	10 ± 5	155	171	16

Retrogression treating to t^*_{min} at 200 and 225 ºC produced the hardest material after paint baking. This is good for RRA forming because the retrogression treatments that allow for the longest processing windows also yield the hardest material after paint baking. While the amount of hardness recovered by the PBC increased with retrogression temperature, the final hardness typically decreased as retrogression temperature increased. The AMAG specimen retrogressed at 225 ºC did not respond to the PBC. The reason for this is unclear because AMAG specimens retrogressed at 200 and 250 ºC each produced a positive PBC response.

The ALCOA material was more sensitive to paint baking after retrogression to t^*_{min} than was the AMAG material. The ALCOA material produced a greater response to the PBC than the AMAG material for each retrogression temperature. This is most likely because hardness was reduced more in the ALCOA material than the AMAG material during retrogression treatments, as shown in Figures 4.1 and 4.2. Though, the final hardness after paint-baking was comparable between the two materials.

In summary, the PBC was not capable of reaging specimens back to the peak-aged condition after retrogression treating to the local hardness minimum. It is unlikely that peak-aged hardness can be obtained by reaging at the PBC temperatures currently used in the auto industry. However, the PBC can improve hardness to within 5 percent of the peak-aged hardness when retrogression treating is conducted at 225 ºC or below. In addition, hardness recovered after retrogressing increased with retrogression temperature when specimens were retrogressed to the local minimum hardness. However, hardness

after the PBC decreased as retrogression temperature increased. According to these results, the best RRA forming temperature for achieving the highest final hardness is 200 ºC when reaging is by the PBC alone.

4.3. Material Retrogression Treated, Intermediate Aged at 120 ºC, and Paint Baked

Intermediate aging was performed before the PBC and after retrogression treating to determine if hardness after the PBC could be improved. Specimens were subjected to intermediate aging at 120 ºC for 24 hours after retrogression treating and prior to paint baking. Hardness data for these specimens and specimens reaged with the PBC only after retrogression treating are plotted against retrogression time in Figure 4.5.

There was no substantial benefit from intermediate aging before the PBC compared to reaging with the PBC alone. Like reaging with the PBC alone, specimens subjected to intermediate aging were most likely over-aged. It is suspected that the PBC coarsens existing η precipitates and evolves existing η' precipitates into larger η precipitates. This decreases the total number of precipitates in the microstructure and reduces hardness. In conclusion, intermediate aging at 120 ºC before the PBC was not beneficial compared to reaging with the PBC alone.

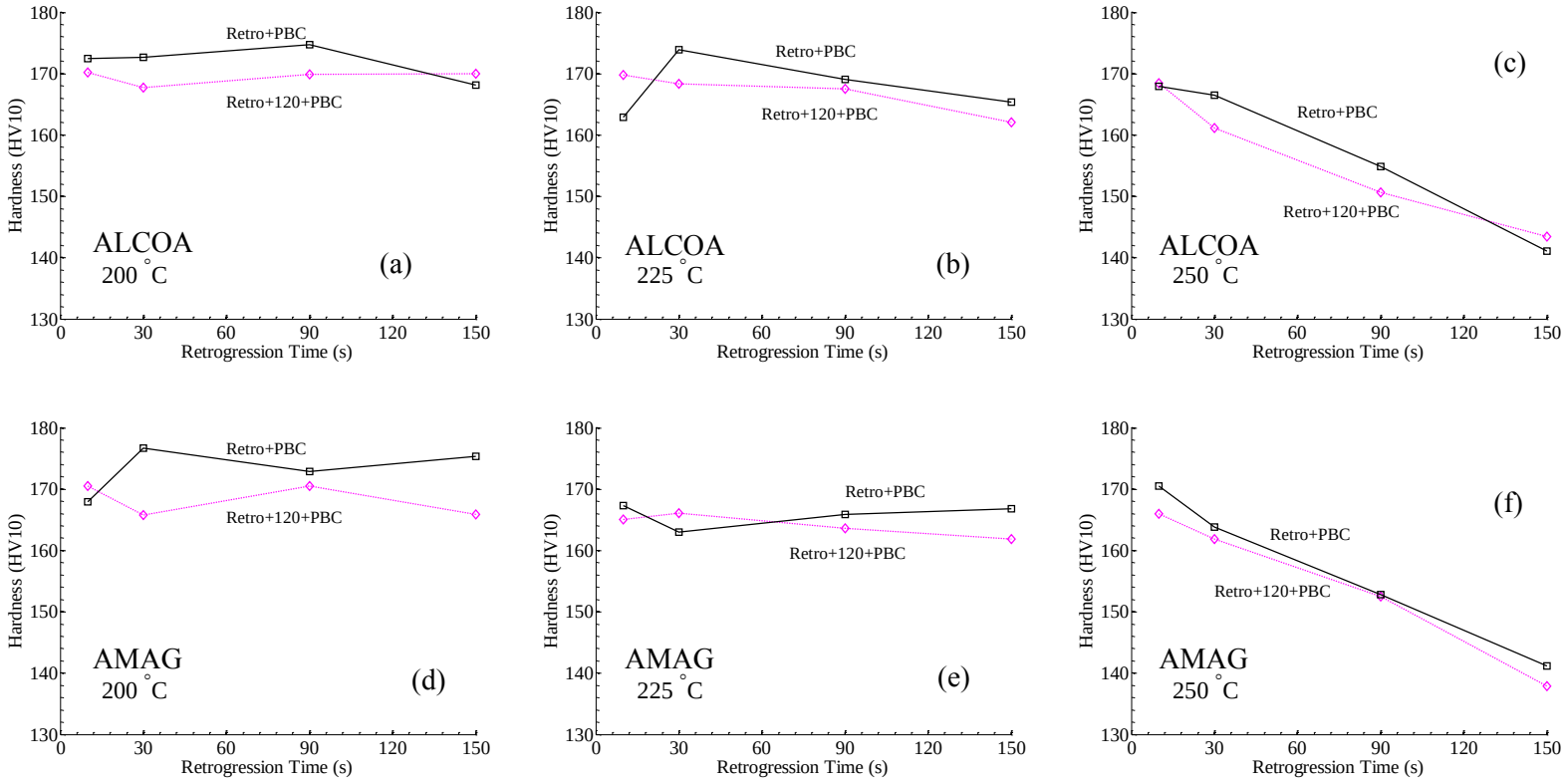

Figure 4.5: Hardness data are plotted against retrogression time for retrogression treated specimens subsequently intermediate aged at 120 ºC for 24 hours and paint baked and specimens reaged with the PBC alone after retrogression treating. Retrogression temperatures of 200, 225, and 250 ºC are shown individually for (a,b,c) ALCOA and (d,e,f) AMAG materials.

4.4. RRA Forming Discussion

RRA forming was introduced as a way to improve upon the room-temperature formability of AA7075-T6. RRA forming behavior was evaluated by tensile testing at 200 and 225 ºC. These temperatures were chosen because retrogressing to t^*_{min} at 200 and 225 ºC produced the hardest material after the PBC. Tensile tests conducted at these temperatures with rapid direct resistance heating indicate that formability is improved at elevated temperatures. Effective local elongation data are plotted against test temperature for uniaxial tensile tests in Figure 4.6.

Forming AA7075-T6 at RRA temperatures greatly improved ductility compared to forming at room temperature. Effective local elongations produced at RRA temperatures were more than double those produced at room temperature. Percent elongations of 40 to 50 percent were measured. These are greater than the elongation measurements available from the literature, also presented in Figure 4.6. This is most likely a result of effective local elongation being monitored through video during this study, as opposed to with a contact extensometer or by monitoring crosshead displacement. The video analysis permitted effective local elongation measurements of local deformation after the onset of necking to be obtained. Data from the available literature were reported as total elongation, which does not account for local elongation after necking. Total elongation was not determined during this study for RRA forming tests because of the large temperature variation along the gauge length caused by rapid electrical heating. Reduction in area was also much greater at RRA forming temperatures

than at room temperature. Reduction in area is presented as a function of test temperature in Figure 4.7. In general, reduction in area and effective local elongation measurements at RRA forming temperatures were in good agreement. Reduction in area measurements were not reported in the available literature. Thus, no comparisons with literature data are possible.

Specimens tested at 200 and 225 ºC failed by shear fracture after considerable necking. Necking at retrogression temperatures was much more severe than at room temperature. This may have been influenced by the steep temperature variation along the specimen gauge length. Regardless, ductility was still much greater than at room temperature.

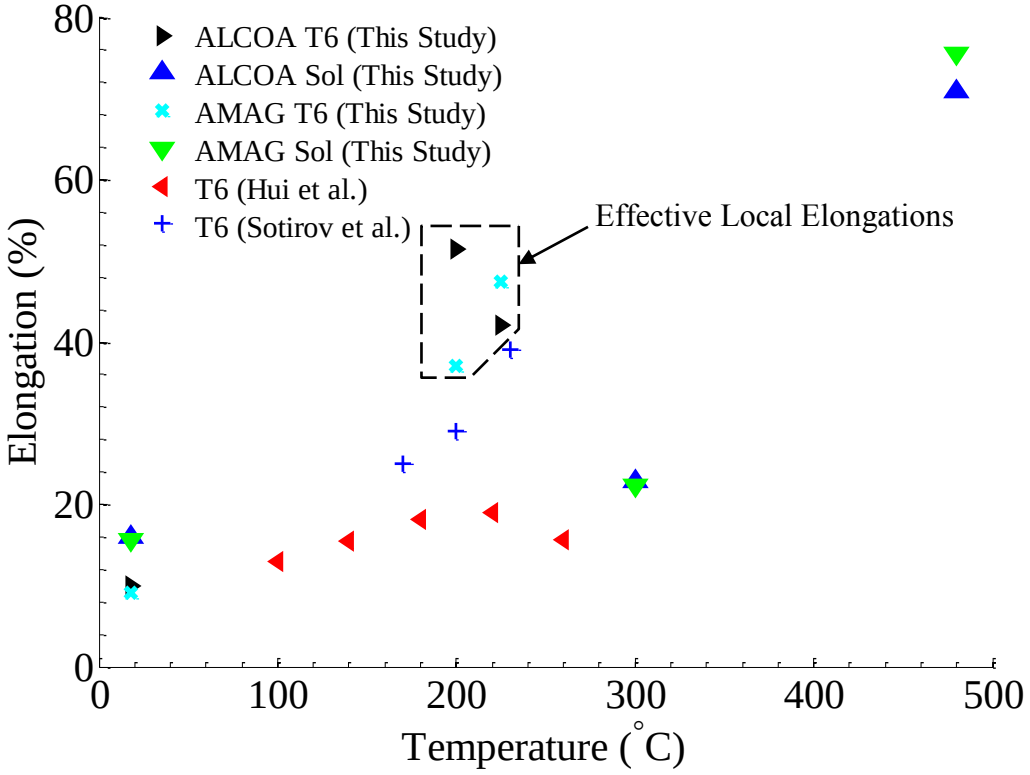

Figure 4.6: Elongation data are plotted against test temperature for uniaxial tensile tests of AA7075 from this study, and elongation is plotted against test temperature for data reported in the available literature [26-27]. The boxed data are effective local elongations determined from video analysis. Strain rates range from 0.001 to 0.078 s^{-1}.

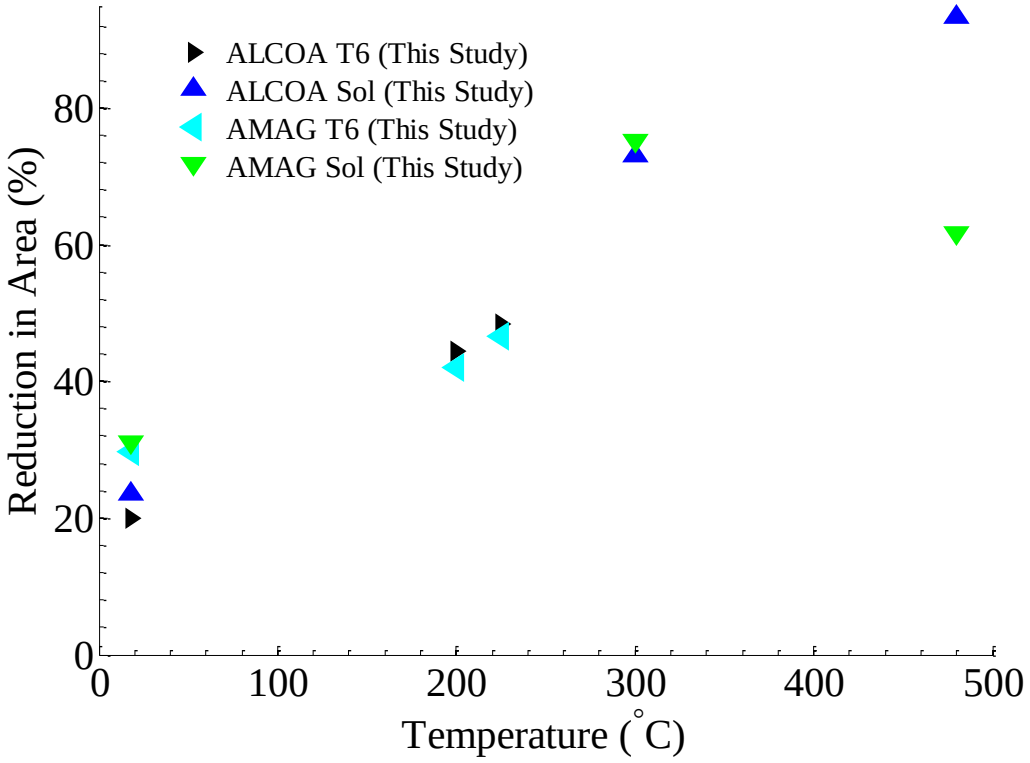

Figure 4.7: Reduction in area data are plotted against test temperature for uniaxial tensile tests of AA7075 from this study. Tests were all conducted at an initial strain rate of 0.05 s^{-1}.

RRA forming greatly improves the ductility of AA7075-T6 over room-temperature forming techniques, such as cold stamping. Both effective local elongation and reduction in area measurements confirm that forming at retrogression treatment temperatures can double ductility compared to forming at room-temperature. Elongation measurements for several materials and various forming techniques are presented in Table 4.3. Ductilities of AA7075-T6 at RRA forming temperatures are comparable, if not greater than, the room-temperature ductility of many commonly used HSLA steels.

Though, ductilities from RRA forming of AA7075-T6 are less than the ductility from hot stamping of AA5083. Table 4.3 suggests that RRA forming may allow auto manufacturers to replace many room-temperature formed steel components with RRA-formed AA7075 components without reducing part complexity.

Press-quench forming (PQF) is a possible forming operation that could be used with RRA forming. AA7075-T6 would be rapidly heated to retrogression temperatures and then stamped in either cold or warm dies to quench the material back to room-temperature during forming. The rapid quenching during forming preserves the retrogressed microstructure, allowing the mandatory PBC to improve final part hardness. Because cooling of the sheet by the dies requires close contact between the two, most cooling occurs after the sheet has been formed in the dies. Thus, the sheet is still hot when formed and retains the high ductility available at elevated temperature while it forms.

In addition to improving ductility, yield strength was reduced in tensile tests conducted at RRA forming temperatures. At room temperature, AA7075-T6 exhibits a tensile yield strength of 530 MPa. This is reduced to 300 to 320 MPa at RRA forming temperatures. Because of this, forming AA7075-T6 sheet with RRA forming techniques would require less force than current cold stamping operations used in the auto industry.

Table 4.3: Elongation data are presented for several materials and forming techniques used in the automotive industry. Elongations denoted with a superscript * are effective local measurements determined from video analysis.

Material Condition Before Forming	Forming Technique	Forming Temperature (°C)	Elongation (%)	Strain Rate
Super-plastic grade AA5083	SPF	500	≥300 [7]	10^{-3}
AA5083	Hot Stamping	340	~120 [42]	10^{-1}
AA7075-Sol.	Solution Forming	480	≥70	20^{-1}
AA7075-T6	RRA Forming	200 to 225	~40*	20^{-1}
AA6061-T6	RRA Forming	205	28 [2]	20^{-1}
HSLA 260	Cold Stamping	18	≥28 [43]	

4.5. Solution Forming Discussion

Solution forming is another new forming concept designed to improve upon the room-temperature formability of AA7075-T6. Tensile testing was conducted at 300 and 480 ºC to determine if formability could be improved at temperatures greater than RRA forming temperatures. Indeed, ductility at solution forming temperatures was much greater than at room-temperature and at RRA forming temperatures, as shown in Figures 4.6 and 4.7. Elongations during tensile tests at 480 ºC were twice those of tensile tests conducted at 200 and 225 ºC. Elongation at 300 ºC was limited by the onset of rapid

necking, as was also the case at RRA forming temperatures. Reduction in area, however, was greater at 300 ºC than at RRA forming temperatures. In summary, the ductility of AA7075 is greatest at solution-forming temperatures.

Failure from cavitation occurred with or without necking for all specimens tested at solution-forming temperatures. This suggests ductility is improved at solution-forming temperatures compared to RRA forming temperatures. Tensile yield strengths at solution-forming temperatures were 143 and 32 MPa for 300 and 480 ºC, respectively. This is very low for AA7075. Because of this, forming stress will be substantially lower for solution-forming operations compared to cold stamping or RRA forming operations of AA7075.

Solution forming of AA7075 produces ductilities greater than those of HSLA steel during cold stamping and AA7075 during RRA forming. The formability of AA7075 during solution forming is still less than the formability of AA5083 during superplastic forming and hot stamping. Furthermore, solution forming of AA7075 requires a longer and more exhaustive aging treatment to reach the peak-aged condition after forming compared to RRA forming. Forming at higher temperatures is also more expensive to implement and operate.

Chapter 5: Conclusions and Future Work

5.1. Conclusions

5.1.1. Aging Behavior

The retrogression and reaging (RRA) behavior of AA7075-T6 was studied. Retrogression treating below 250 ºC produced typical retrogression behavior. This allowed hardness to be recovered during reaging. In particular, retrogression treating to the local minimum hardness was shown to be the optimal retrogression treatment because it produced the hardest material after reaging. This is consistent with the available literature [8, 13-24]. After retrogression treating, reaging was performed with a simulated paint-bake cycle (PBC) conducted at 180 ºC for 30 minutes. Reaging with the PBC after retrogression treating to the local minimum hardness did not return material to the peak-aged condition. However, nearly peak-aged hardness was produced by the PBC after retrogressing to the local minimum hardness for retrogression temperatures below 250 ºC. It is believed that peak-aged hardness was not produced by the PBC because of slight over-aging compared to the standard reaging process conducted at 121 ºC. Adding intermediate aging at 120 ºC prior to the PBC and after retrogression did not improve hardness compared to reaging with the PBC alone.

5.1.2. Forming Behavior

Two high-temperature forming concepts for AA7075 were studied. These were the RRA forming and solution forming concepts. Both forming concepts were evaluated with uniaxial tension tests. RRA forming was evaluated at 200 and 225 ºC, and solution forming was evaluated at 300 and 480 ºC. The ductility of AA7075 at each forming temperature improved upon the room-temperature ductility of AA7075-T6. Ductilities of AA7075-T6 at RRA temperatures were double those produced by room-temperature forming. While ductilities during solution forming were four times greater than the ductility of AA7075-T6 at room-temperature.

RRA forming of AA7075-T6 produces ductilities comparable to the ductilites of many HSLA steels formed at room-temperature. In addition, nearly peak-aged hardness can be produced by the mandatory PBC after forming. This suggests that RRA-formed AA7075-T6 components could replace room-temperature formed HSLA steel components used in the auto industry. This would reduce overall vehicle mass and improve gas mileage. Press-quench forming (PQF) could be used with RRA forming of AA7075-T6. Material would be rapidly heated to the retrogression temperature and stamped in either warm or cold dies. During forming, the material would be quenched to room-temperature through contact with the dies. After forming, the RRA-formed AA7075 component would be reaged to near peak-aged hardness by the PBC. The PQF technique preserves the retrogressed microstructure after forming, allowing hardness to be recovered during the PBC.

Solution forming of AA7075 improves upon the ductility of AA7075 during RRA forming, but it requires more heat treating after forming to reach nearly peak-aged hardness. Ductility of AA7075 at 480 ºC is more than double the ductility of many HSLA steels at room-temperature. However, multiple-step aging treatments would be needed prior to the PBC to produce a nearly peak-aged hardness in the final part.

5.2. Future Work

The forming behavior of AA7075-T6 during PQF operations should be investigated. This can be accomplished by controlling quench rates during tension tests that mimic RRA forming. This would provide information about the formability of AA7075 during simultaneous deformation and quenching.

During this study RRA forming of AA7075-T6 was evaluated at an initial strain rate of 0.05 s^{-1}. Tension tests that mimic RRA forming should be conducted at additional strain rates. Tests that cover strain rates ranging from 0.001 to 1 s^{-1} would provide the strain-rate sensitivity of AA7075-T6 at RRA forming temperatures.

The RRA behavior of AA7075-T6 between 180 and 200 ºC should be evaluated. Retrogression treatments at these lower temperatures could expand the potential processing window of RRA forming. Hardness may be improved after paint baking as retrogression treatment temperatures decrease. Ductilies are expected to be lower than

forming at temperatures above 200 ºC but still may be suitable for RRA forming of AA7075-T6.

The RRA forming behavior of 6000-series aluminum alloys should be investigated. The recommended peak-aging temperatures for these alloys are similar to the PBC temperatures currently used in the auto industry. Because of this, 6000-series aluminum alloys may also be suitable for RRA forming operations.

Appendix A: Experimental Design and Procedures

A.1. Detailed Retrogression Treating Procedure

Molten salt baths were used to perform retrogression treatments on the AA7075-T6 material provided by General Motors. Retrogression treatments were performed on two separate occasions. The first retrogression treatments were performed on June 11th and June 12th of 2013 and material was retrogressed at 200, 250, 300, and 350 °C. The second retrogression treatments were performed on July 23rd of 2013 and material was retrogressed at 200, 225, and 250 °C. The same procedure was used for each retrogression treatment and is described below.

Retrogression Treating Procedure:

1. Small rectangular specimens were machined from the as-received material, and a small hole was drilled into the top of each specimen.

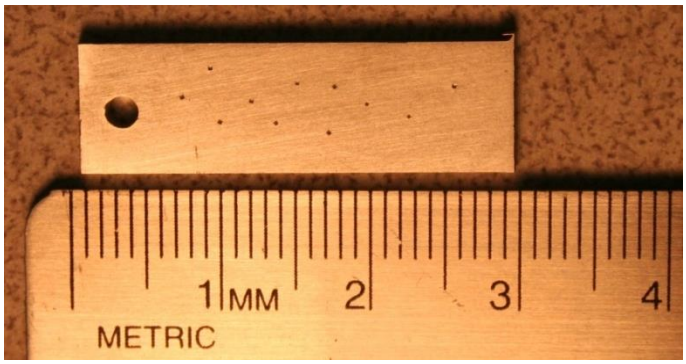

Figure A.1: Aging Specimen.

2. Specimens undergoing the same retrogression treatment were strung onto a long nickel wire and aligned such that they could not contact each other during the retrogression treatment.

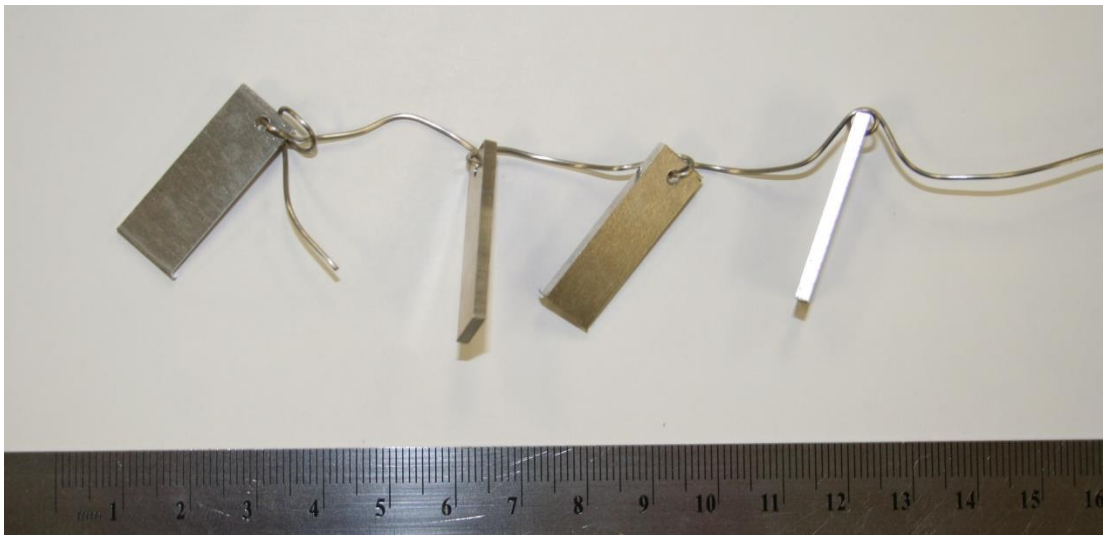

Figure A.2: Aging specimens secured to the nickel wire.

3. The molten salt baths were set to the lowest treatment temperature and allowed 24 hours to reach temperature. Two Inconel (Alloy 600) sheathed type-K thermocouples were submerged in the molten salt bath and an Omega HH501DK thermocouple readout was used to monitor temperature.

Figure A.3: Omega HH501DK hand-held thermocouple readout and metal sheathed type-K thermocouples.

4. Once at temperature, specimens were completely submerged in the molten salt bath and treated for 10, 30, 90, and 150 seconds. Retrogression treatment times were monitored with a stopwatch and computer-based timer.
5. Specimens were immediately quenched to room-temperature in water upon removal from the molten salt bath.
6. The molten salt baths were given 1 hour to stabilize at the next test temperature. Steps 4 and 5 were then repeated at the new test temperature.

A.2. Artificial and Natural Aging after Retrogression Treating

Artificial and natural aging of the material retrogressed on June 11th and June 12th of 2013:

Two specimens were retrogressed at 200 °C and 250 °C for each retrogression time.

- One sample was naturally aged without any other heat treating.
- One was aged at 175C for 30 min to simulate a typical paint bake cycle (PBC) and then naturally aged.

Three specimens were retrogressed at 300 °C and 350 °C for each retrogression time.

- One sample was naturally aged without any other heat treating.
- One was aged at 175C for 30 min to simulate a typical PBC and then naturally aged.
- One was aged at 120 °C for 24 hours, aged at 175C for 30 min to simulate a typical PBC, and then naturally aged.

Aging at 120 °C for 24 hours was performed on June 12th of 2013. Aging at 175 °C for 30 minutes was performed on June 18th of 2013.

Artificial and natural aging of the material retrogressed on July 23rd of 2013:

Five specimens were retrogressed at 200 °C, 225 °C, and 250 °C for each retrogression time.

- One was aged at 175 °C for 30 min to simulate a typical PBC and naturally aged.

- Four were aged at 120 °C for 3, 6, 12, and 24 hours, respectively, aged at 175 °C for 30 min to simulate a typical PBC, and naturally aged.

Aging at 120 °C was performed on July 24th and 25th of 2013. Aging at 175 °C for 30 minutes was performed on July 30th and 31st of 2013.

Specimen Preparation for Hardness Testing:

1. Specimens were washed in a mixture of water and Simple Green™ with an ultrasonic bath.
2. Each side of the specimen was lightly ground with 800-grit and then 1200-grit silicon-carbide paper until a smooth and uniform surface finish was achieved.
3. Specimens were washed again in a mixture of water and Simple Green™ with an ultrasonic bath.
4. Specimens were then tested with a Buehler Macro Hardness Tester, Model 1900-2005.

Figure A.4: Buehler Macro Hardness Tester, Model 1900-2005 used for hardness testing.

A.3. Detailed Heat Transfer Model

Nomenclature:

θ – temperature (kelvin)

θ_o – ambient temperature (kelvin)

x – distance along bar (meters)

C_p – specific heat (Joule/kilogram-Kelvin)

d – density (kilogram/meter^3)

t – time (seconds)

λ – thermal conductivity (Watts/meter-Kelvin)

I – current (Amps)

ρ – resistivity (ohm-meter)

A – cross-sectional area (meter^2)

h – convective heat transfer coefficient (Watts/meter^2-Kelvin)

ε – radiative heat transfer coefficient (Watts/meter^2-Kelvin^2)

v_e – volume of finite difference element (meters^3)

i – time iteration

n – distance iteration

The heat transfer model used to aid in the design the rapid direct electrical heating tensile coupons was adapted from the work of Karunasena on electrical resistance heating of flat steel bars [36]. The governing equation used to derive the model was developed by a power balance performed across the length of the gauge region and is shown by Equation A.1.

$$C_p d\frac{d\theta}{dt} = \frac{\partial}{\partial x}\left(\lambda\frac{\partial\theta}{\partial x}\right) + \frac{I^2\rho}{A^2} - hA\left(\theta-\theta_o\right) - \varepsilon A\left(\theta^4-\theta_o^4\right) \qquad (A.1)$$

Several assumptions were made to limit the complexity of the model. It was assumed that current was evenly distributed throughout the cross-section and power generation remained constant throughout the thickness and length of the gauge region. In addition, temperature was only allowed to vary along the length of the gauge region. Because the specimens being design were small, it is believed these assumptions are fairly accurate. Variation of resistivity and thermal conductivity with temperature was accounted for.

Equation A.1 was solved for temperature and discretized in terms of time, subscript i, and distance, subscript n, along the gauge region [36-37]. This took the form of Equation A.2 and is presented visually in Figure A.5.

$$\theta_{i+1,n} = \left(\frac{\Delta t}{C_p v_e d}\right)[\text{Conduction} + \text{JouleHeating} - \text{ConvectionLoss} - \text{RadiationLoss}] \qquad \text{(A.2)}$$

$$\text{Conduction} = \left(\frac{A}{\Delta x}\right)\left[\left(\lambda_{i,n+1} - \lambda_{i,n-1}\right)\left(\theta_{i,n+1} - \theta_{i,n-1}\right) + \left(\lambda_{i,n}\right)\left(\theta_{i,n+1} + \theta_{i,n-1} - 2\theta_{i,n}\right)\right]$$

$$\text{JouleHeating} = I^2 \rho_{i,n} A \Delta x$$

$$\text{ConvectionLoss} = hA\left(\theta_{i,n} - \theta_o\right)$$

$$\text{RadiationLoss} = \varepsilon A\left(\theta_{i,n}^4 - \theta_o^4\right)$$

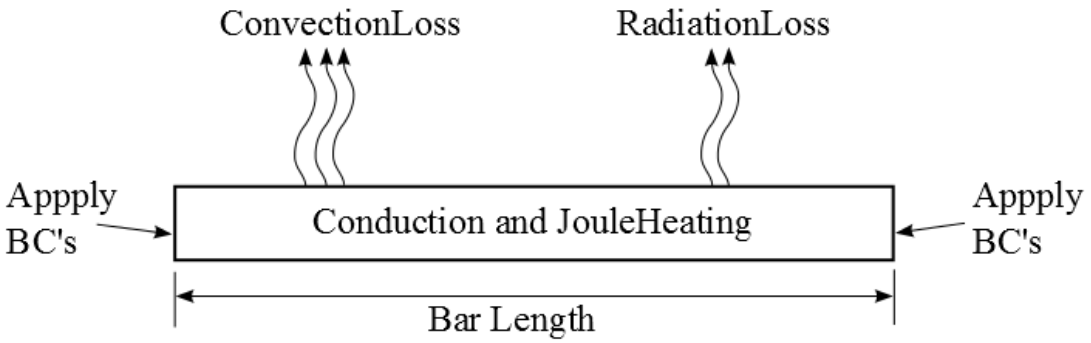

Figure A.5: Visual representation of the heat transfer model.

Boundary conditions needed to be specified before the model could be run. This included specifying the ambient air temperature and the temperature of each end of the gauge region. The ambient air was held constant at 20 °C. The initial temperature at each end of the bar was also taken to be 20 °C, but was linearly increased to 100 °C during the simulation. This was done because Karunasena observed a temperatures increase at the end of the bar in his work [36]. The convection and radiation heat transfer coefficients were initially determined by fitting to data provided by Karunasena. They were later adjusted to more accurately match the behavior observed in this study. The geometry of the specimens made calculations of these values impractical. MATLAB was used to run each simulation of the one-dimensional finite difference model. The code used to run these simulations is presented below.

```
function trans_heat_paper1
% Heating model of Aluminum rectangular bars.
%  Volume multiplied in and conventional conduction,
radiation and
% convection heat transfer are accounted for.

% Initial Temperature (K)
T_initial = 293.15;

% Properties
% Density (kg/m^3)
rho = 2810;
% Specific heat (J/kg-K)
cp = 1000;

% Tensile °Coupon Dimensions
L = 0.155; % bar length (m)
W = 0.005; % bar width (m)
```

```
TH = 0.002; % bar thickness (m)
SA = L*W; % Surface area m^2
V = L*W*TH; % volume m^3
CA = W*TH; % cross-sectional area m^2


% °Current (Amps)
A = 250;

% °Current Density (Amps/m^2)
J = A/CA;

% Thermal Properties
h = 280; % convection heat transfer coefficient W/m^2-K
Radcof   =   2.103E-7;   %   W/m^2-K^2   --   emissivity*stefan
boltzman constant
                  % -- emissivity = 0.09


% Time and distance steps used to run the simultion
dx = 0.00775; % distnace step (m)
dt = 0.1; % time step (s)
VE = W*TH*dx; % elemnet volume (m^3)
SAE = W*dx; % elemnent surface area (m^2)

% °Counting variables
i = 1; % time
n = 1; % distance
j = 1; % initial condition counter
v = 0; % intial temperature heating counter

final_time = 60; % seconds
final_dist = L;

% step sizes
time_step = final_time/dt;
dist_step = final_dist/dx;

    % loop for Initial conditions
    while j <= dist_step;

        % Initial °Conditions
        T1(1,j) = T_initial;
```

```
        %counter to build conditions
        j = j + 1;


    end

    % set other end of bar starting temperature
    T1(1,dist_step+1) = T_initial;

    % Iterative Loop for time
    while i < time_step;

        % Boundary °Conditions
        T1(i+1,1) = T1(i,1) + (v)*(40/time_step);
        T1(i+1,(dist_step+1))    =    T1(i,(dist_step+1))    +
(v)*(30/time_step);

        % reset location on the the Al bar back to the
begining
        n = 2;

        %iterative loop for distance along section
        while n <= dist_step;

            % °Constant used in calculations
            °Cons = dt/(cp*rho*VE);

            % Thermal conductivity for varying  temperature
W/m-K
            Lam1 = 0.17*T1(i,n) + 80; % heat cond. coeff at
                                      %  initial  time  and
temp
            Lam3 = 0.17*T1(i,n-1) + 80; % heat cond. coeff
at
                                        %          location:
(initial location - dx)
            Lam4 = 0.17*T1(i,n+1) + 80; % heat cond. coeff
at
                                        %          location:
(initial location + dx)

            % Electrical Resistivity with temp in ohm-m
            resist = ((1.36E-10)*T1(i,n)) + 1.42E-8;
```

```
            % °Calculations for Temp at time (i), and
            % distance (n) along the Al bar
            °Conduction = (((((Lam4-Lam3))*CA)/(dx))*...
                          ((((T1(i,n+1)-T1(i,n-1))))))+...
                          (((Lam1*((T1(i,n+1)+...
                         T1(i,n-1)-(2*T1(i,n)))))*CA)/dx);
            JHeat = ((J^2)*resist*dx*CA);
            HLoss = ((h)*(SAE)*((T1(i,n)-T_initial)))+...
                    ((Radcof)*(SAE)*((T1(i,n)^4)-
(T_initial^4)));

            T1(i+1,n)             = °Cons*(Conduction+JHeat-
HLoss)+T1(i,n);

            % move to next point along the bar
            n = n + 1;

        end

        % time counter
        i = i + 1;
        v = 1;

    end

% initial conditions for surface plot
distance(1) = 0;
time(1) = 0;
p = 1;
q = 1;

    while p < (time_step);

        time(p+1) = p*dt;
        p = p +1;

    end


    while q <= (dist_step);

        distance(q+1) = q*dx;
        q = q + 1;
```

```
    end


% counting for plots
B = (L/dx)/2;
t_final = (final_time/dt)-1;


% change temperature to degress celcius (C)
T2 = T1 - 273.15;


% Surface plot
figure1 = figure;
surf(distance,time(1:590),T2(1:590,:),'LineStyle',':','Edge
Color',...
    [0.313725501298904                    0.313725501298904
0.313725501298904]);
title('Finite Difference Temperature Span');
xlabel('Distance Along Bar(m)');
ylabel('Time (s)');
zlabel('Temperature (C)');
colorbar

% temperature at L/2 vs time
figure2 = figure;
plot(time,T2(:,B));
title('Temperature at Mid-point');
xlabel('Time (s)');
ylabel('Temperature (C)');

% temperature at t_final across bar
figure3 = figure;
plot(distance,T2(t_final,:));
title('Temperature span at Steady State');
xlabel('Distance Along Bar (m)');
ylabel('Temperature (C)');
```

A.4. Testing and Verification of the Rapid Heating System

A table-top heating rig was built as a precursor to using electrical resistance heating during tensile testing. The table-top rig allowed for the heating system to be easily tested and calibrated prior to tensile testing. It was also used to measure the temperature profile produced by each tensile coupon. A 3-D model of the assembly is displayed in Figure A.6. Specimen lengths of 100 to 230 mm can be accommodated by the table-top rig. However, once the specimen is secured, length cannot be adjusted to account for thermal expansion. This was not expected to affect measurements during testing.

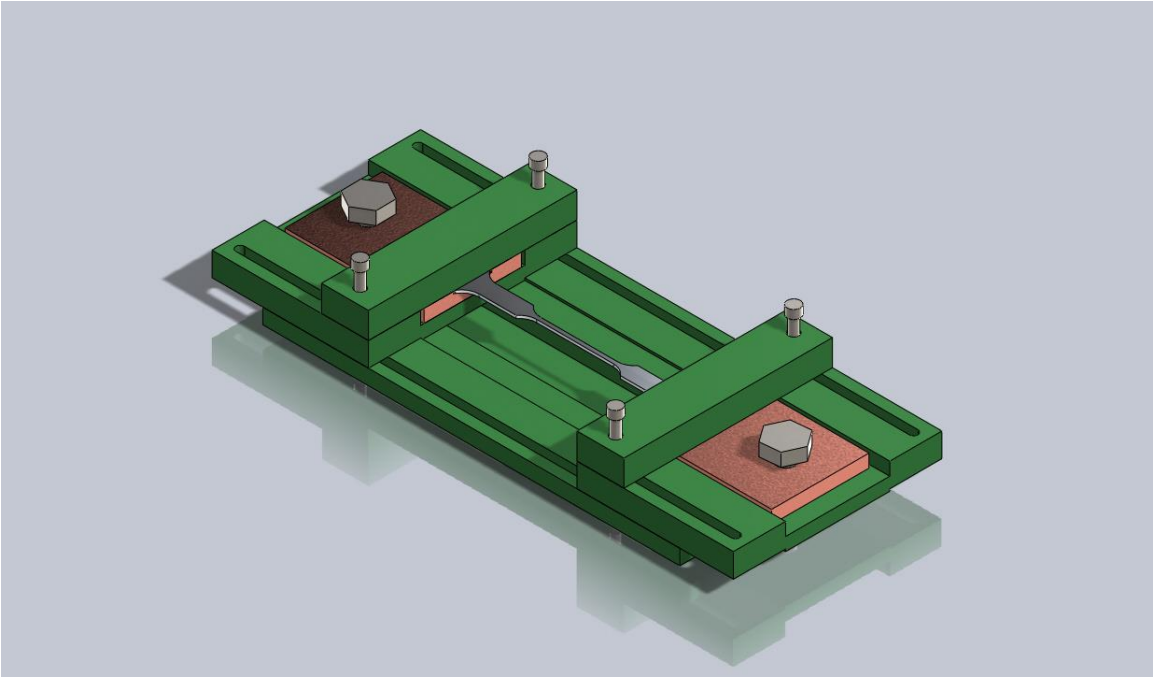

Figure A.6: 3-D model of the table-top testing rig.

The design consists of seven components; one stationary base, two mobile platforms, two specimen holders, and two cover boards. The stationary base keeps the mobile platforms aligned and contains a slot for a refractory material to catch any melted material. The mobile platforms house the copper specimen holders. The cover boards are laid on top of the specimen and bolted through the base board to secure the tensile coupon in the specimen holder. The cover bolt holds the assembly together. The specimen holders were made of C110-H02 copper flat-bar. Copper provided the necessary electrical conduction between the specimen holder and the tensile coupon. The other components were constructed with G-10 phenolic composite, a fiberglass-epoxy laminate composite with excellent electrical insulation properties. Technical drawings of each component are presented in Figures A.7-A.10.

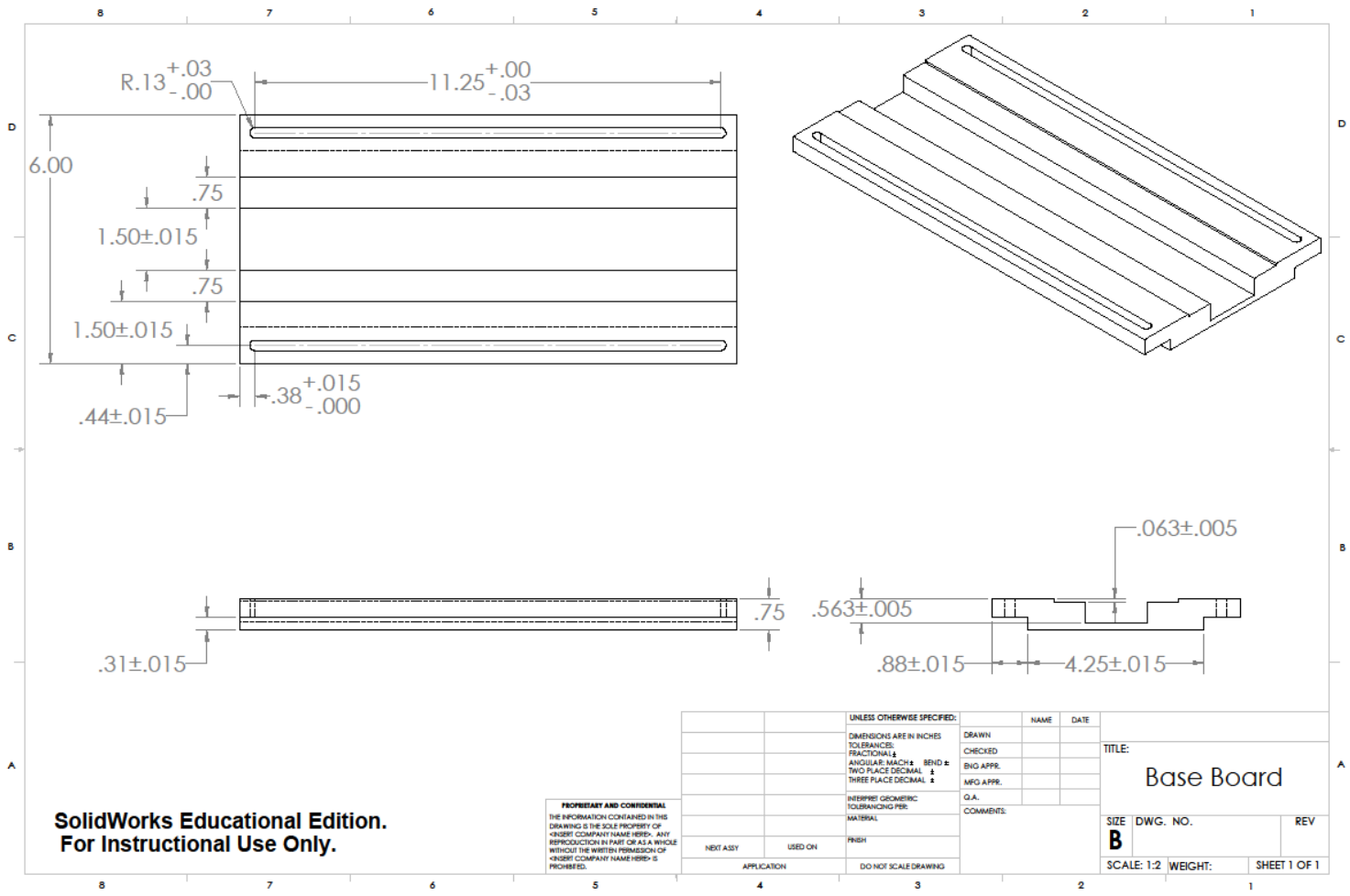

Figure A.7: Technical drawing of the G-10 stationary base. All dimensions in inches.

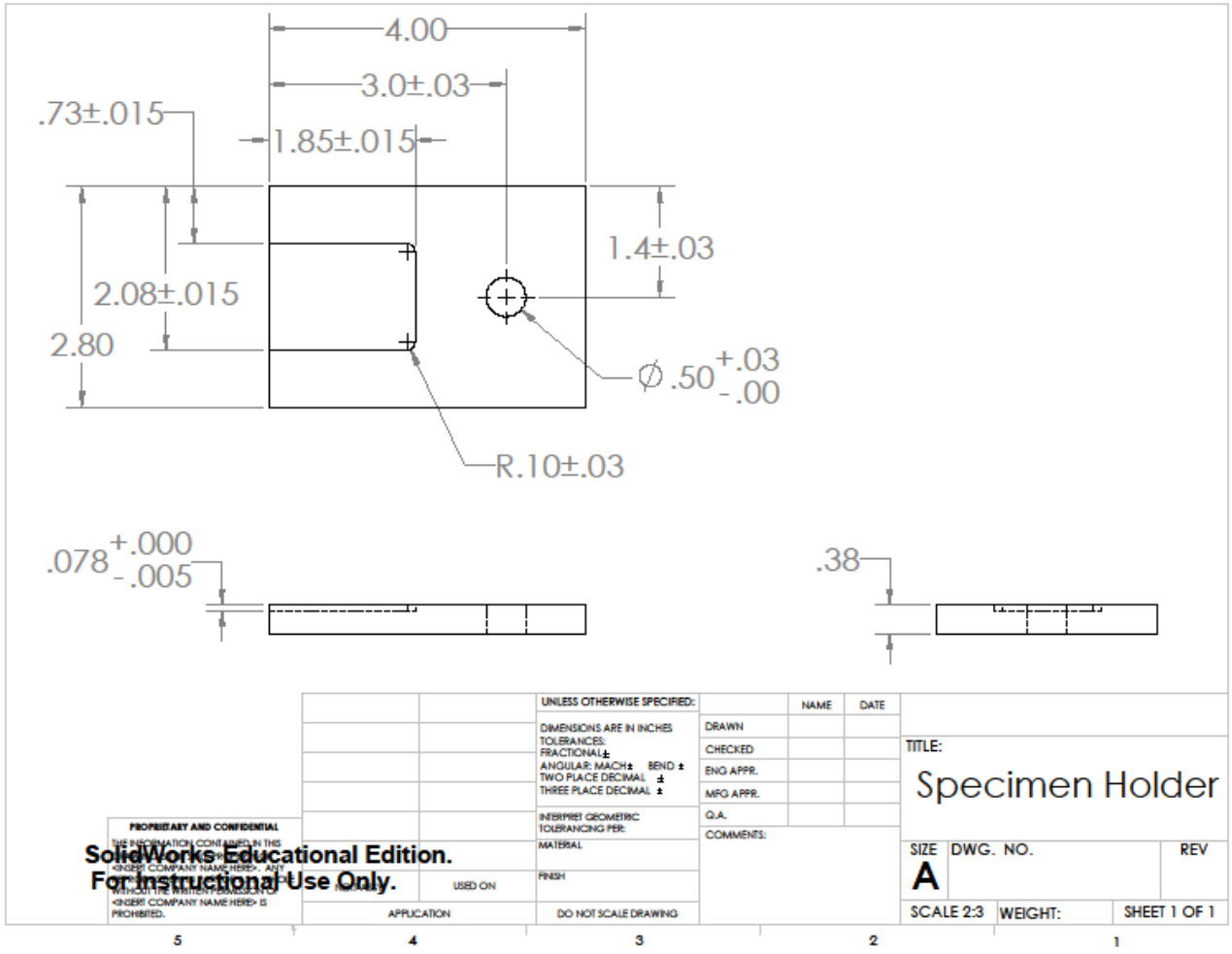

Figure A.8: Technical drawing of the copper specimen holder. All dimensions in inches.

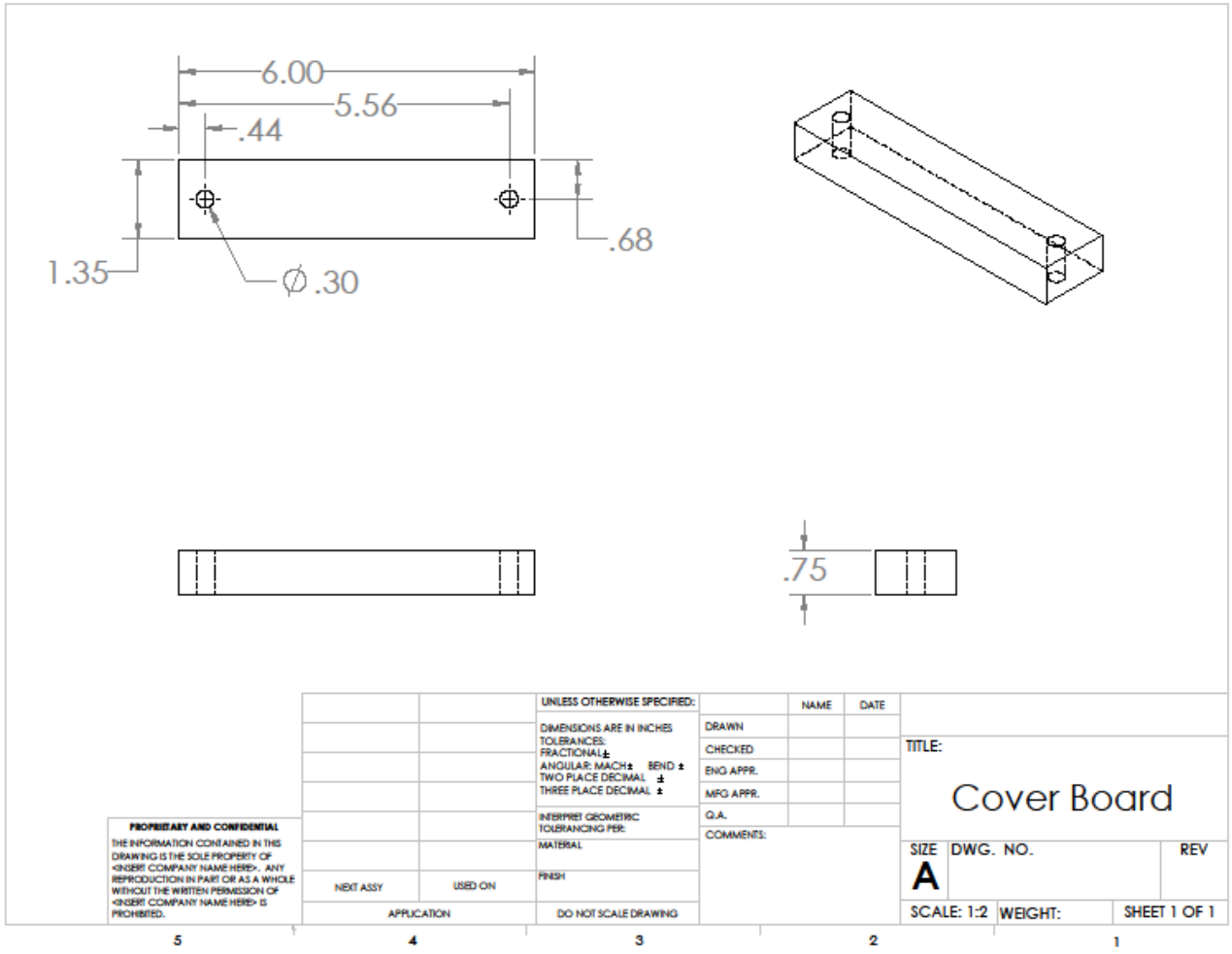

Figure A.9: Technical drawing of the G-10 cover board. All dimensions in inches.

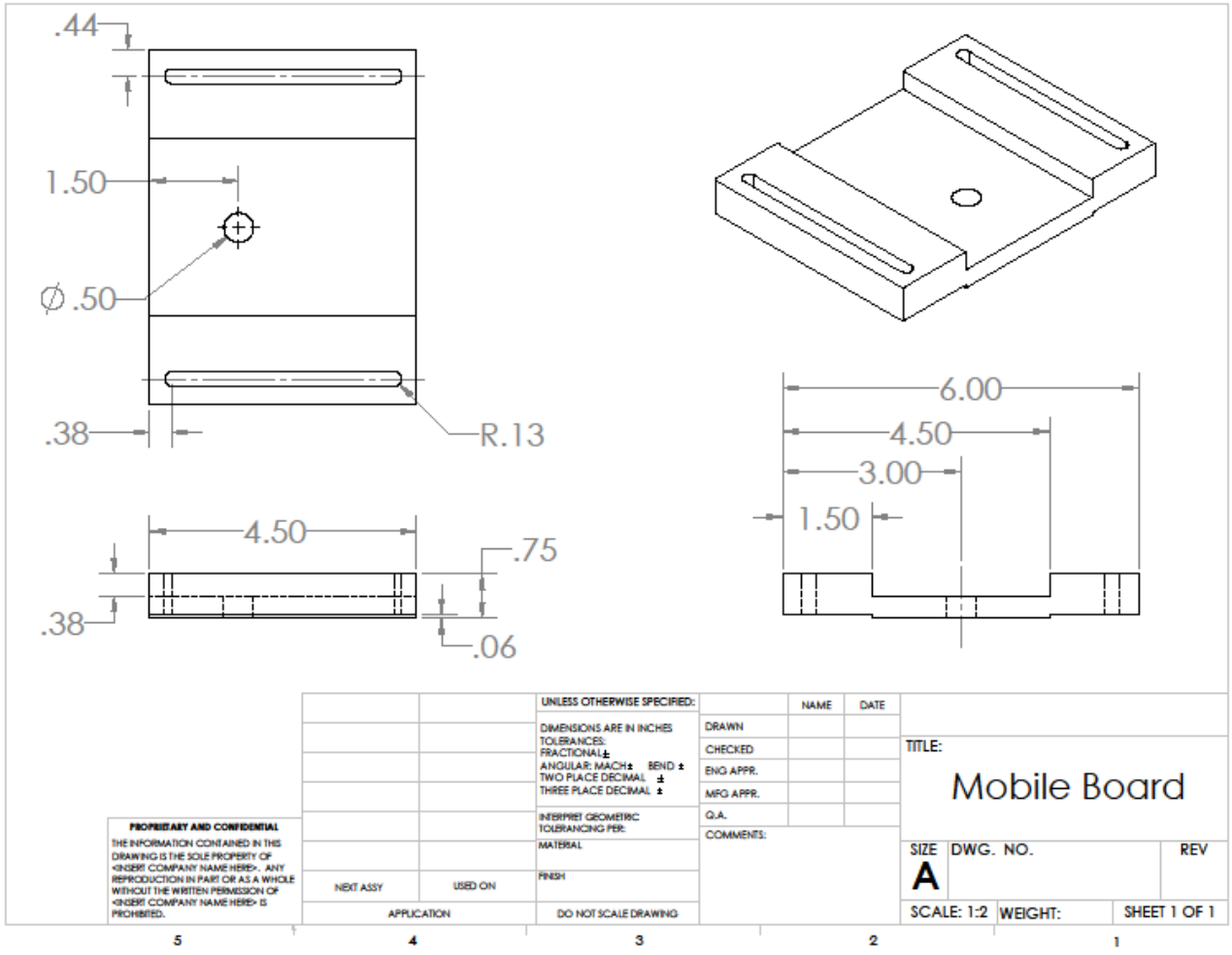

Figure A.10: Technical drawing of the G-10 mobile platform. All dimensions in inches.

A.5. Rapid Electrical Heating Tensile Grip Design

Tensile grips were specifically designed for rapid electrical heating tensile tests. The critical design criteria are listed below:

- Withstand loads of 2000 lbs.
- Electrically isolate the specimen holders from the electro-mechanical test frame.
- Facilitate easy loading and unloading of specimens.
- Don't heat up during testing.
- Connect to the load cell.

The grip assembly consisted of four components; a stainless steel adapter, a G-10 spacer, a copper specimen holder, and a G-10 cover plate. A description of each component follows.

The stainless steel adapter connected the grip assembly to the load cell. It slipped into a collar attached to the load cell and was pin loaded with a half inch diameter steel rod. The adapter was machined from a solid 3 inch diameter rod of 303 stainless steel. Stainless steel was used to prevent rusting. The spacer connected the stainless steel adapter with the specimen holder. The spacer was used to electrically isolate the specimen holder from the electro-mechanical test frame. It was machined from G-10 phenolic. G-10 has a dielectric strength of 800 V/mm and a tensile strength of 45 ksi. The fibers in the composite were oriented parallel to the tensile direction to maximize

strength. The specimen holder was used to house the specimen grip face and provided a location to attach the power supply. It was machined from C110-H02 copper to provide ample conduction between the power supply and the specimen. The specimen was held by its shoulders and was secured to the holder with the cover plate and specimen bolt.

Stainless steel bolts, washers, and nuts were used to assemble the grips, attach the power lead, and hold the specimen in place. An exploded 3-D model of the grip assembly is shown in Figure A.11, followed by the technical drawings for each component shown in Figures A.12-A.15. Tolerance was ± 0.005 inches for all dimensions unless otherwise noted.

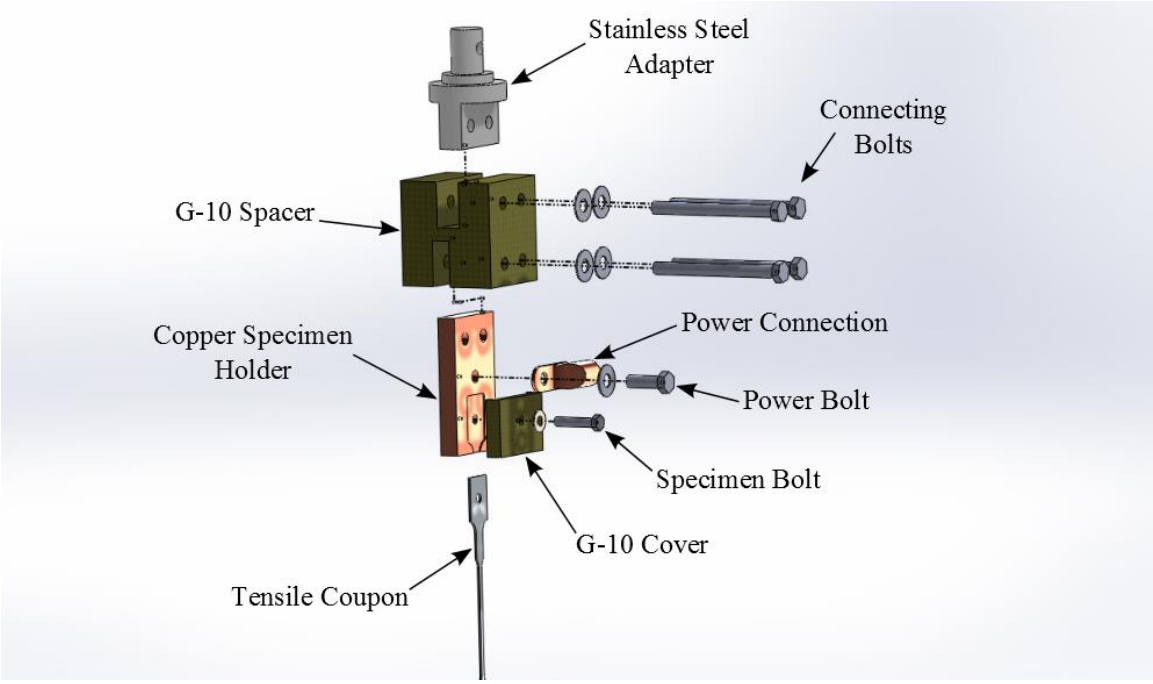

Figure A.11: 3-D exploded assembly view of the direct resistance heating grips.

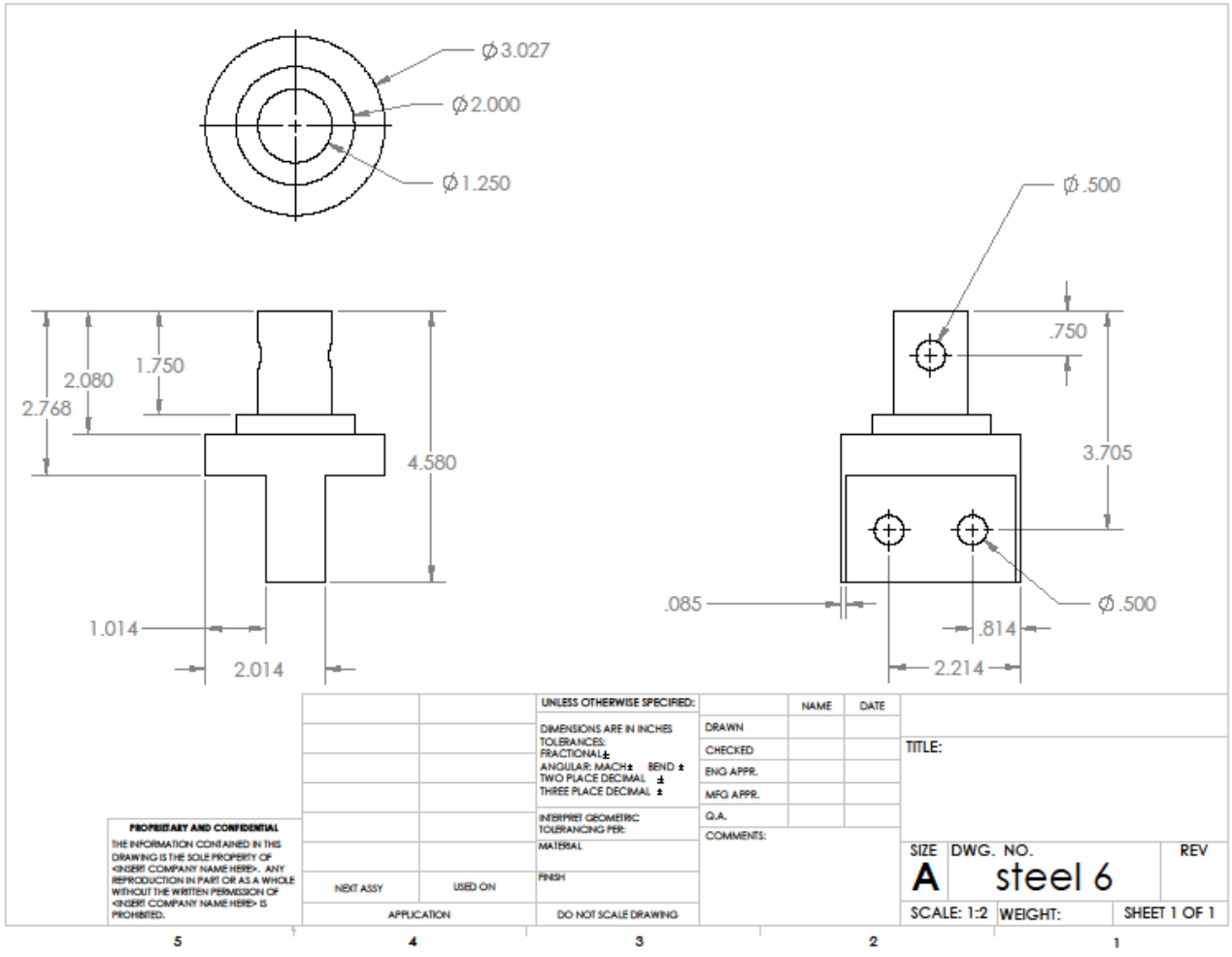

Figure A.12: Technical drawing of the 303 stainless steel adapter. All dimensions in inches.

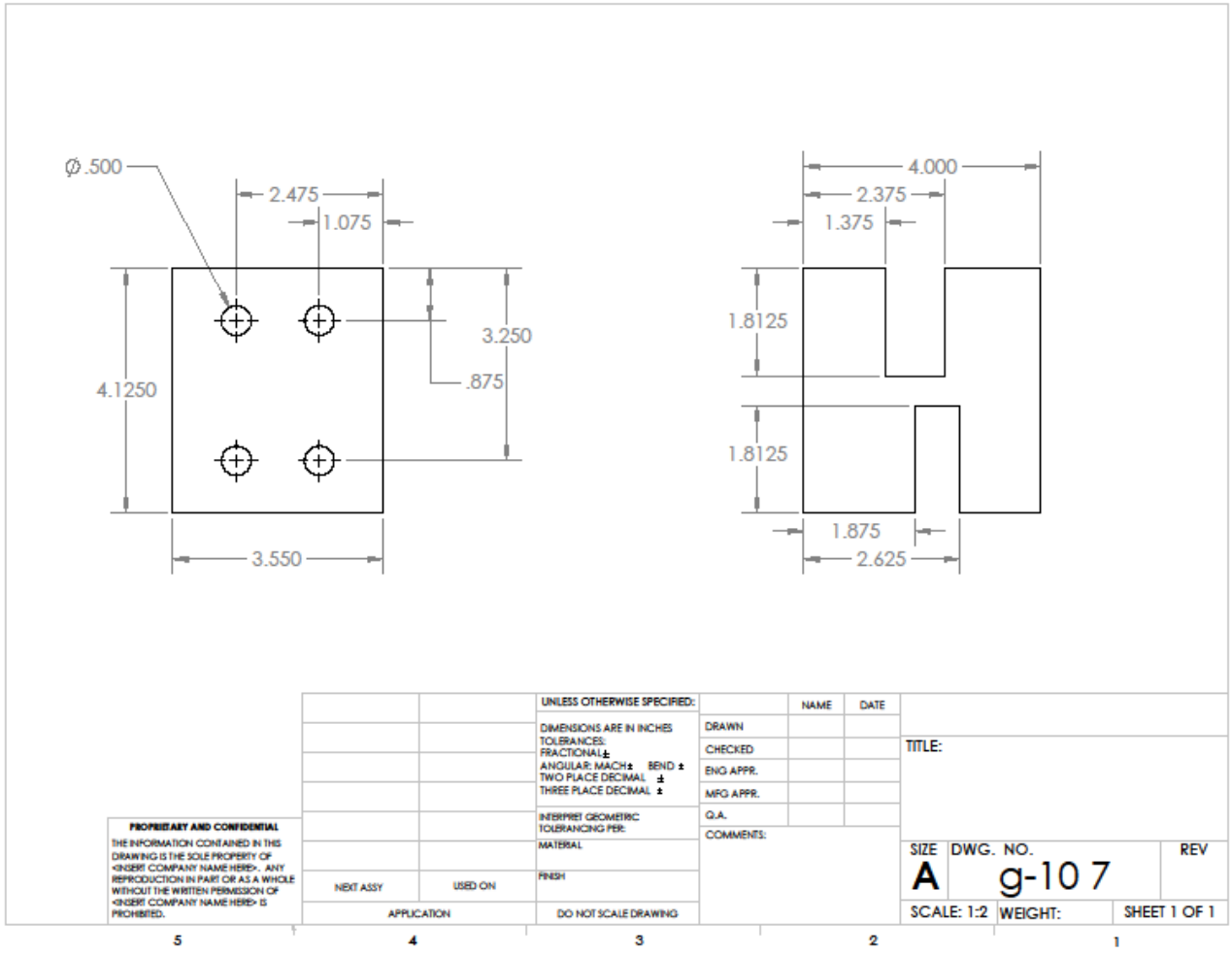

Figure A.13: Technical drawing of the G-10 spacer. All dimensions in inches.

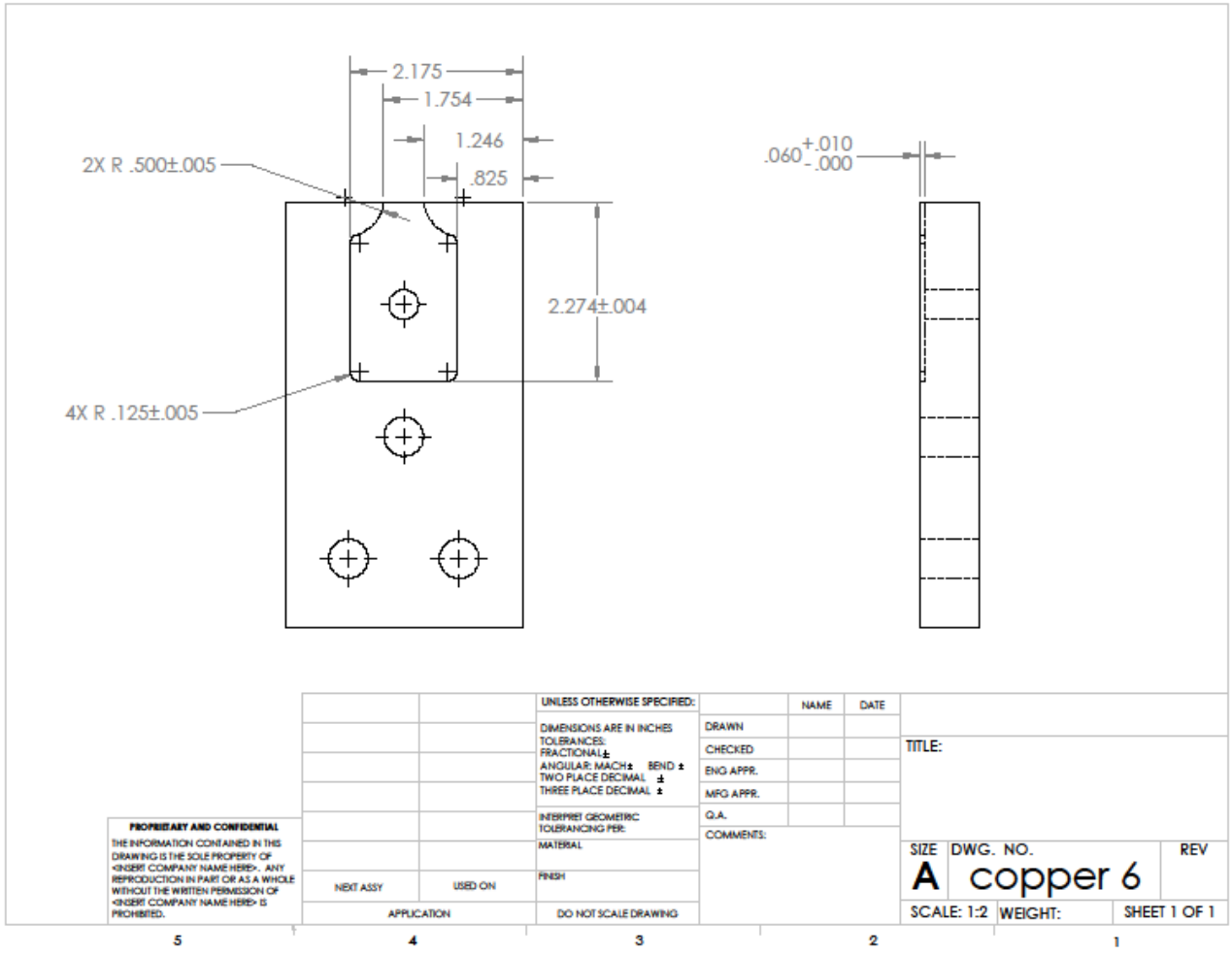

Figure A.14: Technical drawing of the copper specimen holder. All dimensions in inches.

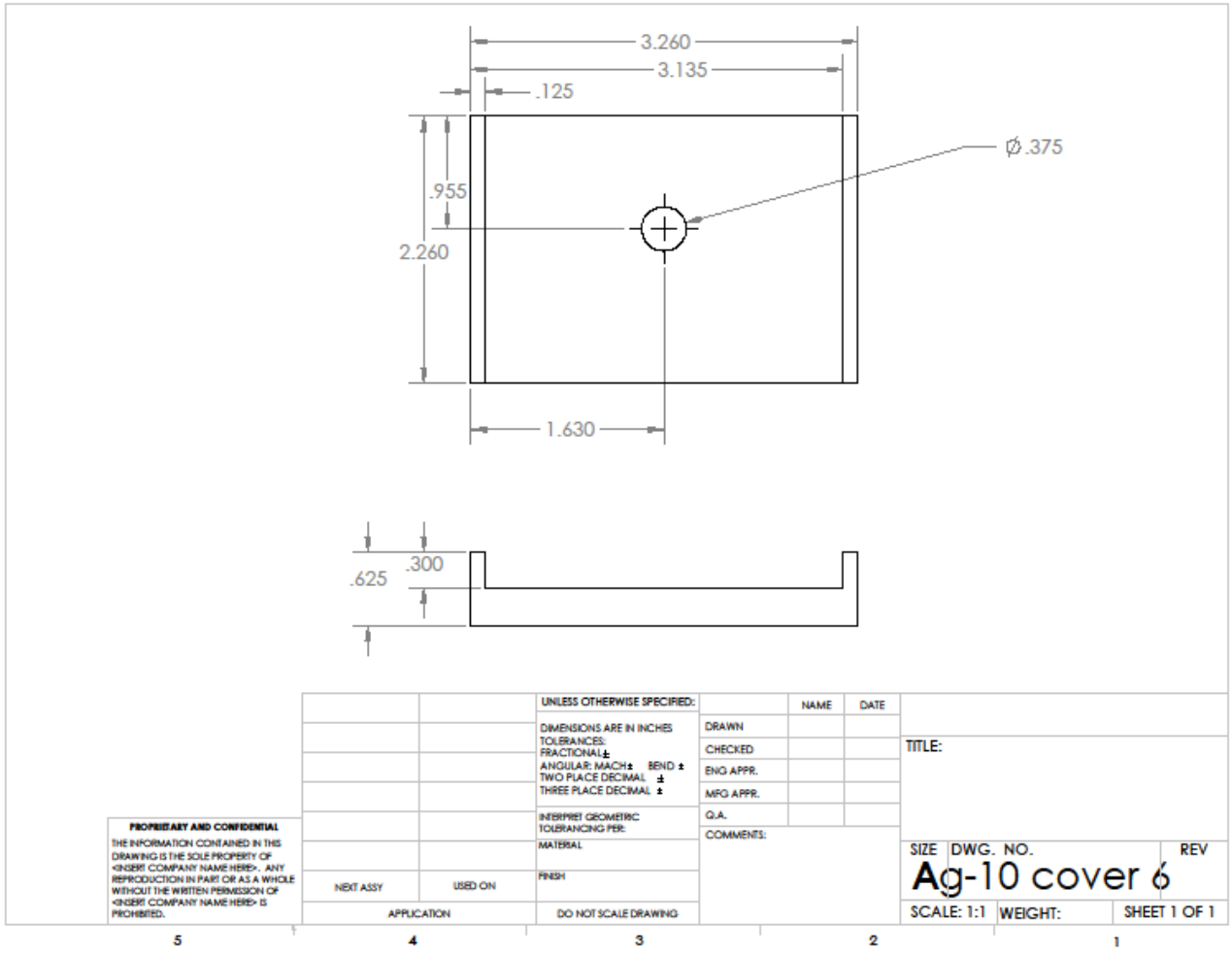

Figure A.15: Technical drawing of the G-10 cover board. All dimensions in inches.

A.6. LabVIEW Control Program Design

A LabVIEW program was used to control and monitor the rapid electric heating system. A screenshot of the program interface is shown in Figure A.16. Temperature determined from the IR is monitored and recorded every millisecond. A case structure was implemented to automate the heating and cool down procedure. It consists of three states.

- The “Start Up” state opens first. This state allows the user to turn on all of the equipment, define the temperature profile for the test, and limits the output of the welder to 15 amps.
- The next state is “Testing”. This is triggered by clicking the “start test” button. In this state the temperature profile begins to run, and the output from the welder is automatically adjusted to keep the temperature determined by the IR as close to the temperature profile. The welder output is controlled by a LabVIEW PID algorithm.
- Once the profile is completed, the program enters the “Stopping” state. This state limits the output of the welder to 15 amps.

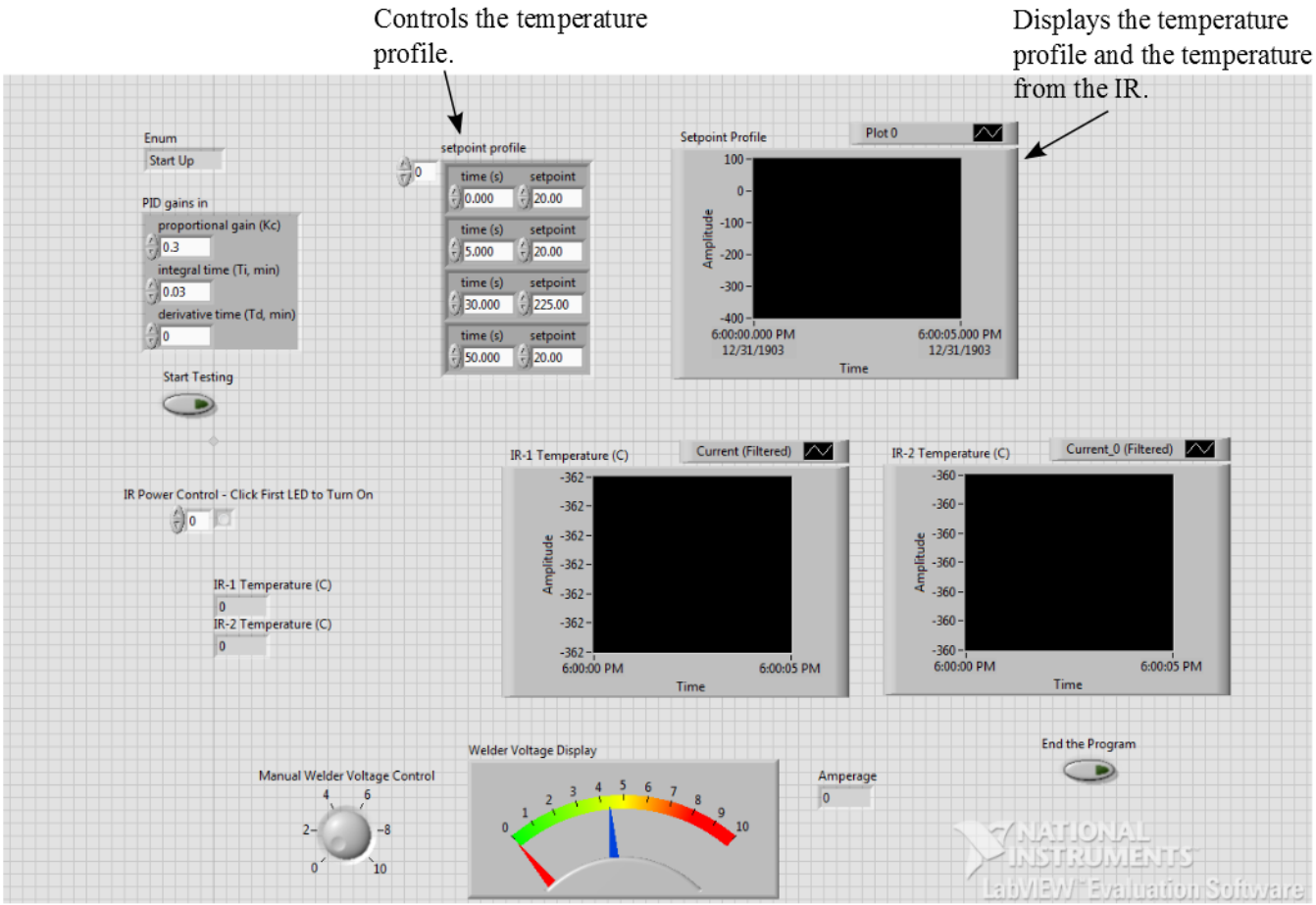

Figure A.16: Screenshot of the LabVIEW interface control program user interface

A.7. Equipment Wiring

System Wiring

A National Instruments PCI 6221 board and SCC-2345 Series carrier were used to control the welder and monitor the IR sensor. Two SCC-FT01 modules were used to connect the SCC-2345 with the wires from each component.

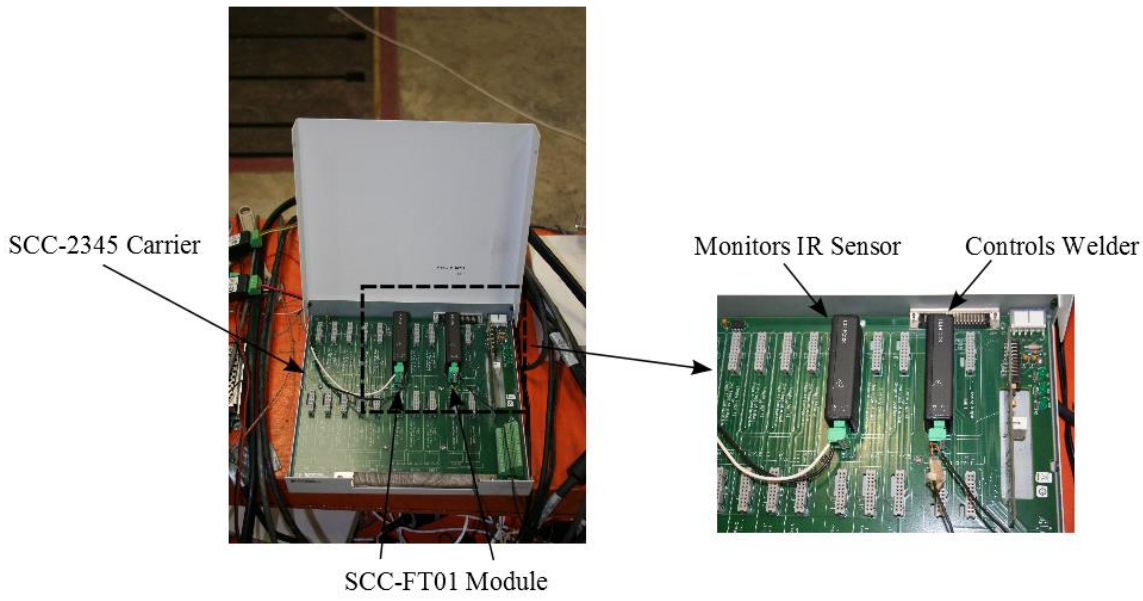

Figure A.17: National Instruments SCC-2345 carrier and SCC-FT01 modules used for data collection.

Welder Wiring – Miller XMT 350 MPA

- The welder is controlled by LabVIEW through the "remote" receptacle on the front of the welder.

Figure A.18: Photograph of the Miller XMT 350 MPA welder.

- In the open end of the remote wire, connect terminal A to terminal B with a small wire. Connect terminal D to the ground terminal and terminal E to the positive

output terminal on the SCC-FT01 module. This module is plugged into an analog output channel on the SC-2345 carrier.

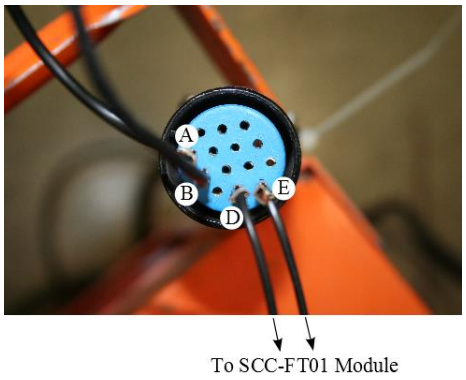

Figure A.19: Photograph of the wire connections on the end of the welder remote control wire.

Infrared Sensor Wiring – Omega 0S550 series infrared pyrometer

- The IR sensor is wired to the corresponding LCD display box from Omega.

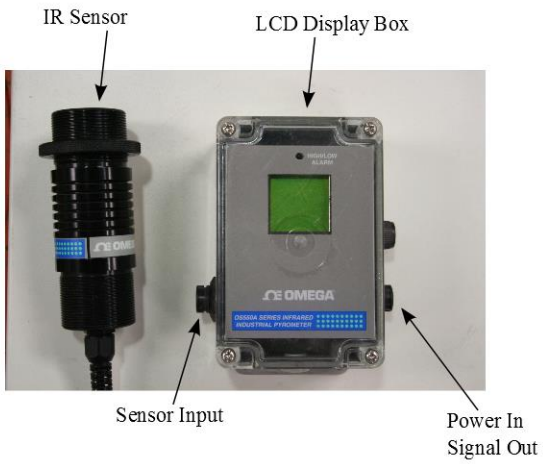

Figure A.20: Photograph of the Omega 0S550 IR pyrometer and corresponding LCD display box.

- A 25 volt power supply is wired through a Digital I/O channel on a National Instruments USB 6525 DAQ to power the IR sensor. The USB 6525 digitally controls the power to the IR sensor.
- The LCD display box outputs a 4 to 20 mA signal. This is signal is converted to temperature. The signal output is wired from the LCD display box to a SCC-FT01 module. This module is plugged into an analog input channel on the SCC-2345 carrier. The signal was run through a low pass RC filter prior to entering the SCC-FT01 module.
- The optimal distance between the lens on the IR sensor and the surface of the specimen is 15.2 mm. The diameter of the spot size is 3.9 mm at this spacing. The spot size is the area captured by the IR sensor.

A.8. Room-Temperature Tensile Testing

Testing was performed with a Series 1600 universal testing machine from Applied Test Systems (ATS). An Epsilon Tech 3542 axial extensometer was used to measure tensile elongation.

Tensile coupon preparation:

1. Specimens were milled from the as-received material.

2. Specimens were tested in the as-received condition and after solution treating.
3. Specimens were solution treated at 480 °C for 30 minutes and immediately water quenched to room-temperature. Solution treating was completed with a Therm-Pro Inc. TF-12C resistance tube furnace.

Figure A.21: Photograph of the tensile coupon used for room-temperature tensile tests.

Tensile testing procedure:

1. The wedge loading grips were loaded in the electro-mechanical test frame.
2. Specimens were aligned in the grips, and the grips were tightened.
3. The extensometer was secured to the middle of the gauge region with rubber-bands. A pin kept the displacement at zero during setup and was removed prior to testing.

Figure A.22: Photograph of the room-temperature tensile testing setup.

4. The ATS software was used to define a constant cross-head speed for testing.
5. The tensile test was performed.

A.9. Solution Forming Tensile Testing

Testing was performed with a MTS Systems 810 materials testing system.

Tensile coupon preparation:

1. Specimens were milled from the as-received material.
2. Specimens were solution treated at 480 °C for 30 minutes and immediately water quenched to room-temperature. Solution treating was completed with a Therm-Pro Inc. TF-12C resistance tube furnace.

Figure A.23: Photograph of the tensile coupon used for solution-temperature tensile tests.

Tensile testing procedure:

1. The three-zone high temperature furnace was turned on. It usually took a few hours to reach the desired testing temperature.
2. The MTS software was used to define a constant cross-head speed for testing.
3. The specimen to be tested was loaded into the high-temperature shoulder loading grips. Thermocouples were attached to the top and bottom grips through a small hole machinced on the front of the grips. The thermocouples were forced to make contact with the specimen. Once the furnace reached the desired testing

temperature, the grips were loaded into the MTS frame. A small pre-load is applied to the specimen to secure it in the grips and account for thermal expansion.

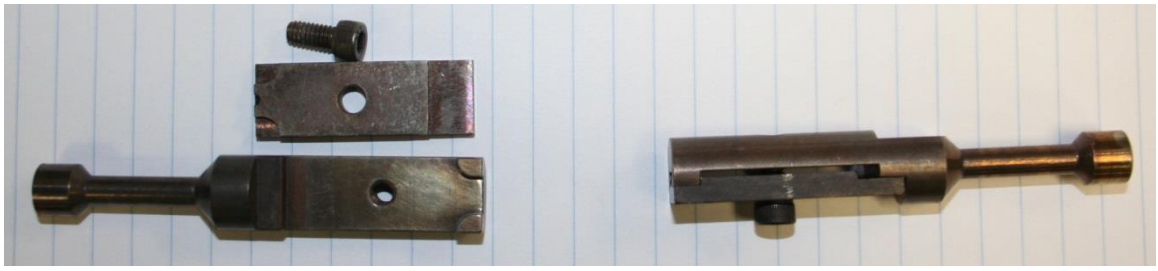

Figure A.24: Photograph of the high temperature tensile grips.

4. Temperature was continuously adjusted to maintain a constant temperature in the testing region. Specimens were given 20 to 30 minutes to reach the testing temperature.
5. The tensile test was performed.
6. Upon sample failure, the specimens were immediately quenched to room-temperature with water.

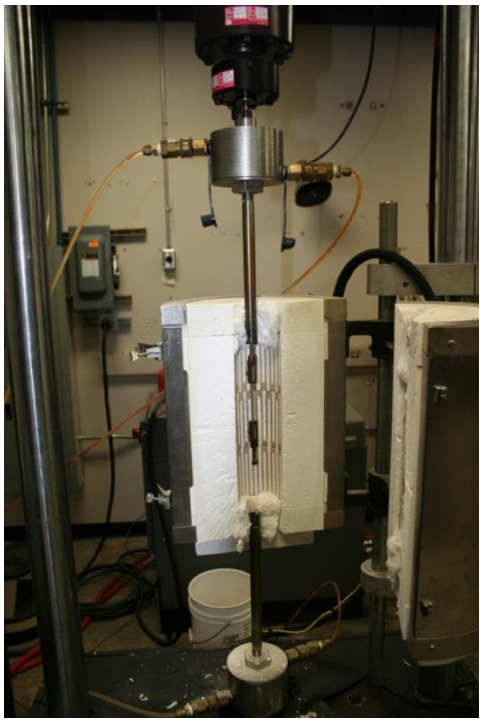

Figure A.25: Photograph of the high temperature tensile testing setup.

A.10. RRA Forming Tensile Testing

Testing was performed with an Applied Test Systems (ATS) Series 1600 universal testing machine.

Tensile coupon preparation:

1. Specimens were water-jetted from the as-received material.
2. A 3/8 inch diameter hole was drilled through each grip face. This allowed the tensile coupons to be bolted to the specimen holder.

3. Specimens were painted flat back on one side and electrochemically etched on the other.

Figure A.26: Front and back of the tensile coupons used for RRA temperature tensile tests.

Tensile testing procedure:

1. The rapid electrical heating grips were loaded into the ATS test frame. The power leads were attached to the specimen holders.

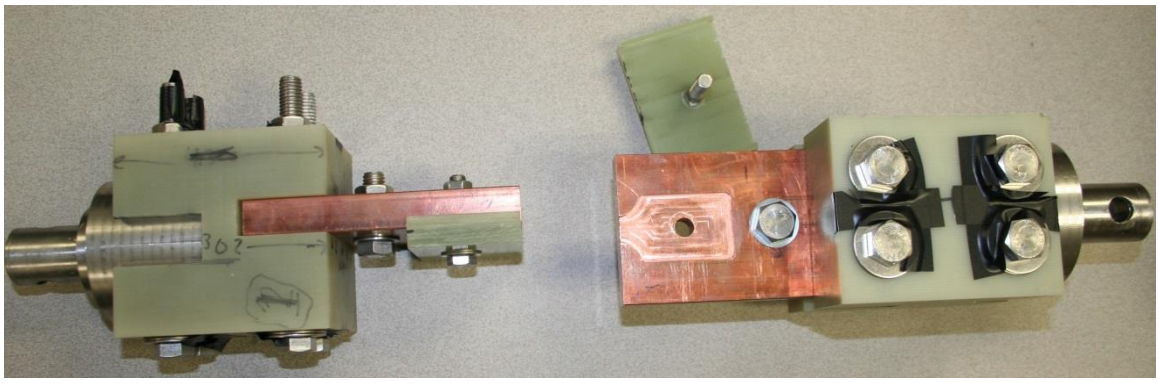

Figure A.27: Direct resistance heating tensile grips.

2. The specimen was loaded into the grips.
3. The IR pyrometer was positioned 15.2 mm (measured from the specimen surface to the IR sensor lens) away from the specimen at the midpoint of the middle-most gauge region. A laser guide was used to check the alignment and removed prior to testing.
4. The video camera used to record each test was positioned across from the IR on the other side of the specimen. It was powered on and focused on the middle of the back of the specimen.

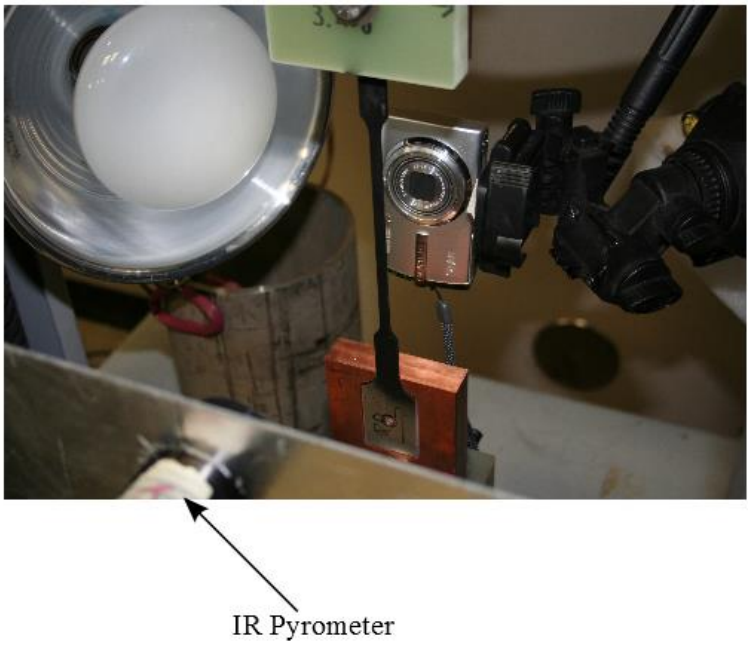

Figure A.28: Close-up photograph of the RRA temperature tensile test setup.

5. The welder mode was set to TIG by turning the knob on the front of the welder so that current output could be controlled remotely. The output scale knob on the front of the welder was rotated clockwise 3 times to set the peak current output to 350 amps.
6. The LabVIEW control program was opened and the appropriate temperature profile was set for the test.
7. The ATS software was opened, and the data channels were zeroed. An appropriate pre-load was applied to the specimen to account for thermal expansion. The ATS software was used to define a constant cross-head speed for testing.
8. A check was done to make sure everything was clear of the test environment and the rapid electric heating system was not grounded anywhere. The video camera started to record and the welder was powered on.
9. The LabVIEW control program was started by clicking the "start test" button.
10. Once the specimen reached the testing temperature, the motion of the electro-mechanical test frame was started. When the motor engaged, power to the welder was shut off. This was to prevent the sample from arcing upon failure.
11. Specimens were allowed to air cool for 1 to 2 minutes and then removed from the grips.

Appendix B: Tensile Test Results

B.1. RRA Forming Tensile Tests

File name: ALCOA_200_0.05_RDA_S_1			
Material	Tensile Test Temperature (ºC)	Strain Rate (s^{-1})	Rolling Direction Orientation
ALCOA AA7075-T6	200	0.05	Along tensile direction

Temperature profile:

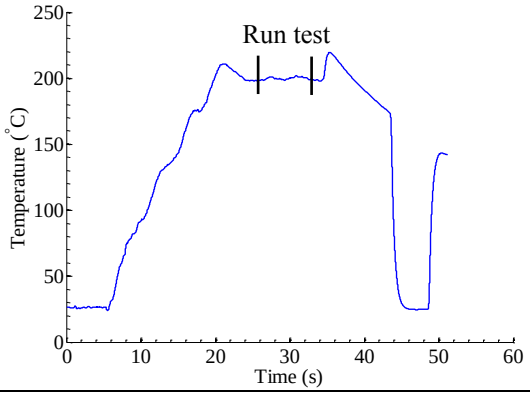

Stress-Strain Curve:

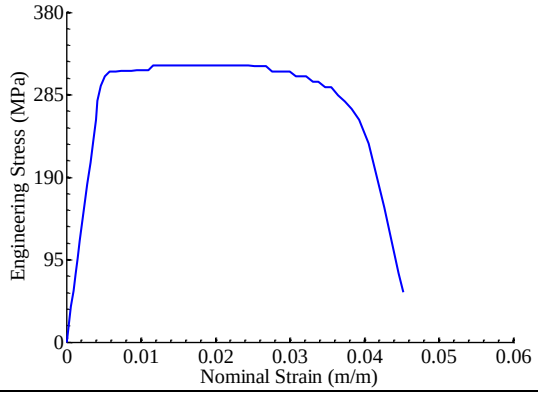

Specimen Photographs:

Scale: 0.5 in.

Before

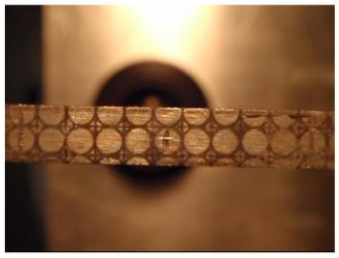

After

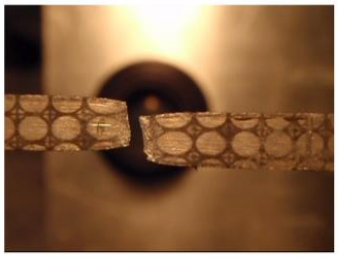

Video Analysis:

First Frame

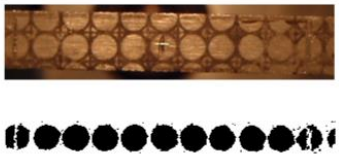

Last Frame

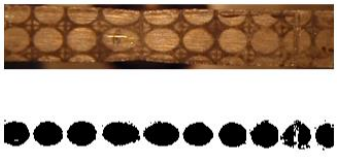

File name: ALCOA_200_0.05_RDP_1			
Material	Tensile Test Temperature (ºC)	Strain Rate (s^{-1})	Rolling Direction Orientation
ALCOA AA7075-T6	200	0.05	Perpendicular to tensile direction

Temperature profile:

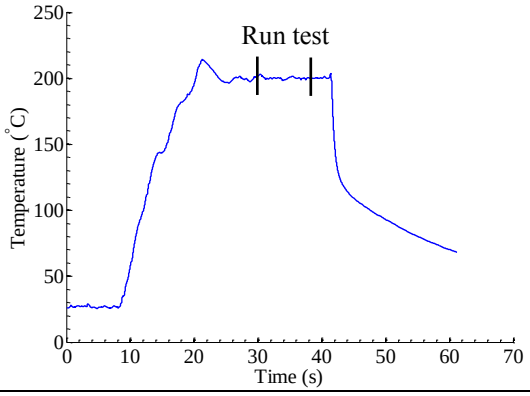

Stress-Strain Curve:

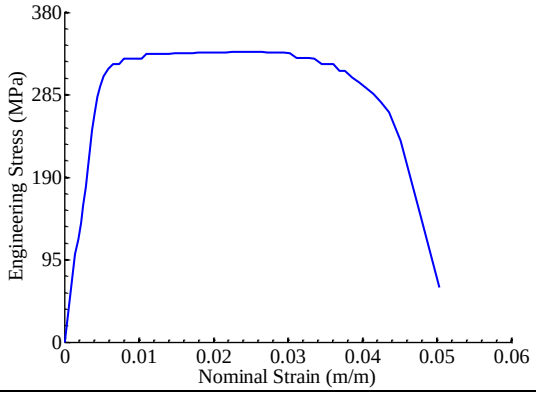

Specimen Photographs:

Scale: 0.5 in.

Before Test

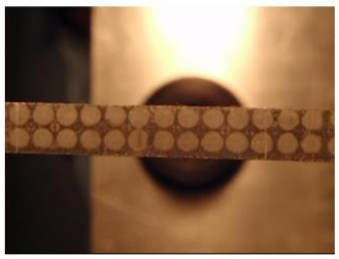

After Test

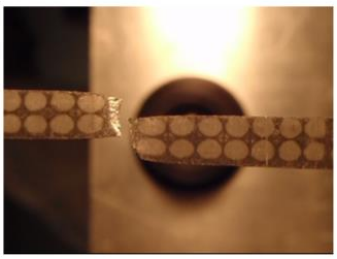

Video Analysis:

First Frame

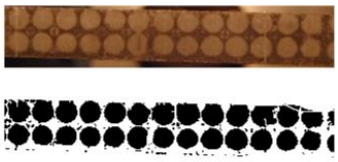

Last Frame

File name: ALCOA_200_0.05_RDP_2			
Material	Tensile Test Temperature (ºC)	Strain Rate (s^{-1})	Rolling Direction Orientation
ALCOA AA7075-T6	200	0.05	Perpendicular to tensile direction

Temperature profile:

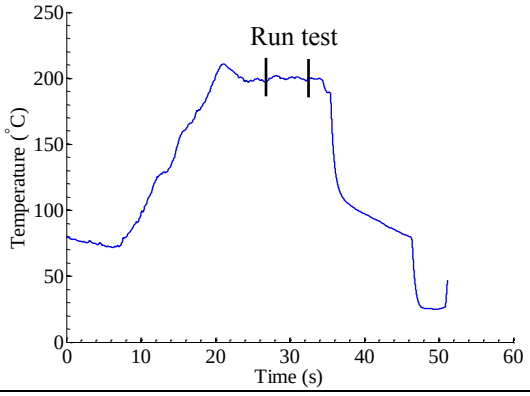

Stress-Strain Curve:

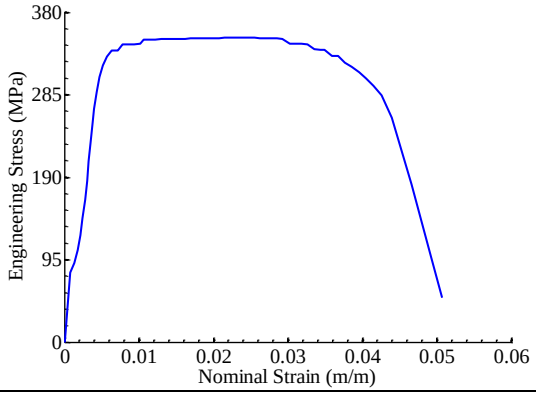

Specimen Photographs:

Scale: 0.5 in.

Before Test

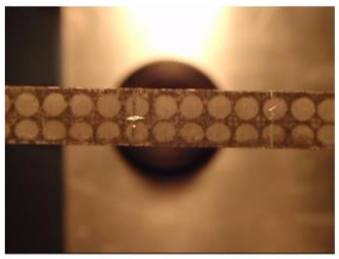

After Test

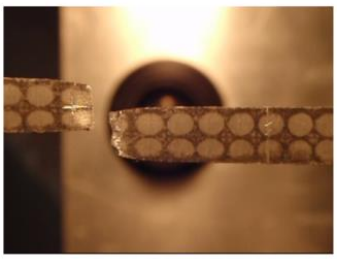

Video Analysis:

First Frame

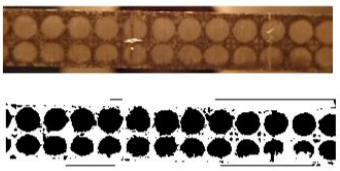

Last Frame

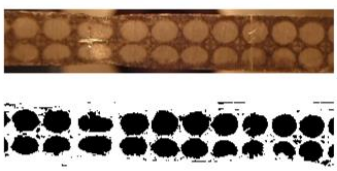

File name: ALCOA_225_0.05_RDA_1			
Material	Tensile Test Temperature (ºC)	Strain Rate (s^{-1})	Rolling Direction Orientation
ALCOA AA7075-T6	225	0.05	Along tensile direction

Temperature profile:

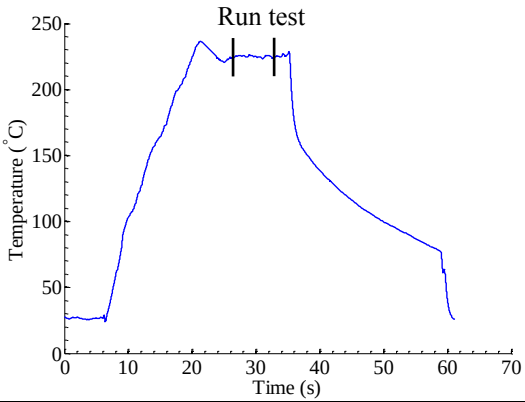

Stress-Strain Curve:

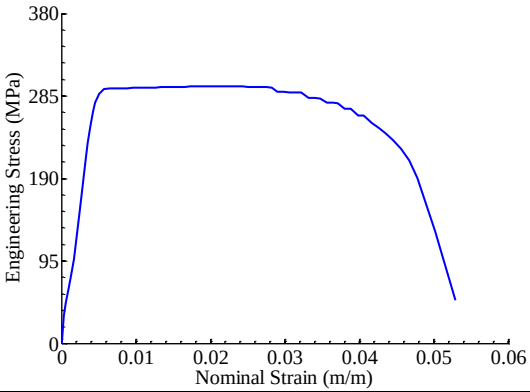

Specimen Photographs:

Scale: 0.5 in.

Before Test

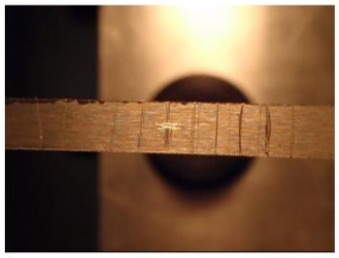

After Test

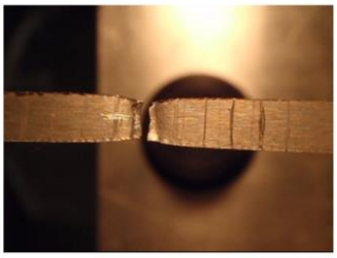

Video Analysis:

First Frame

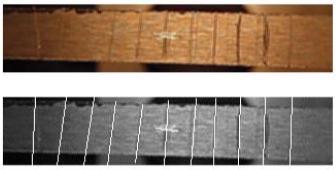

Last Frame

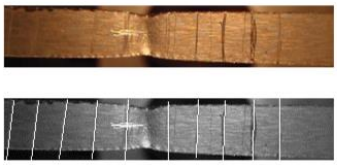

File name: ALCOA_225_0.05_RDA_S_1			
Material	Tensile Test Temperature (ºC)	Strain Rate (s^{-1})	Rolling Direction Orientation
ALCOA AA7075-T6	225	0.05	Along tensile direction

Temperature profile:

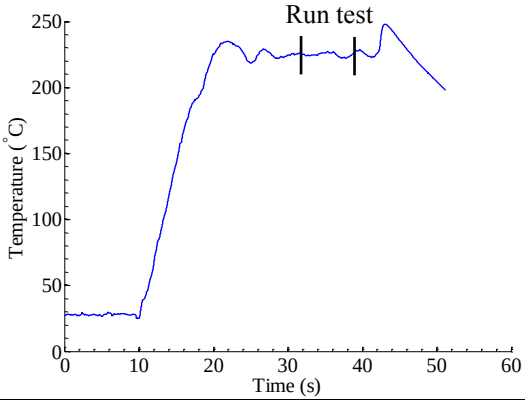

Stress-Strain Curve:

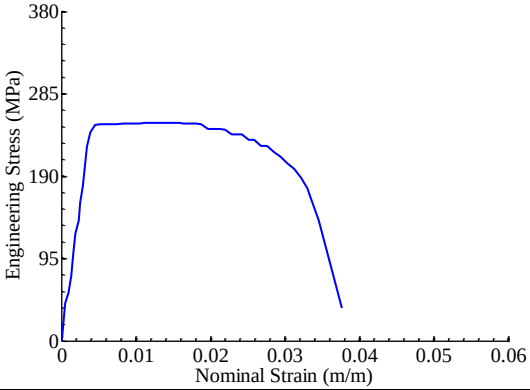

Specimen Photographs:

Scale: 0.5 in.

Before Test

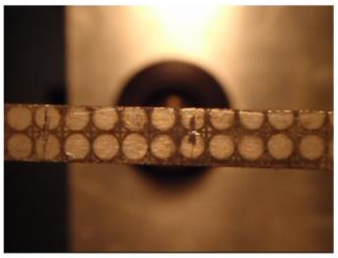

After Test

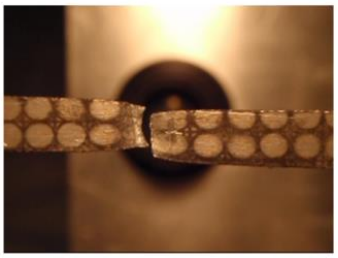

Video Analysis:

First Frame

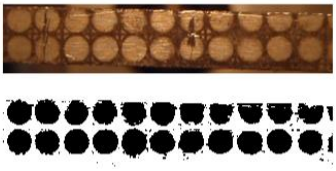

Last Frame

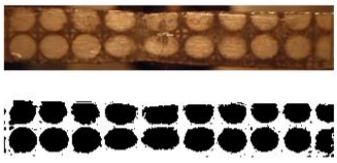

File name: ALCOA_225_0.05_RDP_1			
Material	Tensile Test Temperature (ºC)	Strain Rate (s^{-1})	Rolling Direction Orientation
ALCOA AA7075-T6	225	0.05	Perpendicular to tensile direction

Temperature profile:

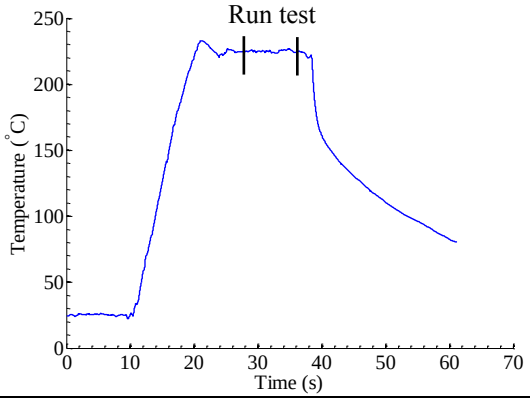

Stress-Strain Curve:

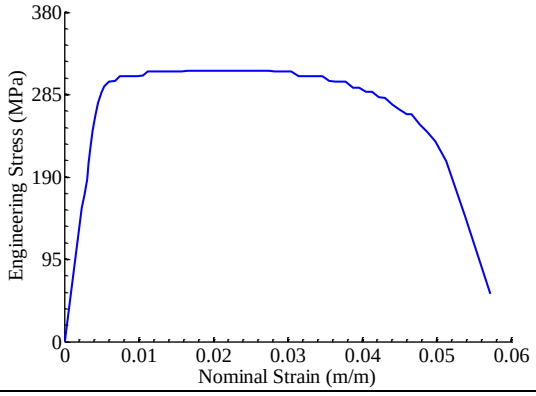

Specimen Photographs:

Scale: 0.5 in.

Before Test

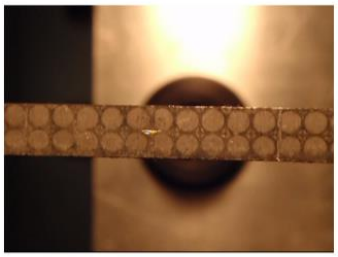

After Test

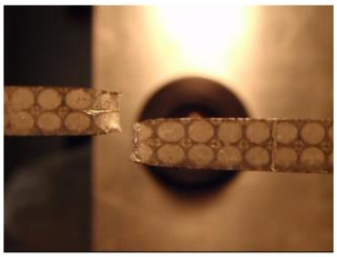

Video Analysis:

First Frame

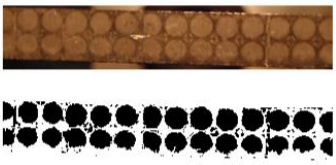

Last Frame

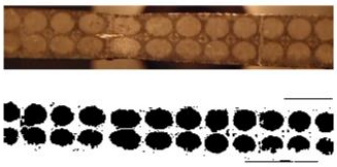

File name: ALCOA_225_0.05_RDP_2			
Material	Tensile Test Temperature (ºC)	Strain Rate (s^{-1})	Rolling Direction Orientation
ALCOA AA7075-T6	225	0.05	Perpendicular to tensile direction

Temperature profile:

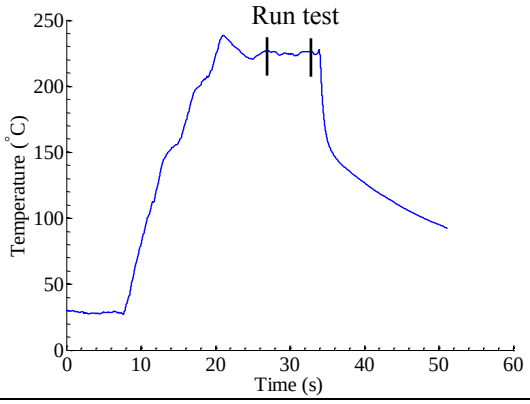

Stress-Strain Curve:

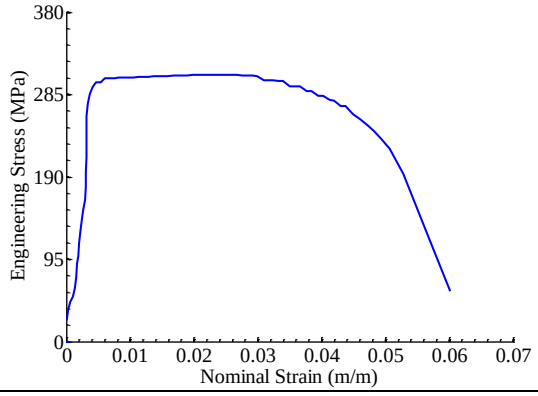

Specimen Photographs:

Scale: 0.5 in.

Before Test

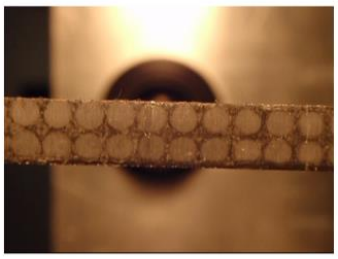

After Test

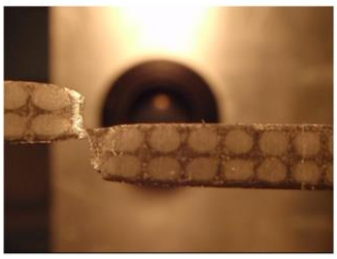

Video Analysis:

First Frame

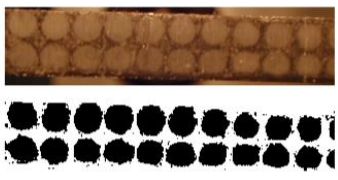

Last Frame

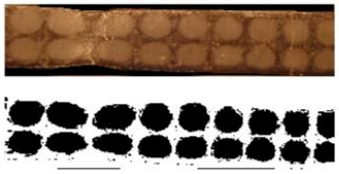

File name: AMAG_200_0.05_RDA_S_1			
Material	Tensile Test Temperature (ºC)	Strain Rate (s^{-1})	Rolling Direction Orientation
AMAG AA7075-T6	200	0.05	Along tensile direction

Temperature profile:

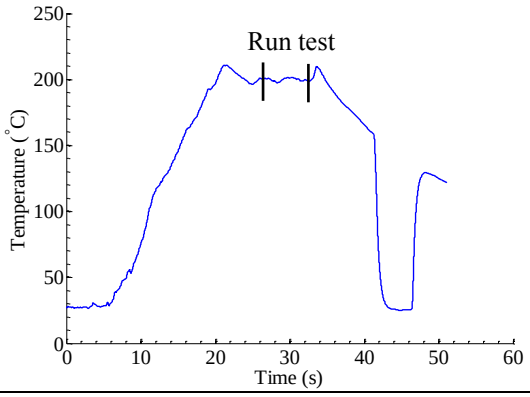

Stress-Strain Curve:

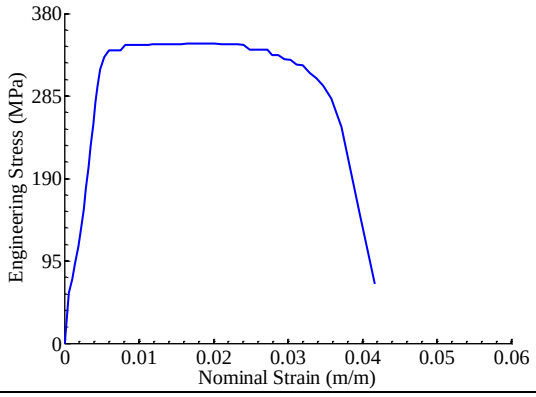

Specimen Photographs:

Scale: 0.5 in.

Before Test

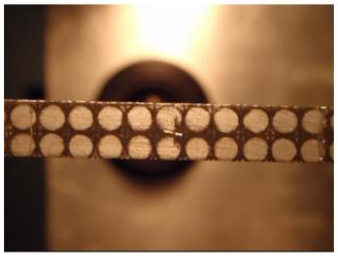

After Test

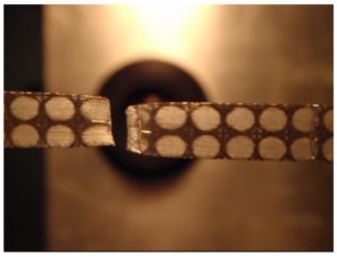

Video Analysis:

First Frame

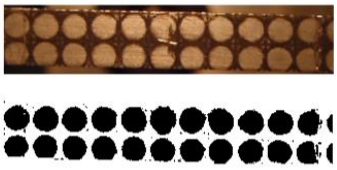

Last Frame

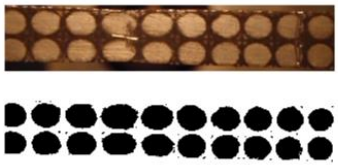

File name: AMAG_200_0.05_RDP_1			
Material	Tensile Test Temperature (ºC)	Strain Rate (s^{-1})	Rolling Direction Orientation
AMAG AA7075-T6	200	0.05	Perpendicular to tensile direction

Temperature profile:

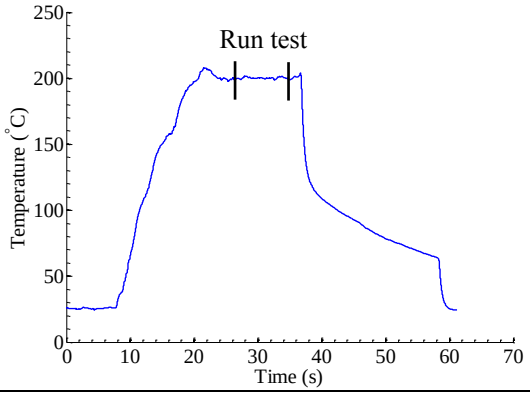

Stress-Strain Curve:

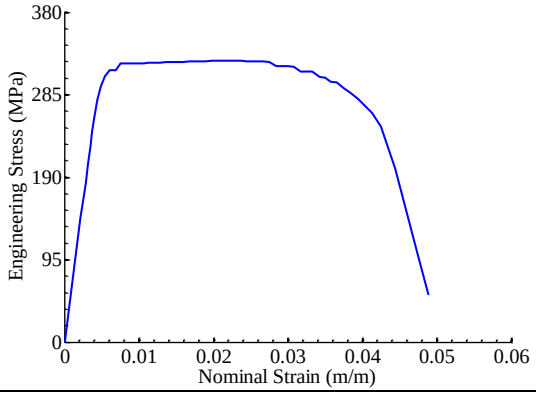

Specimen Photographs:

Scale: 0.5 in.

Before Test

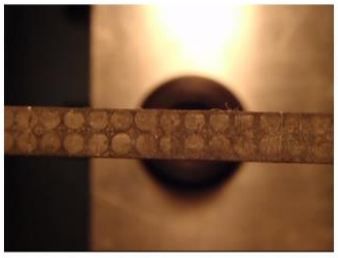

After Test

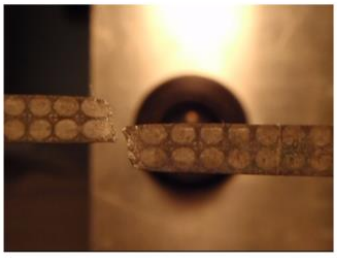

Video Analysis:

First Frame

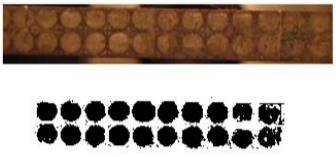

Last Frame

File name: AMAG_200_0.05_RDP_2			
Material	Tensile Test Temperature (ºC)	Strain Rate (s^{-1})	Rolling Direction Orientation
AMAG AA7075-T6	200	0.05	Perpendicular to tensile direction

Temperature profile:

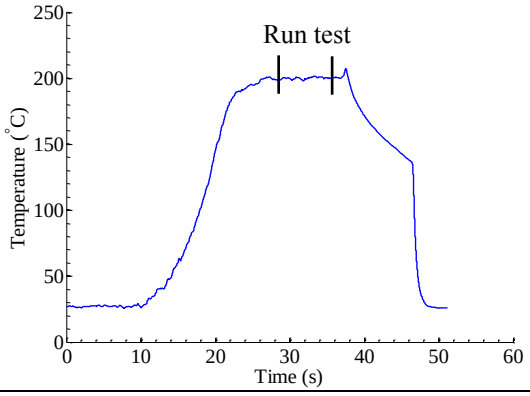

Stress-Strain Curve:

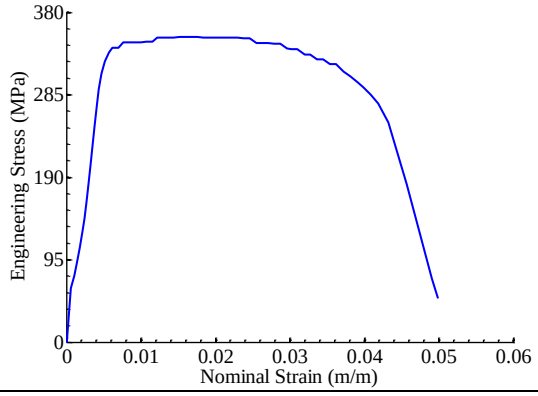

Specimen Photographs:

Scale: 0.5 in.

Before Test

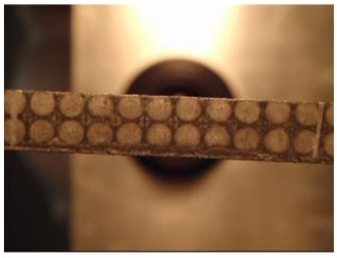

After Test

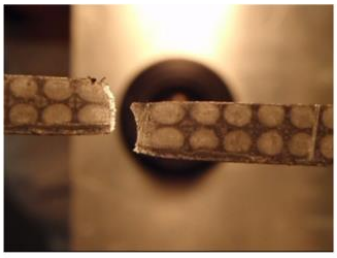

Video Analysis:

First Frame

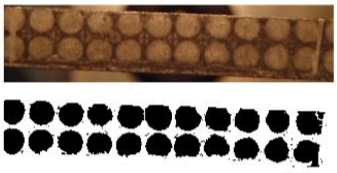

Last Frame

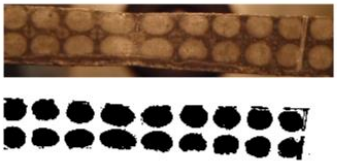

File name: AMAG_225_0.05_RDA_1			
Material	Tensile Test Temperature (ºC)	Strain Rate (s^{-1})	Rolling Direction Orientation
AMAG AA7075-T6	225	0.05	Along tensile direction

Temperature profile:

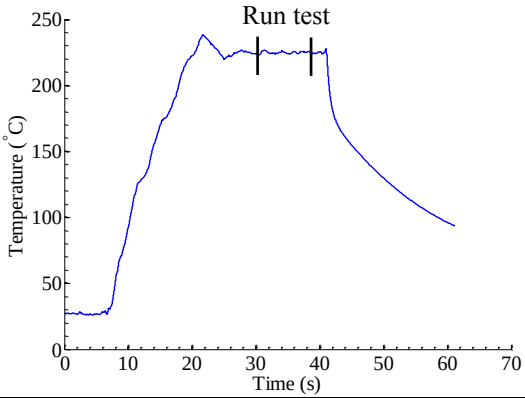

Stress-Strain Curve:

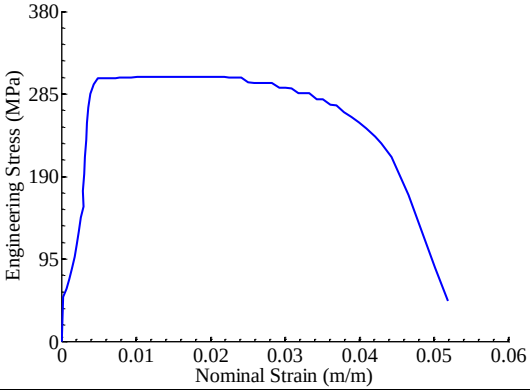

Specimen Photographs:

Scale: 0.5 in.

Before Test

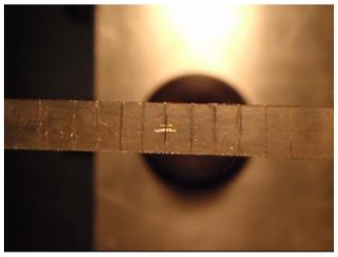

After Test

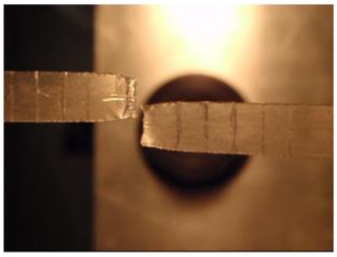

Video Analysis:

First Frame

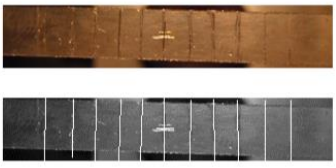

Last Frame

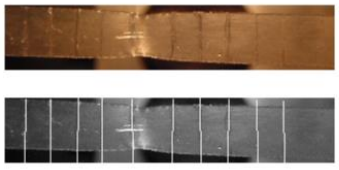

File name: AMAG_225_0.05_RDA_S_1			
Material	Tensile Test Temperature (ºC)	Strain Rate (s^{-1})	Rolling Direction Orientation
AMAG AA7075-T6	225	0.05	Along tensile direction

Temperature profile:

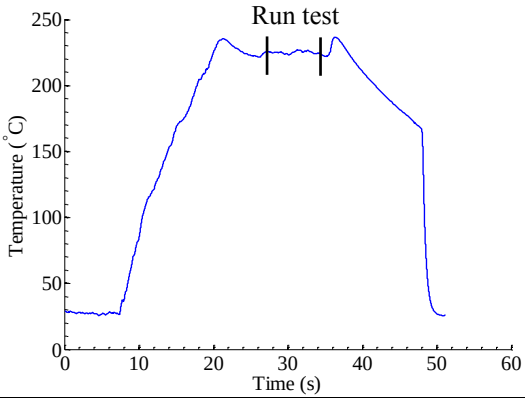

Stress-Strain Curve:

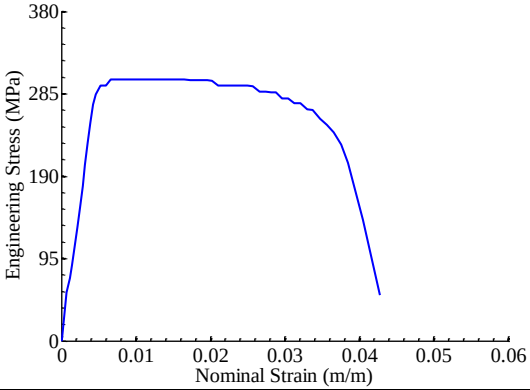

Specimen Photographs:

Scale: 0.5 in.

Before Test

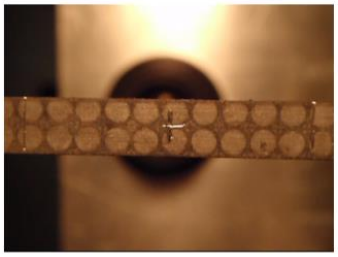

After Test

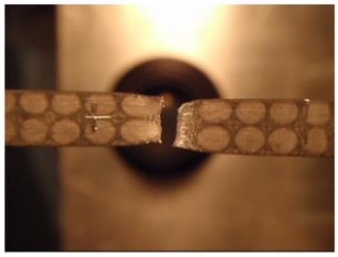

Video Analysis:

First Frame

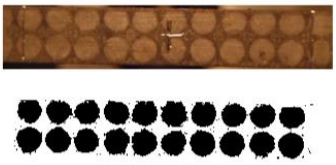

Last Frame

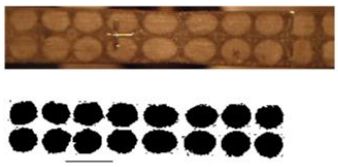

File name: AMAG_225_0.05_RDP_1			
Material	Tensile Test Temperature (ºC)	Strain Rate (s^{-1})	Rolling Direction Orientation
AMAG AA7075-T6	225	0.05	Perpendicular to tensile direction

Temperature profile:

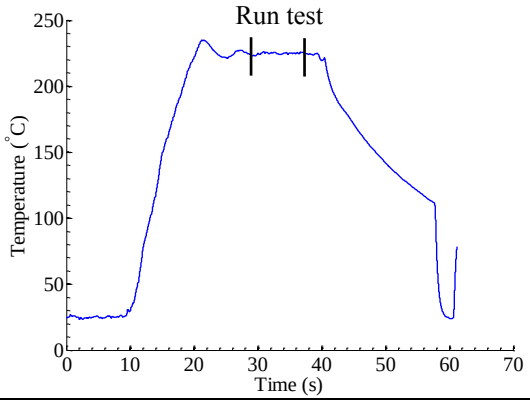

Stress-Strain Curve:

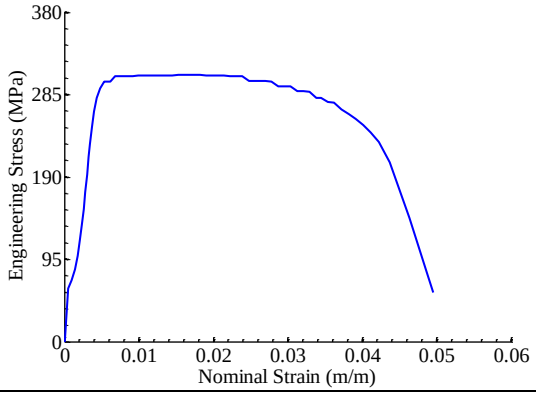

Specimen Photographs:

Scale: 0.5 in.

Before Test

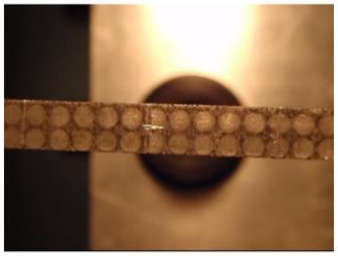

After Test

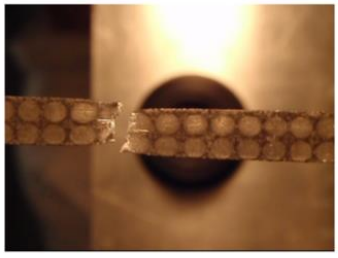

Video Analysis:

First Frame

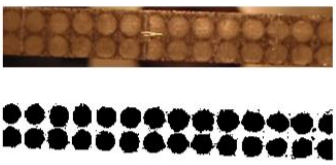

Last Frame

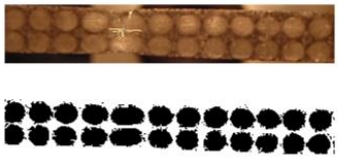

File name: AMAG_225_0.05_RDP_2			
Material	Tensile Test Temperature (ºC)	Strain Rate (s^{-1})	Rolling Direction Orientation
AMAG AA7075-T6	225	0.05	Perpendicular to tensile direction

Temperature profile:

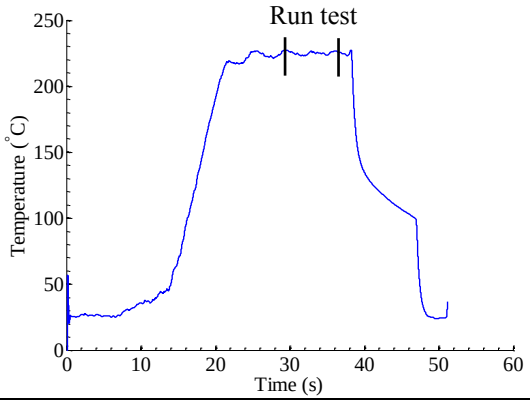

Stress-Strain Curve:

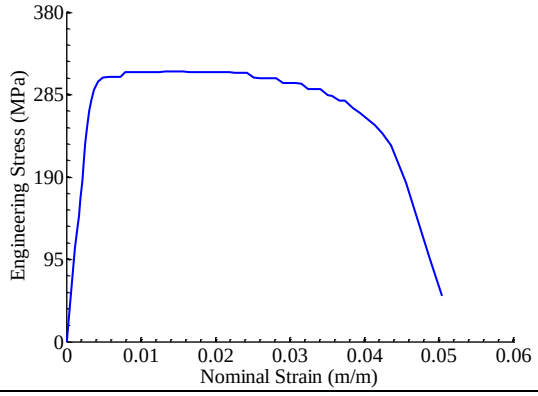

Specimen Photographs:

Scale: 0.5 in.

Before Test

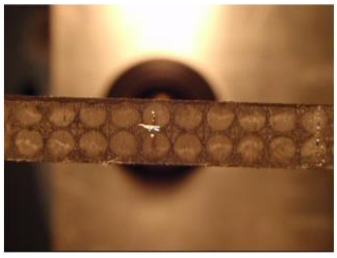

After Test

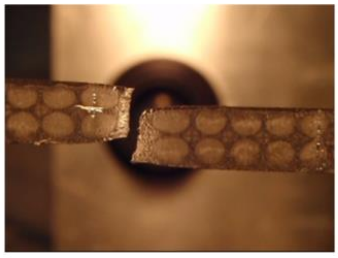

Video Analysis:

First Frame

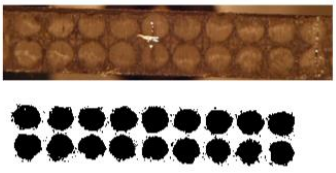

Last Frame

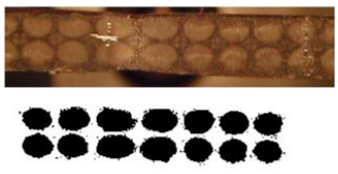

B.2. Solution Forming Tensile Tests

File name: ALCOA_300_1			
Material	Tensile Test Temperature (ºC)	Strain Rate (s^{-1})	Rolling Direction Orientation
ALCOA AA7075-Sol. Treated	300	0.05	Along tensile direction

Stress-Strain Curve:

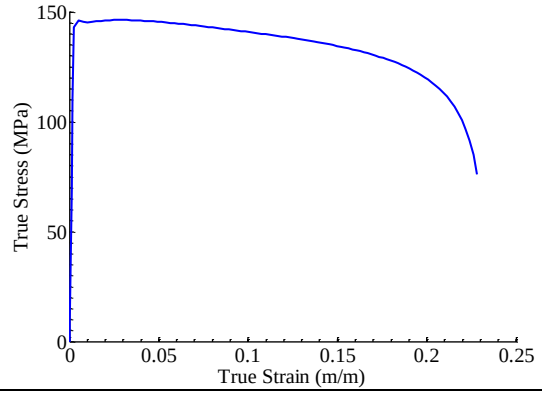

Specimen Photographs:

Generic Specimen Before Test:

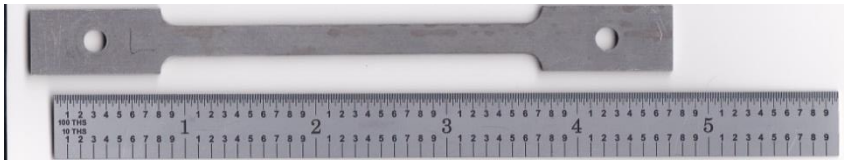

Specimen After Test:

File name: ALCOA_480_1			
Material	Tensile Test Temperature (ºC)	Strain Rate (s^{-1})	Rolling Direction Orientation
ALCOA AA7075-Sol. Treated	480	0.05	Along tensile direction

Stress-Strain Curve:

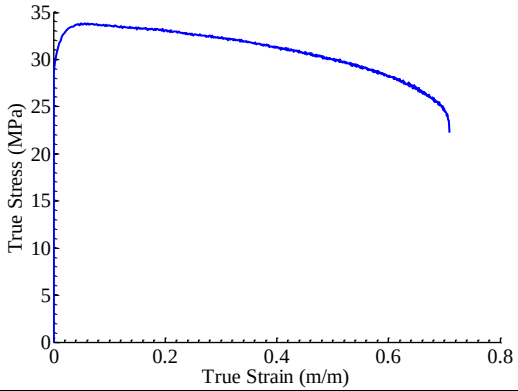

Specimen Photographs:

Generic Specimen Before Test:

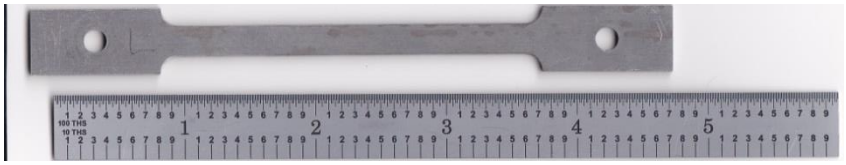

Specimen After Test:

File name: ALCOA_480_2			
Material	Tensile Test Temperature (ºC)	Strain Rate (s^{-1})	Rolling Direction Orientation
ALCOA AA7075-Sol. Treated	480	0.05	Along tensile direction

Stress-Strain Curve:

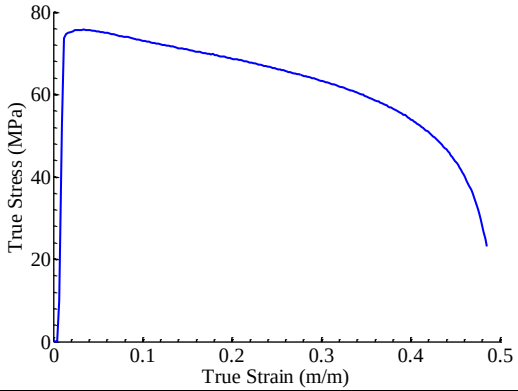

Specimen Photographs:

Generic Specimen Before Test:

Specimen After Test:

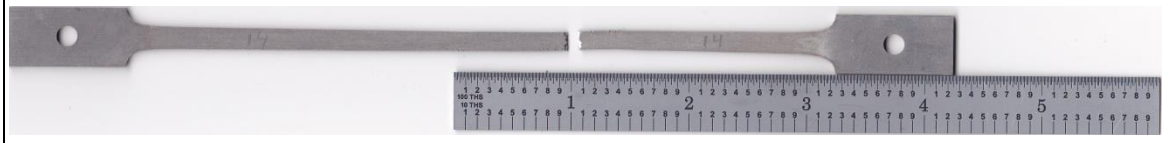

File name: AMAG_300_1			
Material	Tensile Test Temperature (ºC)	Strain Rate (s^{-1})	Rolling Direction Orientation
AMAG AA7075-Sol. Treated	300	0.05	Along tensile direction

Stress-Strain Curve:

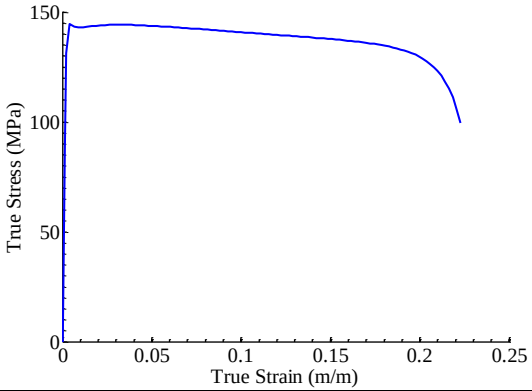

Specimen Photographs:

Generic Specimen Before Test:

Specimen After Test:

File name: AMAG_480_1			
Material	Tensile Test Temperature (ºC)	Strain Rate (s^{-1})	Rolling Direction Orientation
AMAG AA7075-Sol. Treated	480	0.05	Along tensile direction

Stress-Strain Curve:

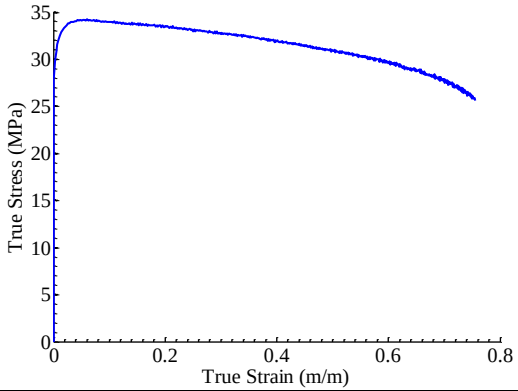

Specimen Photographs:

Generic Specimen Before Test:

Specimen After Test:

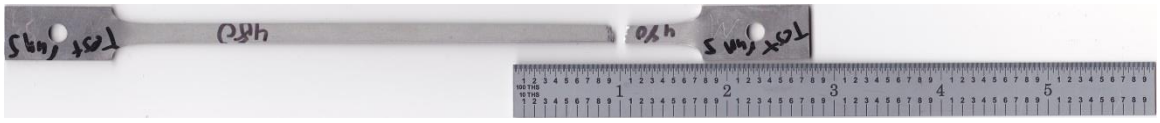

File name: AMAG_480_2			
Material	Tensile Test Temperature (ºC)	Strain Rate (s^{-1})	Rolling Direction Orientation
AMAG AA7075-Sol. Treated	480	0.05	Along tensile direction

Stress-Strain Curve:

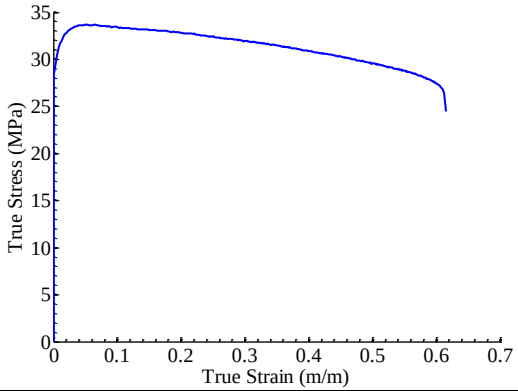

Specimen Photographs:

Generic Specimen Before Test:

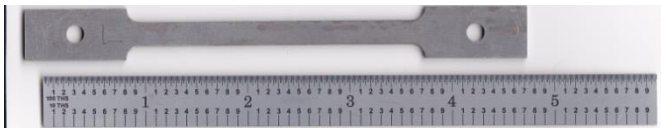

Specimen After Test:

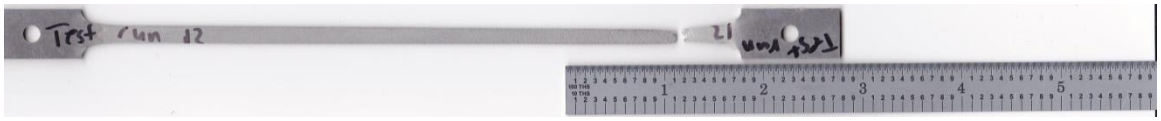

B.3. Room-temperature Tensile Tests

File name: ALCOA_RT_T6			
Material	Tensile Test Temperature (ºC)	Strain Rate (s^{-1})	Rolling Direction Orientation
ALCOA AA7075-T6	300	0.05	Along tensile direction

Stress-Strain Curve:

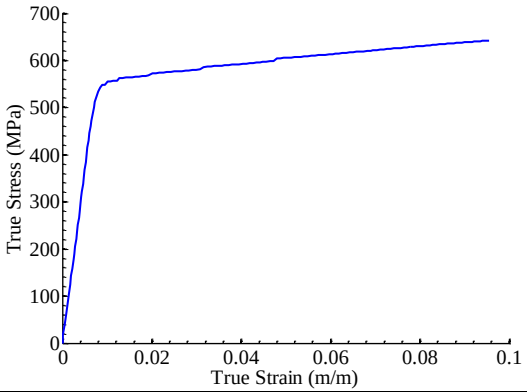

Specimen Photographs:

Generic Specimen Before Test:

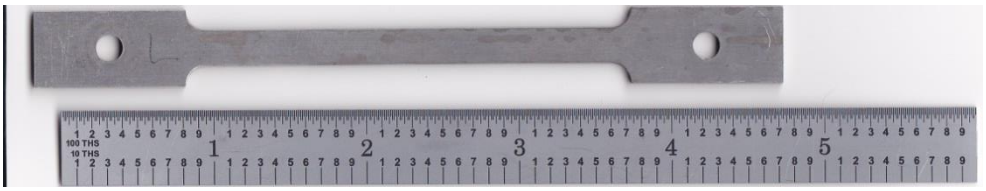

Specimen After Test:

File name: ALCOA_RT_Sol			
Material	Tensile Test Temperature (ºC)	Strain Rate (s^{-1})	Rolling Direction Orientation
ALCOA AA7075-Sol. Treated	300	0.05	Along tensile direction

Stress-Strain Curve:

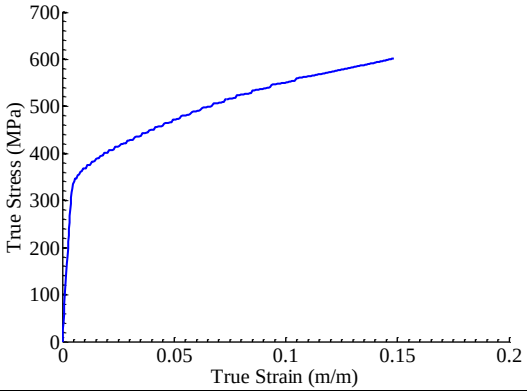

Specimen Photographs:

Generic Specimen Before Test:

Specimen After Test:

File name: AMAG_RT_T6			
Material	Tensile Test Temperature (ºC)	Strain Rate (s^{-1})	Rolling Direction Orientation
AMAG AA7075-T6	300	0.05	Along tensile direction

Stress-Strain Curve:

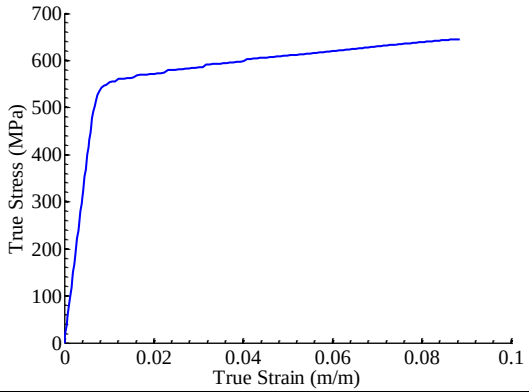

Specimen Photographs:

Generic Specimen Before Test:

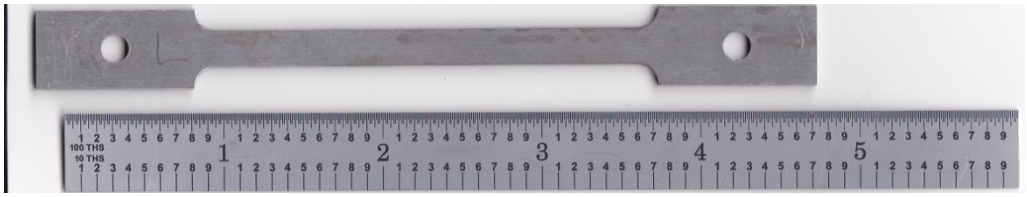

Specimen After Test:

File name: AMAG_RT_Sol			
Material	Tensile Test Temperature (ºC)	Strain Rate (s^{-1})	Rolling Direction Orientation
AMAG AA7075-Sol. Treated	300	0.05	Along tensile direction

Stress-Strain Curve:

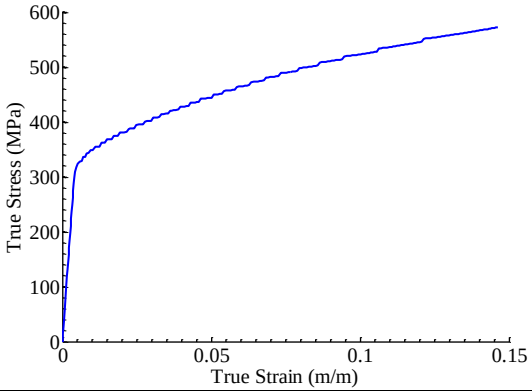

Specimen Photographs:

Generic Specimen Before Test:

Specimen After Test:

References

[1] Federal Register. Part II, Environmental Protection Agency, Department of Transportation, National Highway Traffic Safety Administration, 77 (2012) , p. 62627.

[2] Davis, J. R. (1993). ASM specialty handbook, aluminum and aluminum alloys, ASM international, Davis & Associates.

[3] Davis, J. R. (Ed.). (1990). Properties and selection: nonferrous alloys and special-purpose materials (Vol. 2). Asm Intl.

[4] Polmear, I. J., & Polmear, I. J. (1989). *Light alloys: metallurgy of the light metals* (p. 21). London: Edward Arnold.

[5] Luo, A. A. (2002). Magnesium: current and potential automotive applications. *Jom*, *54*(2), 42-48.

[6] J. R. Davis (ed.), Alloying: understanding the basics (#06117G), in: ASM Handbook, ASM Int. Materials Park, Ohio (2001),pp. 193 – 202.

[7] Kulas, M., Green, W. P., Taleff, E. M., Krajewski, P. E., & McNelley, T. R. (2005). Deformation mechanisms in superplastic AA5083 materials. *Metallurgical and Materials Transactions A, 36*(5), 1249-1261.

[8] Reducing the susceptibility of alloys, particularly aluminium alloys, to stress corrosion cracking. U.S. Patent 3,856,584, issued December 24, 1974.

[9] Taleff, E. M., Nevland, P. J., & Krajewski, P. E. (2001). Tensile ductility of several commercial aluminum alloys at elevated temperatures. *Metallurgical and Materials Transactions A, 32*(5), 1119-1130.

[10] Balderach, D. C., Hamilton, J. A., Leung, E., Cristina Tejeda, M., Qiao, J., & Taleff, E. M. (2003). The paint–bake response of three Al–Mg–Zn alloys. *Materials Science and Engineering: A, 339*(1), 194-204.

[11] McQueen, H. J., Spigarelli, S., Kassner, M. E., & Evangelista, E. (2011). *Hot deformation and processing of aluminum alloys*. CRC Press.

[12] Park, J., & Ardell, A. (1983). Microstructures of the commercial 7075 al alloy in the T651 and T7 tempers. *Metallurgical Transactions A, 14*(10), 1957-1965.Park, J. (1988).

[13] Park, J. K. (1988). Influence of retrogression and reaging treatments on the strength and stress corrosion resistance of aluminium alloy 7075-T6. *Materials Science and Engineering: A*, *103*(2), 223-231.

[14] Rajan, K., Wallace, W., & Beddoes, J. (1982). Microstructural study of a high-strength stress-corrosion resistant 7075 aluminium alloy. *Journal of Materials Science, 17*(10), 2817-2824.

[15] Danh, N. C., Rajan, K., & Wallace, W. (1983). A TEM study of microstructural changes during retrogression and reaging in 7075 aluminum. *Metallurgical Transactions A, 14*(9), 1843-1850.

[16] Park, J., & Ardell, A. (1984). Effect of retrogression and reaging treatments on the microstructure of AA-7075-T651. *Metallurgical Transactions A, 15*(8), 1531-1543.

[17] Kanno, M., Araki, I., & Cui, Q. (1994). Precipitation behaviour of 7000 alloys during retrogression and reaging treatment. *Materials Science and Technology, 10*(7), 599-603.

[18] Bartges, C. (1994). Changes in solid solution composition as a function of artificial ageing time for aluminium alloy 7075. *Journal of Materials Science Letters, 13*(11), 776-778.

[19] Ural, K. (1994). A study of optimization of heat-treatment conditions in retrogressions and reageing treatment of 7075-T6 aluminium alloy. *Journal of Materials Science Letters, 13*(5), 383-385.

[20] Viana, F., Pinto, A., Santos, H., & Lopes, A. (1999). Retrogression and re-ageing of 7075 aluminium alloy: Microstructural characterization. *Journal of Materials Processing Technology, 92*, 54-59.

[21] Ferrer, C., Koul, M., Connolly, B., & Moran, A. (2003). Improvements in strength and stress corrosion cracking properties in aluminum alloy 7075 via low-temperature retrogression and re-aging heat treatments. *Corrosion, 59*(6), 520-528.

[22] Karaaslan, A., Kaya, I., & Atapek, H. (2007). Effect of aging temperature and of retrogression treatment time on the microstructure and mechanical properties of alloy AA 7075. *Metal Science and Heat Treatment, 49*(9-10), 443-447.

[23] Baydogan, M., Cimenoglu, H., Kayali, E. S., & Rasty, J. (2008). Improved resistance to stress-corrosion-cracking failures via optimized retrogression and reaging of 7075-T6 aluminum sheets. *Metallurgical and Materials Transactions A, 39*(10), 2470-2476.

[24] Reda, Y., Abdel-Karim, R., & Elmahallawi, I. (2008). Improvements in mechanical and stress corrosion cracking properties in al-alloy 7075 via retrogression and reaging. *Materials Science and Engineering: A, 485*(1), 468-475.

[25] Dehghani, K., Nekahi, A., & Mirzaie, M. A. M. (2010). Optimizing the bake hardening behavior of Al7075 using response surface methodology. *Materials & Design, 31*(4), 1768-1775.

[26] Sotirov, N., Simon, P., Chimani, C., Uffelmann, D., & Melzer, C. (2012). Warm deep drawability of peak-aged 7075 aluminium sheet alloy. *Key Engineering Materials, 1665*(504), 955.

[27] WANG, H., LUO, Y., FRIEDMAN, P., CHEN, M., & GAO, L. (2012). Warm forming behavior of high strength aluminum alloy AA 7075. *Transactions of the Nonferrous Metals Society of China, 22*(1), 1-7.

[28] Rajamuthamilselvan, M., & Ramanathan, S. (2011). Hot deformation behaviour of 7075 alloy. *Journal of Alloys and Compounds, 509*(3), 948-952.

[29] Smeyers, A., Schepers, B., Braunschweig, W., Bürger, A., Vieregge, K., Khosla, S., & Wise, A. (2011). 7xxx grades for automotive applications. *Aluminium international today: the journal of aluminium production and processing*, *23*(1), 37-39.

[30] Burger, G., Gupta, A., Jeffrey, P., & Lloyd, D. (1995). Microstructural control of aluminum sheet used in automotive applications. *Materials Characterization, 35*(1), 23-39.

[31] Saga, M., Kikuchi, M., Matsuo, M., Sasaki, Y., & Yan, Z. (1996). Effect of pre-aging temperature on the behavior in the early stage of aging at high temperature for al-mg-si alloy. *Materials Science Forum, , 217* 821-826.

[32] ASTM E8. (1997). Standard test methods for tensile testing of metallic materials. *Annual book of ASTM standards*, *3*.

[33] ASTM E21-09. (2009). Standard test methods for elevated temperature tension tests of metallic materials. *Annual book of ASTM standards*, *3*.

[34] *Alloy 7075 Plate and Sheet Technical Sheet*. ALCOA Mill Products.

[35] W. Koster, "Die Temperaturabhangigkeit des ElisatizitatsmodulsreinerMetalle," ZeitschrietfurMetallkunde, 39 (1948), pp. 1–9.

[36] Karunasena, W. G., Greene, G. W., & Chen, N. N. (1978). Direct resistance heating characteristics of rectangular sheet blanks. *Industry Applications, IEEE Transactions on*, (3), 282-288.

[37] Çengel, Yunus A., and Afshin J. Ghajar. (2010). *Heat and Mass Transfer: Fundamentals & Applications*.

[38] *Industrial Laminate Specifications Glass-Based Phenolics NEMA G-3, G-5, G-7, G-9, G-10, G-11 Grades. (n.d)* Retrieved 2014, from http://www.boedeker.com/ilamg_p.htm

[39] Schindelin, J., Arganda-Carreras, I., Frise, E., Kaynig, V., Longair, M., Pietzsch, T., & Cardona, A. (2012). Fiji: an open-source platform for biological-image analysis. *Nature methods*, *9*(7), 676-682. Retrieved 2014, from http://fiji.sc/Fiji

[40] Gale, W. F., & Totemeier, T. C. (Eds.). (2003). *Smithells metals reference book*. Butterworth-Heinemann.

[41] Hisayuki, K., Yamane, T., Takahashi, T., Minamino, Y., Hirao, K., & Araki, H. (1999). Diffusion of zinc in commercial al-zn alloys under high pressure. *Journal of Materials Science, 34*(10), 2449-2454.

[42] Bariani, P. F., Bruschi, S., Ghiotti, A., & Michieletto, F. (2013). Hot stamping of AA5083 aluminium alloy sheets. *CIRP Annals-Manufacturing Technology*, *62*(1), 251-254.

[43] High strength low alloy (HSLA) steels for cold forming. ArcelorMittal (2013).